



Norwegian University of
Science and Technology

Subsea regeneration of triethylene glycol (TEG) for natural gas dehydration.

Natalie Therese Josefsen

Chemical Engineering and Biotechnology

Submission date: July 2017

Supervisor: Liyuan Deng, IKP

Co-supervisor: Luca Ansaloni, IKP
Kristin Dalane, IKP

Norwegian University of Science and Technology
Department of Chemical Engineering

Preface

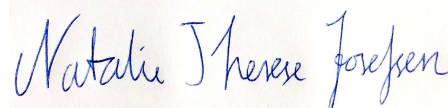
This thesis was written as the final work of the master program in Chemical Engineering at the Norwegian University of Science and Technology NTNU.

Foremost, I would like to express my deepest gratitude towards my supervisor professor Associate Professor Liyuan Deng for her guidance and inquisitive attitude to my work. I would like to thank my co-supervisor Luca Ansaloni for his motivation and help, whether it is experimental work or data analysis, also on weekends. I would like to thank my co-supervisor PhD candidate Kristin Dalane for her sharing of knowledge and encouragement. Furthermore, I would like to thank Zhongde Dai for meaningful discussions and for proof reading the thesis.

My fellow master's students at the MEMFO group also deserves acknowledgement. The open and sharing environment with you has helped me throughout this thesis. And thanks to all of my friends in Trondheim for supporting me and making the time as a student rememberable. At last, thanks to my mum for encouragement and support in troubled times and late night discussions.

Declaration of Compliance

I hereby declare that this thesis is an independent work in agreement with the exam rules and regulations of the Norwegian University of Science and Technology.



Natalie Therese Josefsen
19 July 2017, Trondheim

Abstract

The scope of this thesis was to examine the use of pervaporation technology with membranes for the regeneration of triethylene glycol (TEG) in natural gas dehydration. To reduce the need for offshore installations, subsea separation processes have been proposed. The subsea natural gas dehydration near the well is desirable as it results in smaller volume stream of natural gas and less water to damage the pipes. However, the conventional method of dehydration is not feasible for subsea operations due to factors, such as bulky design, large heating requirements and the need for continuously attention and maintenance, and another approach is needed. An alternative method for the natural gas dehydration is by using a closed loop membrane process design, using TEG as liquid absorbent.

Literature results on membrane absorbers using TEG for natural gas dehydration are available, but there is a lack of information about TEG dehydration using pervaporation technology, therefore experimental data is needed to validate computational models for process analysis. In this thesis, an experimental study of dehydration of TEG with pervaporation technology has been carried out using composite membranes with porous support of polypropylene (PP) and dense layer of Teflon AF2400. The addition of porous nanoparticles to the dense AF2400 layer was examined and innovative multi-layered membranes were developed for future use in pervaporation. The membranes were characterized in terms of compatibility to TEG, morphology and surface properties with scanning electron microscopy (SEM), scanning transmission electron microscopy S(T)EM and contact angle measurements. Furthermore, a method for analyzing TEG in aqueous solutions was developed with gas chromatography mass spectrometry (GC/MS) as this was vital to the pervaporation study.

The use of AF2400 as a dense layer in the composite membrane was confirmed as a suitable polymer after a compatibility study, as no TEG uptake was obtained. Results obtained from the pervaporation study show excellent separation factor of water from TEG, but rather low water flux through the membrane. In general, the water flux increased with increasing operating temperature and higher water content in the feed. The amount of TEG in the permeate was extremely low, increased slightly with increasing temperature and decreased with higher water content in the feed. The water permeance was enhanced with higher temperature and was shown to be rather independent of feed water concentration. The membrane showed long-term stability as the pervaporation experiments were performed over a time span of 1500 hours. The effect of adding ZIF-L nanoparticles to the dense layer of AF2400 in the composite membrane enhanced the water flux through the membrane. However, more TEG was found in the permeate, resulting in a lower separation factor, higher TEG permeability and lower water selectivity of the membrane. On the other side, the separation factor was still extremely high (>10000), suggesting that the addition of ZIF-L to the composite membrane with PP and AF2400 can be a suitable approach to improve the water permeance through the membrane.

Sammendrag

Hensikten med denne masteravhandlingen har vært å undersøke bruken av pervaporasjonsteknologi med membraner for regenerering av trietylene glykol (TEG) i naturgasstørking. For å redusere behovet for offshore installasjoner, subsea separasjonsprosesser har blitt foreslått. Subsea gasstørking nærme brønnen er ønskelig da det resulterer i mindre vann som kan skade gassledningene og et mindre gassvolum. Den konvensjonelle metoden for gasstørking er ikke gjennomførbar for subsea operasjoner på grunn av faktorer som klumpete design, oppvarmingskrav og kontinuerlig overvåking og vedlikehold, og en ny tilnærming kreves. En alternativ metode for tørking av naturgass er ved å bruke et "closed loop" prosessdesign med TEG som absorbent.

Det eksisterer minimalt med litteratur for fjerning av vann fra TEG ved pervaporasjonsteknologi, det trengs derfor eksperimentelle data for å validere datamodeller for prosessanalyse. I denne avhandlingen har det blitt utført et eksperimentelt studie av fjerning av vann ved å bruke komposittmembraner med polypropylen (PP) og Teflon AF2400. Tilføring av porøse nanopartikler til AF2400 ble undersøkt og innovative multi-lag-membraner ble utviklet for fremtidig bruk i pervaporasjonsteknologi. Membranene ble karakterisert i form av kompatibilitet til TEG, morfologi- og overflateegenskaper med skanning elektronmikroskopi (SEM), skanning transmisjon elektronmikroskopi S(T)EM og måling av kontaktvinkler. Videre ble en metode for å analysere TEG i vannløsninger utviklet med gass kromatografi masse spektrometer (GC/MS) da dette var absolutt nødvendig for pervaporasjonsstudiet.

Valget av AF2400 som yterste lag i komposittmembranen ble bekreftet som egnet polymer etter kompatibilitetsstudie uten TEG absorbering og med kontaktvinkeltester som viste hydrofob karakteristikk. Resultatene fra pervaporasjonsstudiet ga utmerket separasjonsfaktor for vann over TEG, men en lav vannfluks gjennom membranen. Generelt sett økte vannfluksen med høyere vannkonsentrasjon i føden. Mengden TEG i permeatet var ekstremt lav og økte noe med økende temperatur og høyere vanninnhold i føden. Vannpermeansen økte med høyere temperatur og den viste seg å være uavhengig av vannkonsentrasjonen i føden. Membranen viste langtidsstabilitet da pervaporasjonseksperimentene gikk over et tidsspenn på 1500 timer. Tilføring av ZIF-L nanopartikler til AF2400-laget i komposittmembranen økte vannfluksen gjennom membranen. Når det er sagt, så var det var det mer TEG i permeatet og dermed en lavere separasjonsfaktor, høyere TEG-permeabilitet og lavere vannselektivitet for nanokomposittmembranen. På den andre siden var separasjonsfaktoren fortsatt ekstremt høy (>10000), som antydte at tilføring av ZIF-L til komposittmembranen med PP og AF2400 kan være et egnet tilnærming for å forbedre vannpermeansen gjennom membranen.

Contents

1	Introduction	1
1.1	Motivation	1
1.2	Research objective	3
2	Theory	4
2.1	Dehydration of natural gas	4
2.1.1	Transport in pervaporation	7
2.2	Membranes for pervaporation	12
2.2.1	Choice of membrane material	12
2.2.2	Mixed matrix membranes	14
2.2.3	Composite membranes	19
3	Experimental	22
3.1	Materials	22
3.2	Characterization techniques	23
3.2.1	Compatibility experiments	23
3.2.2	Contact angle measurement	23
3.3	Membrane preparation	25
3.3.1	Composite membranes	25
3.3.2	Multi-layered membrane development	27
3.4	Morphological characterization	28
3.4.1	Effect of water exposure	30
3.5	Gas Chromatography Mass Spectrometer	31
3.5.1	Technical conditions	32
3.5.2	Sample preparation	32
3.5.3	Method development	33
3.5.4	Method validation	33
3.6	Pervaporation	35
3.6.1	Experimental setup	35
4	Results and Discussion	37
4.1	Compatibility measurements	37
4.1.1	Submerging test	37
4.1.2	Contact angle	41
4.2	Morphological characterization	42
4.2.1	Composite membrane PP-AF2400	42
4.2.2	ZIF particles	43

4.2.3	Nanocomposite membrane	44
4.3	Gas Chromatography Mass Spectrometer	47
4.3.1	Method development	47
4.3.2	Method validation	52
4.4	Pervaporation	55
4.4.1	Pervaporation performance of PP-AF2400	56
4.4.2	Pervaporation performance of PP-AF2400-ZIF-L	63
4.4.3	Effects of aging	66
4.4.4	Comparison to literature data	67
4.5	Further membrane development	68
4.5.1	Optimizing the dip coating process	68
4.5.2	Multi-layered membrane development	69
5	Conclusion	75
6	Suggestions for Future Research	78
	Appendix A - Risk assessments	i
	Appendix B - Membrane images	i
	Appendix C - S(T)EM images	ii
	Appendix D - standard deviation	iii
	Appendix E - Pervaporation graphs	iii
	Appendix F - Activity coefficients	iv
	Appendix G - Apparent activation energy	v

List of Figures

2.1.1 Conventional dehydration system	4
2.1.2 Closed loop membrane process	5
2.1.3 Solution-diffusion model	7
2.1.4 Ideal and non-ideal sorption isotherms	8
2.1.5 Specific volume	9
2.2.1 Schematic representation of aMixed matrix membrane.	14
2.2.2 Morphologies of nanoparticles in MMM.	15
2.2.3 Molecular structure of ZIF-8.	16
2.2.4 Network of zinc atoms in ZIF-L and ZIF-8.	17
2.2.5 Transport paths of TEG and water in MMM of ZIF-L and ZIF-8.	17
2.2.6 Illustration of different composite membranes	19
3.2.1 Contact angle apparatus.	23
3.2.2 Contact angle, schematic representation	24
3.3.1 Dip coating procedure for composite membranes (Technique A).	25
3.3.2 Membrane preparation apparatus.	26
3.3.3 Image of filtration procedure and plasma cleaner	27
3.4.1 Pictures of SEM TM3030 PLUS and S(T)EM 5500 from HITACHI.	28
3.4.2 Scanning electron microscope illustration	29
3.4.3 Experimental water exposure apparatus.	30
3.5.1 Illustration of the GC/MS analytical tool.	31
3.5.2 Picture of the GC/MS setup.	32
3.5.3 Graphs of the mass spectra obtained with GC/MS	33
3.6.1 Experimental pervaporation setup	35
3.6.2 Pictures of the experimental pervaporation setup.	36
4.1.1 Graph, compatibility of different membranes	38
4.1.2 Nafion and Nexar molecule structure	39
4.1.3 Molecular structure of PIM-1 and PTMSP	39
4.1.4 Molecular strucutre of polyimide, PDMS, AF2400.	40
4.1.5 Contact angle measurements of AF2400 and PP.	41
4.2.1 SEM images of PP-AF2400 composite membrane	42
4.2.2 S(T)EM images of the ZIF particles characterized.	43
4.2.3 S(T)EM images of 4 and 8 sonications of ZIF-L in composite membranes PP- AF2400-ZIF-L	44
4.2.4 S(T)EM images of composite membranes with PP coated with MMM of AF2400 and ZIF-L	45

4.2.5 S(T)EM surface images composite membrane PP-AF2400-ZIF-8 before and after water wash	46
4.3.1 GC/MS chromatograms, effect of changing split from 10 to 2.	48
4.3.2 GC/MS chromatograms, effect of increasing the inlet oven temperature.	50
4.3.3 GC/MS chromatogram, Restek temperature program.	50
4.3.4 GC/MS chromatograms, different amount of sample injected.	51
4.3.5 GC/MS, calibration curve.	52
4.4.1 Effect of feed water concentration on total flux and TEG concentration in permeate in PP-AF2400 membrane.	56
4.4.2 Effect on feed water concentration on water flux and TEG flux in PP-AF2400 membrane.	57
4.4.3 Separation factor as a function of water concentration in feed in PP-AF2400 membrane.	57
4.4.4 Effect of water concentration in feed on water and TEG permeance in PP-AF2400 membrane.	58
4.4.5 Effect of water concentration in feed on ideal selectivity in PP-AF2400 membrane.	59
4.4.6 Effect of temperature on separation factor, TEG flux, ideal selectivity in PP-AF2400 membrane.	60
4.4.7 The effect of temperature on permeance and ideal selectivity in in PP-AF2400 membrane.	61
4.4.8 Arrhenius type of relation with permeance in PP-AF2400 membrane.	62
4.4.9 Effect of feed water concentration on total flux, TEG concentration in permeate and separation factor in PP-AF2400-ZIF-L membrane.	63
4.4.10 Effect of feed water concentration on permeability and ideal selectivity in PP-AF2400-ZIF-L membrane.	65
4.4.11 Graph, aging of membrane in PP-AF2400	66
4.4.12 A comparison of literature data and the obtained data for pervaporation.	67
4.5.1 Examination of the dip coating technique. a) Thickness of coating as a function of AF2400 concentration. b) Thickness of coating as a function of total dipping time.	68
4.5.2 S(T)EM images of multi-layered membranes with PP and a crystalline layer of ZIF-L	69
4.5.3 The effect of plasma treatment on the contact angles of water on PP.	70
4.5.4 Effect of plasma treatment on adhesion between PP and ZIF-L.	71
4.5.5 Effect of water exposure on particle ZIF-L layer.	72
4.5.6 Effect of 100% humidity on ZIF-L particle layer.	73
4.5.7 S(T)EM images of multi layered membrane with PP-ZIF-L coated with a layer of AF2400.	74
.0.1 Pictures of the multi-layered membranes when detachment occurred.	i
.0.2 SEM/S(T)EM surface images of self standing membranes with AF2400, with and without zif-l nano particles.	ii
.0.3 TEG concentration as a function of water concentration in feed.	iv

List of Tables

2.2.1 Literature data for pervaporation of EG, DEG, TEG	12
3.3.1 Overview of the composite membranes that were experimentally made.	25
4.3.1 GC parameters.	47
4.3.2 Summation of the different temperature oven programs that were tested.	49
4.3.3 Parameters for the validation of the GC-MS method.	52
4.3.4 GC/MS, method repeatability.	53
4.3.5 GC/MS, method accuracy.	54
4.4.1 Compatibility tests of AF2400-ZIF-L.	64
.0.1 Activity coefficient of water	v
.0.2 Activity coefficient of TEG	v
.0.3 Activation energy found from permeance	vi

Abbreviations

	Explanation
BSE	Backscattered electron
CMS	Carbon molecular sieves
CNT	Carbon nanotubes
DEG	Diethylene glycol
EDX	Energy dispersive X-ray
EG	Ethylene glycol
FFV	Fractional free volume
FID	Flame ionization detector
FT-IR	Fourier transform infrared spectroscopy
GC	Gas chromatography
GC/MS	Gas chromatography mass spectrometry
GPTMS	Glycidyoxypropyltrimethoxysilane
Hmim	2-methylimidazole
ICH	Council for Harmonisation
IPA	Isopropanol
IS	Internal standard
LN ₂	Cold liquid N ₂
LOD	Limit of detection
LOQ	Limit of quantification
m/z	Mass over ion ratio
MMM	Mixed matrix membrane
MS	Mass spectrometry
NaCl	Sodium Chloride
PAN	Polyacrylonitrile
PD	Polydopamine
PDMS	Polydimethylsiloxane
PEI	Polyethylenimine
PFC	Perfluorocopolymers
PI	Polyimide

	Explanation
PP	Polypropylene
PPM	Parts per million
PSf	Polysulfone
PSI	Pervaporation separation index
PV	Pervaporation
PVA	Poly(vinyl alcohol)
PVAm	Polyvinylamine
PVDF	Polyvinylidene difluoride
PTMSP	Poly[1-(trimethylsilyl)-1-propylene
RSD	Relative standard deviation
S/N	Signal to Noise
SA	Sodium alginate
SEM	Scanning electron microscopy
SIM	Selected ion monitoring
STEM	Scanning transmission electron microscopy
SCF	Standard cubic feet
TEOS	Tetraethoxysilane
TEG	Triethylene glycol
THF	Tetrahydrofuran
VOC	Volatile organic compounds
XRD	X-ray diffraction
ZIF	Zeolitic imidazolate frameworks
TEOS	Tetraethoxysilane
TEG	Triethylene glycol
THF	Tetrahydrofuran
VOC	Volatile organic compounds
XRD	X-ray diffraction
ZIF	Zeolitic imidazolate frameworks

Symbols

	Unit	Explanation
a	-	Activity
A	m^2	Membrane area
D	m^2/s	Diffusivity
E_J	J/mol	Apparent activation energy
g	m/s^2	Gravitational constant
J_0	-	Preexponential factor
J_i	g/m^2h	Flux of component i
l	m	Membrane thickness
L_i	-	Proportionality constant of component i
p	Pa	(hydraulic)Pressure
p^0	Pa	Saturation vapor pressure
p_p	Pa	Pressure on the downstream side
P_i	$m^3/m^2s.Pa.m$	Permeability
Q	kg	Total mass permeated
R	$J/mol.K$	Ideal gas constant
R^2	-	Squared correlation coefficient
S	$m^3/m^3.Pa$	Solubility coefficient
SU	%	Solvent uptake
T	K	Temperature
T_g	K	Glass transition temperature
t	s	Time
V_0	m^3	Volume at 0K
V_f	m^3	Free volume
V_T	m^3	Observed volume
W_d	kg	Weight of dry membrane
W_s	kg	Weight of the swollen membrane
x_i	-	Mole fraction of liquid
y_i	-	Mole fraction of vapor
α	-	Selectivity
γ	N/m	Surface tension
μ	-	Micro
ρ	kg/m^3	Density
θ	-	Angle

Chapter 1

Introduction

1.1 Motivation

Natural gas is a vital part of the world's energy supply. It is one of the cleanest fossil fuels, safest and most useful energy source [1]. The world uses almost 100 trillion scf (standard cubic feet) of natural gas every year, and the total consumption is increasing every year [2]. The bottom hole natural gas consists of a gas mixture containing mostly of methane and other hydrocarbons, but also impurities, such as water, H_2S and CO_2 . In order to be able to use the natural gas, it must go through several stages of separation and purification. All natural gas must be dried before it enters the distribution pipelines to control corrosion and avoid formation of hydrates or solid hydrocarbons [3]. Out of this large gas processing market, only 5% is covered by membranes where almost all membranes are used for the removal of CO_2 [2].

Membrane technology is a relatively new and growing technology with large potential for several applications including natural gas dehydration. Membrane separation has several advantages compared to conventional separation processes, such as low capital costs, no moving parts, low environmental impacts and easy scale-up due to modular design. Furthermore, the process is simple, has a compact design, is reliable and can be operated unattended, which are vital requirements in subsea processing where the process takes place on a remote location without the possibility of continuous maintenance [2, 4]. Conventionally, natural gas dehydration has been one of the first steps of the topside production facility, located at a platform or on land with an absorption process using triethylene glycol (TEG). The rich TEG is regenerated in a stripper where the water is separated out of the process so the TEG can be reused [5]. The conventional glycol absorption process is a mature process and is widely accepted in the industry. However, it is not feasible to install this process subsea due several factors, such as large and bulky design, the need for continuously attention and maintenance due to operational problems including foaming, corrosion and contamination of TEG.

An alternative approach is to move dehydration of the gas stream subsea near the well resulting in less water to damage the pipes [3]. The movement of traditional fluid processing closer to the seabed can potentially reduce the cost of the downstream equipment where the pipes can be produced of low cost mild steel with a smaller volume flow, which enables a smaller topside

processing facility. In this view, a closed loop membrane contactor is proposed as a solution where the absorption step is replaced with a membrane process, which contacts the natural gas with TEG, whereas the desorption step is a pervaporation unit. Pervaporation is mass transfer from liquid to vapor phase using a permeable barrier [6]. The membrane process is a promising alternative for subsea regeneration as it has less heating requirements compared to conventional regeneration. The focus in this report will be on the development of membrane materials suitable for the regeneration of TEG with pervaporation dehydration.

The choice of membrane material for pervaporation operations is important as it directly affects the separation properties. The goal is to create a membrane with excellent thermal and chemical stability that shows large water flux through the membrane and high selectivity over a large period of time. Several membrane materials have been used for pervaporation where the most commercially used membrane material is polymeric. The membrane can either be dense or microporous, with homogenous or an asymmetric structure [7]. Promising innovative hybrid materials have been proposed for pervaporation separation, such as mixed matrix membranes(MMM) and nanocomposite membranes with nanoparticles incorporated in the polymer matrix [8].

1.2 Research objective

This thesis is a part of a project by SUBPRO (Subsea production and processing), a centre for Innovation-based research (SFI) to develop new methods of subsea separation. The aim of the project is to investigate membrane materials suitable for subsea dehydration of triethylene glycol with membrane pervaporation technology.

To date, there exists minimal literature on dehydration of TEG by pervaporation. Only comparable data are pervaporation studies of dehydration of ethylene glycol (EG) and a limited amount of diethylene glycol (DEG) studies. Experimental data is therefore needed to validate computational models for process analysis, which will provide information of the possibility of using pervaporation technology subsea. This project focuses on the preparation of membranes, characterization and experimental evaluation of the membrane performance with pervaporation of TEG-water mixtures.

The goal is to develop membrane materials suitable for long-term experimental pervaporation. First, compatibility tests have been performed to reveal the most suitable polymer materials. Hydrophobic Teflon AF2400 was selected due to its tough material properties, chemical and thermal long-term stability and minimal TEG uptake. The membrane permeance and selectivity of hydrophobic materials are quite different compared to those of hydrophilic cross-linked polymers that are commonly used in dehydration by pervaporation [9]. Obtaining a high water flux through the membrane can be challenging with hydrophobic polymers, however Teflon AF2400 holds the material property of high fractional free volume letting water molecules easier through the open rigid perfluor chains[10]. To increase the water flux, composite membranes are made with a thin layer AF2400. A part of the study was therefore to study the preparation techniques of composite membranes.

Preparation and characterization of the membranes have been completed with composite membranes with mechanical support of polypropylene and dense layer of Teflon AF2400 with and without nanoparticles. Furthermore, innovative multi-layered membranes with a crystalline nanoparticle layer have been investigated for future use in pervaporation. The membrane performance of the composite membranes have been studied with pervaporation of TEG-water mixtures with different operating temperatures and TEG concentrations in the feed solution over a long time period. As well, the present research requires the development of a suitable analytical method to detect TEG in the permeate to obtain reliable experimental data. Despite of the challenge of detecting TEG in aqueous solutions, a method for the detection of TEG concentration down to 100ppm was developed with gas chromatography mass spectrometry (GC/MS). This method assured experimental data from the permeate resulting in valuable information for membrane performance in the dehydration of TEG by pervaporation.

Chapter 2

Theory

This section will go through the basics of dehydration of natural gas, transport in pervaporation and the theory behind membrane technology. Furthermore, the choice of membrane materials will be argued, herein mixed matrix membranes and composite membranes.

2.1 Dehydration of natural gas

The most common way to remove water from the gas stream is by using liquid absorption (glycol), solid adsorption or refrigeration. The two first methods use mass transfer between water and a desiccant, while the last method use a combination of condensation of water vapor to liquid and chemical injection [1].

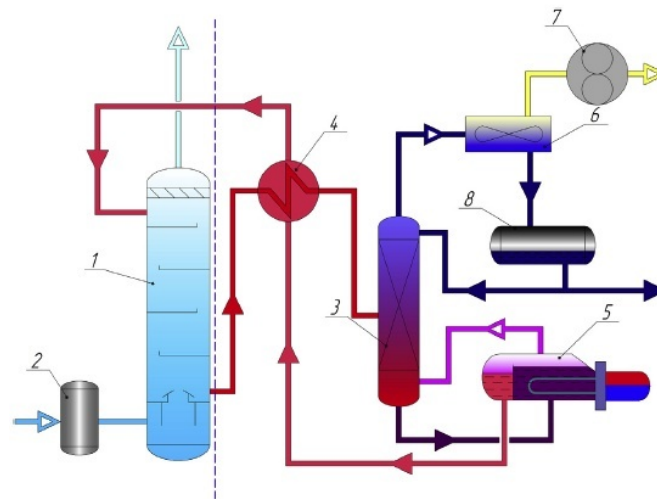


Figure 2.1.1: Conventional dehydration system by TEG absorption with regeneration of TEG in a desorption process; 1 absorber, 2 inlet scrubber, 3(left) stripper, 4 heat exchanger, 5 fired heater, 6 condenser, 7 vacuum pump, 8 reflux tank.(Reprinted from [1])

When removing water with glycol triethylene glycol (TEG) is preferred over ethylene glycol (EG) and diethylene glycol (DEG) as TEG holds several desirable properties such as high boiling point, high decomposition temperature and lower vaporization losses [1].

After using TEG for dehydration of natural gas, it must be dehydrated and regenerated. The conventional method for dehydration of TEG is by desorption of the rich TEG (TEG with high water content) in a stripper. The absorption-desorption process is a temperature swing process, as illustrated in Figure 2.1.1. First, any liquid water or liquid hydrocarbons is removed in a prescrubber before the wet natural gas is contacted with TEG in the absorber. The rich TEG is heated before it enters the stripper where any volatile compounds are flashed and condensed in a condenser at low pressure caused by a vacuum pump before entering a reflux tank. The liquid TEG is heated before it is regenerated to the absorption column as lean TEG (TEG with low water content). Since the process conditions at absorption require temperatures below 50°C , rich TEG must be heated by 100°C before entering the stripper [1, 11]. Lean TEG must be cooled before entering the absorber, which results in large amounts of energy required for the heat exchangers. The large energy requirements and the complicated process system of absorption-desorption makes it unsuitable for subsea operations. The conventional process requires a large footprint, continuous maintenance and has the need for constant attention, hence an alternative approach is needed [12].

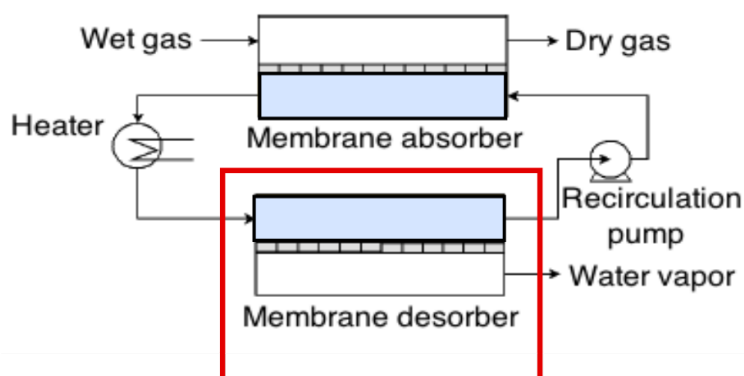


Figure 2.1.2: Schematic representation of the closed loop membrane process [12]. The wet gas is absorbed in a membrane contactor and the wet TEG is regenerated and dehydrated with pervaporation in the membrane desorber.

The use of membrane technology may be a viable alternative to the conventional glycol dehydration process and the use of membranes in subsea dehydration of natural gas could be a possible solution to the subsea dehydration challenge. The potential challenge with the membrane system is the loss of methane to the permeate due to insufficient driving force. To obtain sufficient driving force, the use of a vacuum pump or sweep gas is needed. The addition of a vacuum pump subsea could be a problem, while addition of sweep gas to the process would increase the complexity of the system. A solution proposed by SUBPRO (subsea production and processing) research center is a closed loop membrane process where the water in the natural gas is absorbed by a membrane contactor and the solvent is regenerated with pervaporation [12]. A schematic illustration of the closed membrane loop system is shown in Figure 2.1.2. First, any liquid water

or liquid hydrocarbons must be removed in a prescrubber before the wet natural gas is absorbed in a membrane contactor. Dry gas is exported and the wet TEG is regenerated and dehydrated by pervaporation in the membrane desorber. As Figure 2.1.2 illustrates, heating is required for pervaporation. However, the component involved in the phase change is the minor component of the liquid mixture, which reduces the energy requirement compared to conventional desorption. This factor, plus the possibility of using water selective membranes with high separation efficiency, pervaporation is considered as one of the most cost-effective liquid separation technologies [13, 12].

The main applications of PV have been the separation of azeotropic mixtures or the separation of components with close-boiling points or chemical instability. A typical PV separation is dehydration of organic solvents such as alcohols, acetic acid, tetrahydrofuran (THF), and acetone as all problems regarding azeotropic distillation are avoided with the PV process. Other applications of PV include separation of small amounts of volatile organic compounds (VOCs) from water, for environmental pollution control and food applications [13]. Processes involving phase change are often energy-intensive. Distillation is a perfect example where large amounts of liquid mixture is heated up to the boiling point of one or more components. PV, on the other only deals with the minor components of the mixture, which reduces the energy consumption. In PV the minor components permeates through the membrane, while the rest of the mixture is circulated or regenerated. In addition, the possibility of using membranes with high selectivity can increase the total separation efficiency. The once-through separation factor in PV can be in the range of 2000-10000 when separating water-isopropanol with a 10% water content in the feed, while in distillation, the maximum single plate separation factor is around 2 [14, 15].

To separate two liquids with pervaporation, a liquid mixture contacts a membrane surface; one component permeates through the membrane to a faster rate and is removed from the other side as vapor. The transport is driven by vapor pressure difference between the feed and the permeate side. To obtain high driving force on the permeate side, a vacuum pump can be used. Other alternatives to obtain low pressure are sweep gas or condensation of the permeate vapor. Cooling of the permeate vapor is often preferred industrially over a vacuum pump as it often is more economical [13]. Sweep gas is also an alternative, especially when separating water directly from natural gas where a study by Lin et al. showed that the use of sweep gas decreased both the required membrane area and the possible methane loss of the natural gas [16].

2.1.1 Transport in pervaporation

Solution-diffusion model

The transport through a membrane is highly dependent on the porosity of the membrane. Non-porous membranes are used in pervaporation, while porous membranes are used in microfiltration and ultrafiltration processes. In porous membranes, several molecular sieving models are considered to describe the transport, while in dense membranes the transport mechanism can be considered via a somewhat simple approach: the solution-diffusion model. The model consists of three steps; sorption of the molecule in the membrane, diffusion through the membrane and desorption from the membrane to the downstream part [17]. Figure 2.1.3 illustrates the solution-diffusion principle. The model describes the permeability of a fluid through a dense membrane in terms of solubility and diffusivity and is given by the formula:

$$\text{Permeability}(P) = \text{Diffusivity}(D) \times \text{Solubility}(S) \quad (2.1.1)$$

where the solubility is the amount of a compound that is adsorbed by the membrane, and the diffusivity determines the rate of permeation through the membrane.

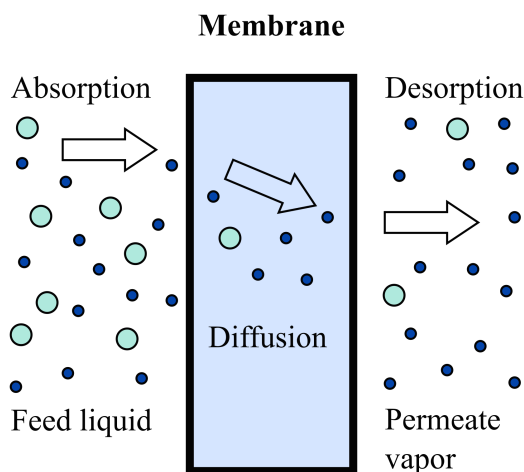


Figure 2.1.3: Schematic representation of the solution-diffusion model.

One compound in the liquid mixture has higher affinity towards the membrane and sorbs favorably at the membrane surface. Subsequently, the compound diffuses through the membrane due to a concentration gradient between the two surfaces of the membrane. Finally, the compound desorbs instantaneously on the membrane surface at the downstream side. Solubility is a thermodynamic parameter, whereas diffusion is a kinetic parameter. Solubility of a component on the membrane is a measure of the amount of penetrant sorbed by the membrane material for the given condition on the surface, whereas the diffusion of a component indicates how fast a penetrant is transported through the membrane [17, 18].

Another factor that is important to consider is the difference between the transport in gases versus liquids. Firstly, the affinity of liquids and polymers are much more significant than that between gases and polymers. The solubility of liquids can be so high that the liquid dissolves the polymer. Several counter measures have been applied, such as crosslinking of polymers or the combination of polymers with different properties. Furthermore, the solubility has a large influence on the diffusivity, in which the polymer chains become more flexible resulting in an increased permeability. In addition, the transport of gases in a mixture flow through a dense membrane flows quite independently, while in liquid mixtures, the transport is affected by flow coupling and thermodynamic interactions [17].

Diffusion of a component through the membrane depends on the size and geometry of the permeating compound and the membrane material. However, with interacting systems, the diffusion coefficient is highly dependent on the concentration of the components. Even large molecules can swell the membrane in such a degree that gives a large diffusion coefficient. For ideal systems, the solubility is independent of the concentration and can be described by Henry's law (Figure 2.1.4 a)), in which the concentration inside of the membrane is proportional to the applied pressure. The ideal case is generally observed with gases in elastomeric polymers, whereas the non-ideal case can occur in both rubbery or glassy polymers depending on the different interactions and solubilities. The sorption isotherm in non-ideal cases is normally curved rather than linear (Figure 2.1.4 b)). For example, permeabilities of large molecules in the rubbery and hydrophobic polymer polydimethylsiloxane (PDMS) can be 5 orders of magnitude higher than those of small molecules. This non-ideal sorption can be described by free volume models or Flory-Huggins thermodynamics [17].

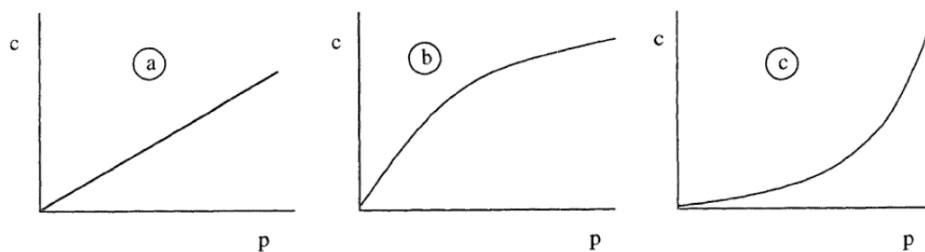


Figure 2.1.4: Ideal and non-ideal sorption isotherm (Reprinted from [17], p165)

Free volume theory

The free volume theory is a quantitative description on the concentration dependence of the diffusion coefficient. It is based on the description of amorphous polymers, whether a polymer is in the the glassy or rubbery state. In the glassy state, the polymer chains are rigid and the chain mobility is very limited. The thermal energy is too small to allow rotation around the polymer chains. Above the glass transition temperature (T_g), in the rubbery state, the polymer is significant more flexible and the polymer chain movements are not limited. Several physical properties are changed when reaching the glass transition temperature, such as density or specific volume. Figure 2.1.5 illustrates the specific volume of a amorphous polymer with

different temperatures and the relations to free volume V_f , observed volume V_T and volume at 0K V_0 . The free volume can be described as the volume created by thermal expansion of the originally closed-packed molecules at temperature 0K (Figure 2.1.2).

$$V_f = V_T - V_0 \quad (2.1.2)$$

And the fractional free volume (FFV) is defined as the ratio of the free volume to the observed volume, found in equation 2.1.3.

$$v_f = \frac{V_f}{V_T} \quad (2.1.3)$$

Where the specific volume at a particular temperature is described by the polymer density, whilst the volume occupied at 0K can be estimated from group contributions.

Some glassy polymers have an especially large fractional free volume and consequently exhibit high permeabilities to gases and vapors. A common feature of the glassy polymers with high FFV is that they have a rigid backbone with bulky side chains, resulting in a mechanical stable polymer with the possibility of permeating components through its free volume. Examples of glassy polymers with high FFVs are: PTMSP, a substituted polyacetylene and AF2400, a per-fluoro copolymer [19].

When considering transport through non-porous membranes, it is important to be aware of the different non-ideal transport cases, as they can significantly affect the separation properties of the membrane. The free volume approach is quite useful for describing the transport of small molecules through polymers. A molecule can only diffuse through the membrane if there is sufficient space or free volume. Consequently, if the molecule size increases, the amount of free volume must also increase.

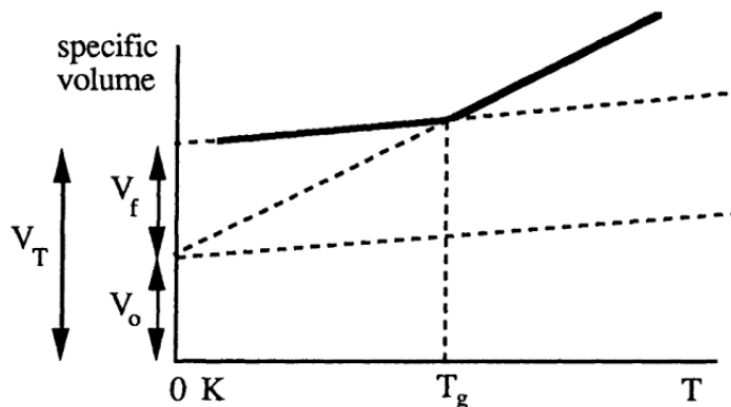


Figure 2.1.5: Specific volume (Reprinted from [17], p178)

Aspects of separation

The transport of a single component can be described by the simple flux equation:

$$J_i = -L_i \frac{d\mu_i}{dx} \quad (2.1.4)$$

in which L_i is the mobility coefficient and μ_i is the chemical potential of component i. With assumed isothermal conditions (constant temperature) and constant pressure within the membrane, the chemical potential is given by:

$$\mu_i = \mu^0 + RT \ln a_i \quad (2.1.5)$$

where the activity coefficient a_i is given by:

$$a_i = \frac{p_i}{p_i^0} \quad (2.1.6)$$

where p_i^0 is the saturation pressure of species i and p_i is the vapor pressure. Since $\frac{d\mu_i}{dx}$ is:

$$\frac{d\mu_i}{dx} = \frac{RT}{p_i} \frac{dp_i}{dx} \quad (2.1.7)$$

equation 2.1.4 becomes:

$$J_i = \frac{L_i RT}{p_i} \frac{dp_i}{dx} \quad (2.1.8)$$

Replacing the differentials with differences, the equation 2.1.8 becomes:

$$J_i = \frac{P_i}{l} \Delta p \quad (2.1.9)$$

where the permeability is $\frac{L_i RT}{p_i}$, the membrane thickness is l , the partial pressure difference is Δp . In the case of liquid feed, the Δp can be written as:

$$J_i = \frac{P_i}{l} (x_i \gamma_i p_i^0 - y_i p_p) \quad (2.1.10)$$

where the permeability P_i of component i is dependent on both composition and temperature. x_i and y_i are the mole fractions of component i, respectively in the liquid feed and vapor phase permeate, p_i^0 is the saturation pressure of pure component i at the given T, p_p is the total pressure on the downstream side and γ_i is the activity coefficient of species i. The activity coefficient in 2.1.10 can be found from semi-empirical equations given in literature. The saturation pressure p_i^0 at a given temperature is normally calculated by the Antoine equation:

$$\log p = A + \frac{B}{T + C} \quad (2.1.11)$$

where A, B and C are constants that can be found in the literature for a number of organic solvents.

The temperature dependence of the permeability P_i can be analyzed by the Arrhenius relationship:

$$P_i = P_0 \exp\left(\frac{-E_J}{RT}\right) \quad (2.1.12)$$

where P_0 is the preexponential factor, R is the universal gas constant, T is the temperature and E_J is the apparent activation energy of the flux, which indicates the temperature dependence of the flux [20]. Both flux, solubility and diffusivity follow a similar Arrhenius temperature dependence [17].

Another important separation parameter in membrane technology is the separation factor or selectivity and can be explained as:

$$\alpha_{A,B} = \frac{y_A/y_B}{x_A/x_B} \quad (2.1.13)$$

where y_A and y_B are the permeate compositions and x_A and x_B are the feed compositions. For a binary mixture, the selectivity of a pervaporation membrane is used to compare the separating capacity of the species. The selectivity in an ideal case is given by the ratio of the permeabilities, where the permeability is given by the multiplication of diffusivity and solubility from eq. 2.1.1:

$$\alpha_{A,B}^{ideal} = \frac{P_A}{P_B} = \frac{D_A S_A}{D_B S_B} \quad (2.1.14)$$

where the selectivity $\alpha_{A,B}^{ideal}$ is a dimensionless factor of species A relative to species B. A selectivity of 1 is no separation, while a selectivity of 5000 is an exceptional separation. Studies have shown a trade-off between the selectivity and the flux in pervaporation.

2.2 Membranes for pervaporation

2.2.1 Choice of membrane material

A limited amount of membranes have been developed for the purpose of removing water from TEG with PV technology. The choice of membrane material for PV operations is crucial for the separation process. The most important material criteria are chemical resistance and mechanical stability in order to ensure a long-term stability and lifetime of the membrane, which is crucial in subsea separation. Furthermore, an outstanding separation factor and permeability of the targeted compound is especially important for the membrane performance [21]. Several membrane materials have been used for pervaporation. Examples are polymeric, inorganic and hybrid materials, such as mixed matrix membranes (MMM) [8]. Table 2.2.1 show a comparison of the performance in literature data using dehydration of glycols with different membrane materials. The research has mainly been focused on the dehydration of MEG. However, the data obtained from MEG dehydration can offer a reasonable prediction for dehydration of TEG. As the kinetic size of TEG is larger than MEG, the separation factor for dehydration of TEG can be larger [12].

Polymeric membranes can be produced in different shapes, sizes and morphologies at a relatively low cost. Therefore, the most commercially used membranes in PV are polymeric membranes. [22]. However, the main drawback of polymeric membranes is the trade-off between permeability and selectivity: when the permeability increases, the selective decreases and vice versa. Several research efforts have been made over the past ten years on the design and fabrication of new polymeric materials that can overcome the performance of other membranes and eliminate this trade-off [8].

Table 2.2.1: Comparison of literature data for pervaporation of EG, DEG and TEG.

Mass ratio	Membrane	T[°C]	Flux [g/m ² h]	α	Ref.
EG/80	PBI/PEI dual-layer hollow fiber membrane	60	1763	115	[20] (2011)
EG/80	NaA zeolite membrane.	120	5003	>5000	[23] (2012)
EG/80	PVA-GPTMS/TEOS	70	60	714	[24] (2006)
EG/90	Chitosan coated zeolite filled cellulose	30	311	50	[25] (2010)
DEG/99	Hybrid Silica(HybSi)	90	70	9800	[26] (2014)
TEG/91	Silica	80	184	2054	[27] (2001)
EG/90	MMM with polydopamine-coated MOF	70	540	2864	[28] (2017)

Inorganic membranes have on the other hand shown exceptionally good chemical and thermal stability compared to polymer membranes, together with excellent separation performances. However, they are more expensive to synthesize making the production process more complicated [22]. Promising inorganic structures with narrow pore size where examples of materials are ceramic and zeolite membranes [8]. Ceramic membranes offer advantages over polymer membranes, such as higher mechanical strength and temperature stability. Van Veen et al. [27] studied the performance of ceramic silica membranes in dehydration of TEG by pervaporation technology, in which the water flux was 184 g/m²h and the selectivity was 2054. The first large-scale PV plant was based on an inorganic membrane and was successfully implemented in 2001 for dehydration of organic liquids. The inorganic membrane used in that plant was a hydrophilic NaA zeolite

membrane layer on porous ceramic support [29]. The uniform pore size distribution of the zeolites makes them ideal for separation where they can act as selective catalysts and adsorbents and separate molecules due to their molecular size [30]. Zeolites are inorganic particles with high surface area, high void volume (30 % of total zeolite volume) and uniform micropores. These zeolite particles have been widely researched, and has shown promising results for membrane separation [31, 32].

To improve the separation properties of the PV membranes and enhance their permeabilities, alternative approaches have been suggested. Examples are chemical modification of polymers, polymer blends or using inorganic particles as fillers in organic polymer matrix (MMM) [33]. Either the membrane is polymeric, inorganic or consists of both, the choice of membrane material is crucial in the membrane separation performance. An important property of the polymer membrane is the hydrophilicity of the membrane material. The membrane permeance and selectivity of hydrophobic materials are quite different compared to those of hydrophilic cross-linked polymers that are commonly used in dehydration by pervaporation [9]. Hydrophilic membranes are significantly affected by water swelling in aqueous solutions due to water-polymer interactions, which can affect the performance and long-term stability of the membrane [20]. This is a contrast to the hydrophobic polymer, which absorbs minimal amount of water or other polar compounds in the mixture. However, obtaining a high water flux through the membrane can be challenging with hydrophobic polymers, hence a high fractional free volume (FFV) is essential. If the purpose was to separate water from TEG, the FFV of the membrane should be high enough to let the water molecules through and retain the TEG molecules. It is the different molecular size that makes it possible to use hydrophobic membranes in dehydration of TEG [9].

2.2.2 Mixed matrix membranes

The mixed matrix membranes (MMM) have received much attention in the past years due to their separation properties and economical benefits over inorganic membranes. Figure 2.2.1 illustrates a schematic representation of a MMM. MMMs consist of inorganic particles incorporated in an organic polymer matrix. Particularly, porous fillers, such as zeolites, metal organic frameworks (MOFs) [33] and carbon nanotubes (CNTs) have been used. MOFs are compounds of metal ions or clusters connected to organic molecules (ligands) forming different structures often with surface areas up to $7000 \text{ m}^2/\text{g}$ [34]. The use of MOFs in MMM can offer a better interaction between the polymer phase and the fillers. The porous structure can enhance permeation through the membrane due to lower diffusion resistance in the porous structure. With suitable pore size, these inorganic fillers can promote molecular sieving effect [35, 36]. However, to achieve enhanced separation performance, the membrane has to be defect-free and the interface between the polymer chains and the inorganic fillers can not have any discontinuity [33].

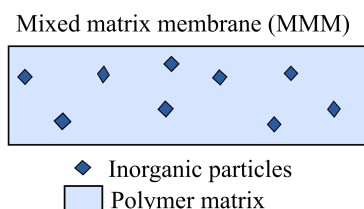


Figure 2.2.1: Schematic representation of a mixed matrix membrane.

The morphology of the mixed matrix membranes affects the transport through the membrane. Firstly, voids are often present in the membrane structure caused by a detachment of the polymeric chains from the particle surface. The effect can easily be diagnosed and will have a "sieve-in-cage" morphology as shown in Figure 2.2.2 as Case C. The interfacial voids can be a result of either repulsive forces between the polymer and the particles, different thermal expansion properties or high rigidity of polymeric chains when using a glassy polymer. Another effect that can attribute to the formation of defects into the polymer matrix is rigidification of the polymer near the particles or partial pore blockage of the particle (Case B) [17]. The third case of non-ideality of the MMM is reduced permeability region within sieve, which can for example be caused by internal pore blockage. Figure 2.2.2 summarizes the relationship between the possible morphologies and the correlating transport properties [37].

A possible solution to obtain the ideal case (case A) in mixed matrix membranes is by ultrasonication. It is one of the easiest and most frequently used approaches for the synthesis of hybrid organic-inorganic membranes when blending two phases. In ultrasonication, ultrasonic (US) waves are applied on polymeric solutions immersed in an aqueous bath [38]. The dispersion of particles in the polymer is associated with the shear forces applied by the liquid on the particle clusters in the solvent solution. External forces, such as stirring or cavitation in the form of ultrasonication are directly responsible for the dispersion. If the affinity between the fillers and the solvent is poor, a low concentration of polymer solution can be used for better dispersion of the inorganic phase with ultrasonication [39].

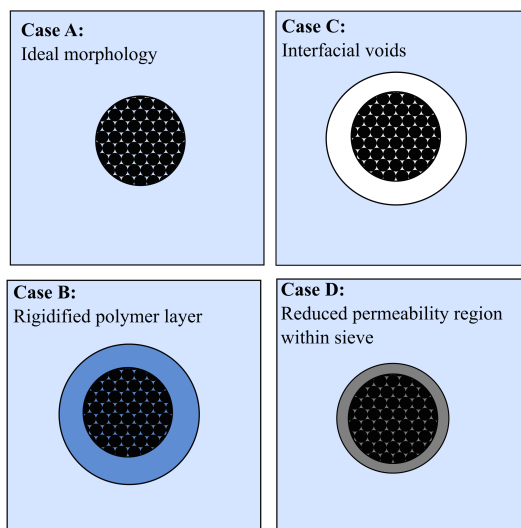


Figure 2.2.2: Schematic representation of the different morphologies nanoparticles in MMM can have. Case A: Ideal morphology, Case B: Rigidified polymer layer, Case C: Interfacial voids and Case D: Reduced permeability region within sieve.

Moore et al. [37] studied non-ideal effects in organic-inorganic materials and offered recommendations and limitations to avoid the non-ideal behaviors. Avoiding voids present in the membrane structure is difficult with polymers that are rigid. The easiest solution is to choose polymers with low T_g or adding plasticizers to lower the T_g . Unfortunately, the transport properties of these materials are not always desirable. To maintain flexibility of the polymer chains during membrane preparation, one could cast at an elevated temperature to maximize stress relaxation. Another solution was to add a compatibilizer to the zeolite surface to improve the adhesion between the organic-inorganic materials.

To eliminate the interfacial voids between the polymer and the zeolite particles, Dogan et al. [25] coated zeolite filled cellulose membranes with chitosan. The coating of the hydrophilic polymer resulted in an uniform coating layer, which suggested that the coating had good adhesion to the zeolite membrane and was successful. Furthermore, the clustering of the inorganic particles in the polymer matrix can affect the separation properties with decreased mass transport through the membrane. To prevent the aggregation of inorganic particles, Guo et al. [24] added successfully a coupling agent to a hybrid organic-inorganic membrane consisting of inorganic particles of tetraethoxysilane (TEOS) and polymer poly(vinyl alcohol)(PVA). The addition of the coupling agent γ -glycidyoxypropyltrimethoxysilane (GPTMS) created a more homogenous distribution of the silica particles in the PVA matrix, which enhanced the separation properties of the PV process.

To improve the compatibility between metal-organic frameworks and the polymer matrix, Zhang et al. [28] used a MMM of PVA and coated the sulfonic acid MOF with a thin and uniform polydopamine (PD) layer for dehydration of ethylene glycol. The coating of the MOF enhanced the formation of hydrogen bonding between the amine group in the PD and the hydroxyl in the PVA matrix, which resulted in better compatibility and improved the separation performance

of the MMM. The water permeability and selectivity increased by respectively 483% and 567% compared to those of pure PVA.

Gao et al. [40] showed that the pore size of the zeolite affects the separation factor of the pervaporation. They studied how different zeolites affected the separation in pervaporation of water and ethanol with hydrophilic PVA composite membranes filled with KA, NaA, CaA, and NaX zeolites. The zeolites with smaller pore size (Ka, NaA) increased the separation factor, while a zeolite as NaX with bigger pore size did not affect the separation factor significantly. Zeolites facilitates the permeation of smaller molecules and hinders the larger molecules, which improves the flux and separation factor of the membrane. The larger the pore size of the Zeolite, the higher is the flux expected. The separation of different alcohol-water mixtures have been tested and the separation factor of water versus bigger alcohol molecules increased, while the separation factor of water with smaller alcohol molecules was not significantly affected due to the molecular sieving effect of zeolites.

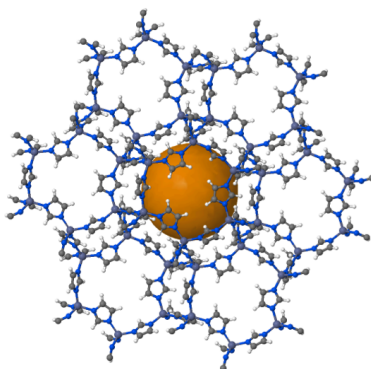


Figure 2.2.3: The molecular structure of ZIF-8, in which the yellow sphere represents the pore size of the ZIF-8 structure and the surrounding blue and gray molecules are the zinc ions coordinated by four imidazolate units [41].

Wu et al. [42] studied the trade-off effect between flux and selectivity in pervaporation of ethanol and water, using MMMs with different inorganic fillers incorporated in PVA polymer matrix. The report shows that there still exists a trade-off effect with the inorganic fillers (KA, NaA, CaA, NaX and clinoptilolite) and the explanation was poor interaction between the inorganic fillers and the polymer matrix. In contrast, by increasing the hydrophobicity of the surface of $MIL - 53 - NH_2$, the MMMs showed an outstanding performance in water permeance and selectivity, breaking the trade-off effect and indicating its potential for further pervaporation study.

The focus in this study has been on developing MMM incorporated with Zeolitic imidazolate frameworks (ZIFs). The ZIFs are a subgroup of MOFs with high thermal and chemical stability. They consist of tetrahedral metal ions bridged with imidazolate creating a three-dimensional structure. The structure of ZIF-8 consists of zinc ions coordinated by four imidazolate rings and the molecule structure is shown in Figure 2.2.3 [41]. By using different imidazolate units, porous structure and topology of the ZIFs can be designed and controlled [43]. The ZIFs have been used as fillers in MMM in areas such as gas separation, pervaporation and nanofiltration.

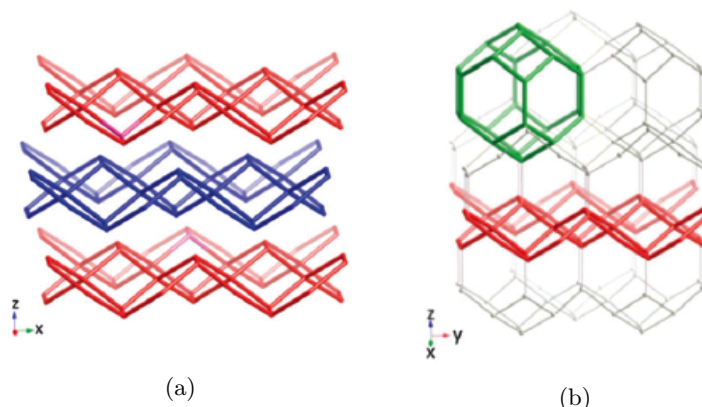


Figure 2.2.4: The network of zinc atoms in ZIF-L and ZIF-8. a) The two-dimensional layer structure of ZIF-L. b) The framework of ZIF-8 (grey color) with a ZIF-8 cage (green color) and the corresponding ZIF-L layer (red color) [43].

ZIF-L consists of the same building blocks as ZIF-8 (Hmim and zinc nitrate), but have different topology, shown in Figure 2.2.4. ZIF-L is a leaf shaped, two dimensional ZIF with a cushion-shaped cavity between the layers. The cushion-shaped cavity is unique, and has proven to accommodate CO_2 molecules well in gas separation [43]. As seen from Figure 2.2.4b, the two ZIFs are very different, which suggests unique pore systems for the use in membrane separation [44]. The narrow pore size of ZIF-8 (3.4 Å) [35] is smaller than the kinetic diameter of glycols (4.5 Å) and bigger than the kinetic diameter of water (2.6 Å) [45], hence ZIF-8 should be capable of separating water from glycols.

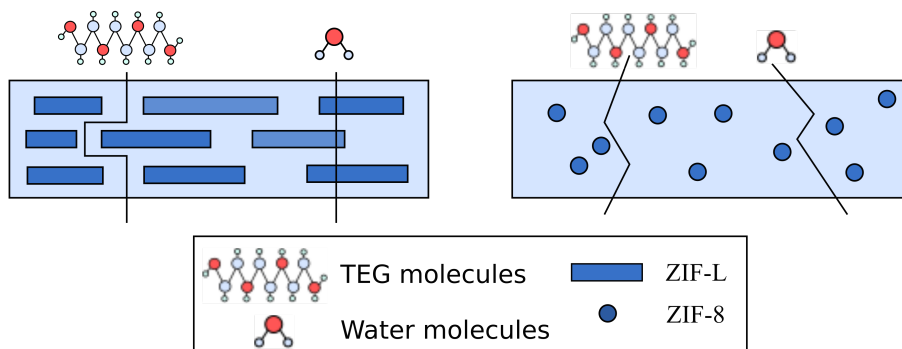


Figure 2.2.5: Illustration of the possible transport paths of TEG and water in MMM consisting of ZIF-L and ZIF-8.

Liu et al. [36] incorporated both ZIF-L and ZIF-8 particles into sodium alginate (SA) matrix for dehydration of ethanol using pervaporation technology. Adding ZIFs to the pure polymer membrane enhanced the separation performance with both higher permeation flux and separation factor. With a ZIF-L filler content of 4 wt%, the permeation flux was $1218 \text{ g/m}^2\text{h}$ and the separation factor was 1840, whereas with ZIF-8 fillers, the permeation flux and separation factor were respectively $879 \text{ g/m}^2\text{h}$ and 678. The exceptional separation performance of the ZIF-L filled membranes was due to the ordered alignment of the ZIF-L particles shown in Figure 2.2.5. The alignment of ZIF-L particles created water channels and rendered the desirable molecular sieving effect for water molecules, whereas large molecules as TEG could not be transported along the same path.

Sorribas et al. [46] improved the water/ethanol separation in pervaporation by incorporating hydrophilic MOF into the commercial polymer polyimide (PI) Matrimid™5218. An incorporation of 40% of the MOF HKUST-1 in the polymer matrix, the water flux increased from $240 \text{ g/m}^2\text{h}$ for the pure PI to $430 \text{ g/m}^2\text{h}$ with the MMM, without significant changes in the separation factor (>200). The incorporation of ZIF-7 into MMM with chitosan in ethanol/water pervaporation resulted in an overall enhanced separation performance. The doped chitosan showed smaller pore size due to cross-linking between the zinc atoms of ZIF-7 and the amino groups of the polymer. This cross-linking resulted in rigidified polymer chain of the MMMs, which gave a lower flux and a higher separation factor. However, in total, the overall separation performance was enhanced [47].

2.2.3 Composite membranes

A composite membrane is a structure consisting of a thin dense top layer and a porous support. An illustration of different composite membranes can be seen in Figure 2.2.6. The dense skin layer provides effective separation, while the porous support gives the membrane the mechanical strength [7]. The main advantage with composite membranes is the possibility of using an (ultra)thin (typically with a thickness $< 1 \mu\text{m}$) dense top layer able to ensure a high transmembrane flux and in the case of liquid feed, the avoidance of the wetting phenomena. The top layer should be selective towards one of the components and should be defect-free, since few defects will drastically affect the selectivity of the membrane. The support should have an open network to minimize the resistance and it should not contain macro voids, which will make the support weak for high-pressure applications.

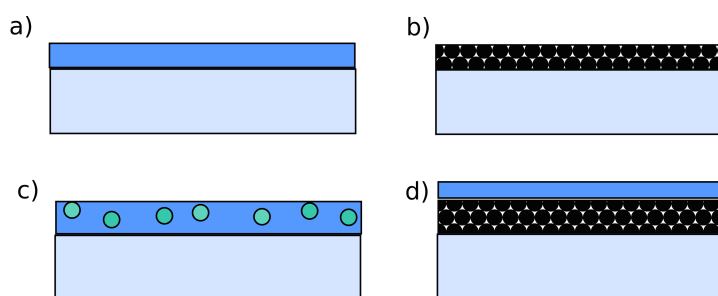


Figure 2.2.6: Illustration of different composite membranes. a) Porous support and a thin dense skin layer. b) Porous support and a dense crystalline MOF layer. c) Porous support and a dense skin layer with embedded nanoparticles. d) Porous support and a dense crystalline MOF layer with a protective polymer layer.

Wu et al. [48] studied thin film composite membranes of polyamide and polydopamine for dehydration of ethylene glycol. The incorporation of polydopamine sublayers into the membrane increased both the permeability and the selectivity of the membrane. The presence of NaCl salt in the feed solution affected the membrane performance. It resulted in a decreased permeation flux and a higher separation factor. The separation factor decreased with higher EG content, while the separation factor increased with NaCl present in the water solution [48].

Huang et al. constructed a composite membrane with an extremely thin perfluoro coating layer on a smooth defect-free cellulose ester membrane for pervaporation of ethanol/water mixtures. The results showed that the water permeance of the composite membrane was lower than the uncoated hydrophilic membrane, however much higher than the pure perfluoro membrane. Furthermore, the composite membrane maintained high selectivity at all feed water concentrations and at high feed water content, the selectivity of the composite membrane was higher than both of the components of the membrane alone. The protective perfluoro layer separated the hydrophilic layer from direct contact with the feed, thereby controlling swelling and plasticization of the hydrophilic layer and maintaining the selective properties of the layer [9]. Results from aging experiments by Nguyen et al. showed that Teflon AF2400 was the most effective hydrophobic thin skin layer material as the reduction in mass transfer coefficient was the lowest of the materials tested [49].

The focus in this work has been on incorporating MOFs in the thin skin layer of the composite membranes, as well as exploring new techniques of utilizing MOFs in composite membranes. Li et al. [50] prepared a mixed matrix composite membrane containing ZIF-7 nano-fillers for gas separation. The composite membrane was made of commercially available poly (amide-b-ethylene oxide) (Pebax[®]1657) mixed with ZIF-7 deposited successfully as a thin layer ($<1\mu\text{m}$) on the porous support of polyacrylonitrile (PAN). To avoid penetration of ZIF-7 particles into the porous support, a flat gutter layer of PTMSP was applied on the porous support. SEM pictures confirmed excellent adhesion and morphology between the polymer phase and the ZIF-7 filler with no observed voids or clusters. The permeability and the gas selectivity were enhanced with low ZIF-7 loading. With a filler loading of 34wt%, the gas selectivity was further enhanced, however; the permeability was reduced compared to pure Pebax[®]1657 membrane. The reason was assumed to be polymer chain rigidification at high filler loading.

An important role in the performance of composite membranes is the nature of the interface between the polymeric support and the MOF. It is vital with good adhesion between the MOF and the support, hence minimal non-selective voids or defects between the layers. It is rather hard to study the interfacial interactions between the layers. However; the ability to prepare new composite materials provides an opportunity to develop innovative surface science techniques to study the interface itself [51]. Hu et al. improved the composite membrane properties by incorporating carbon nanotubes in the thin skin layer of polyvinylamine (PVAm) and polyvinylalcohol (PVA). The incorporation enhanced the separation properties with higher permeation flux and separation factor in the dehydration of triethylene glycol with pervaporation. However, the membranes were only selective to water in low water concentrations (0-20%) and water concentrations above 20% resulted in lower separation factor [52].

The filler size can affect the polymer-filler interactions. With a smaller filler size, the surface area is larger and can provide greater polymer-filler interactions and enhance the polymer-filler compatibility. In addition, small fillers have the advantage in meeting the future requirements of decreasing the membrane thickness to ensure high permeation [53]. Several thin film composite membranes have been prepared with an ultra thin dense layer of a thickness of 100nm [54, 55]. However, industrial membranes consisting of a thin selective layer less than 100nm require a gutter layer between the porous support and the selective layer to achieve high permeance and selectivity in gas separation [56].

Another possibility of preparing composite membranes with MOFs, is to have a crystalline MOF layer directly on the polymer support, with or without an extra protective polymer layer. It is an innovative approach that has limited amount of tests with pervaporation. The idea is that alignment of the ZIF-L particles will create water channels and render the molecular sieving effect for water molecules without having the transport resistance in the dense polymer. If the particles are sensitive to the liquid environment, a ultra-thin protective layer can be coated on top of the crystalline layer, or a MMM consisting of similar nanoparticles to enhance the compatibility between the layers. Several reports describing the preparation of ZIF-8 layers on inorganic supports have been presented [29, 57, 58]. However, high cost and difficult processing techniques associated with the inorganic supports have motivated research with ZIF layers placed on polymeric support. This could offer the alternative of a low-cost and easy processable membrane and benefits for the future chemical industry [59]. ZIFs layers have successfully been grown on several polymer mate-

rials, including polyethylenimine (PEI) [60], polysulfone (PSf) [61] and polyvinylidene difluoride (PVDF) [62]. The experimental synthesis and the material properties of these membranes is vital to obtain a homogenous, dense, thin and selective ZIF layer on top of the porous support [59].

Techniques utilized have been in situ growth or secondary seeded growth. In situ growth is a one-step procedure where the support is immersed in a growth solution, in which the particles are synthesized on the polymer. In situ growth is not straightforward as the growth of ZIF crystals on porous supports are not generally favored [63]. Chacho-Bailo et al. prepared successfully continuous ZIF-8 membranes on porous polysulfone for hydrogen separation [61]. Secondary seeded growth is divided into two parts, in which the seeding crystals are first attached to the support and subsequently the seeded support is immersed in the growth solution. Li et al. [64] compared the two methods at a preliminary stage, in which the defects were determined using nitrogen gas permeation test. In situ growth method for 4h exhibited highest crystallinity and the lowest amount of defects. The method is preferable as it is an easy and fast route of synthesizing high quality ZIF-8 membranes.

Studies have shown that the modification of the polymer support prior to ZIF-8 growth can improve the final membrane performance [59]. The modification can be physical or chemical and the purpose is to create a better adhesion of the ZIF-8 layer and the polymer support. Barankova et al. [60] added ZnO in the polymer support of PEI and it was assumed to have improved the adhesion of the ZIF-8 layer to the polymer support due to a positive effect on the growth of ZIF-8 crystals where the zinc ions can serve as a secondary metal source for ZIF-8 crystal formation. The membrane was successfully synthesized as a four-layered structure consisting of polyester, a mixed matrix membrane of PEI/ZnO, a layer of ZIF-8, and a protective layer of polydimethylsiloxane (PDMS) for gas separation. Another suggestion for better adhesion between the polymer support and the ZIF layer is plasma treatment of the polymer surface. Plasma treatment can alter the physico-chemical properties of the polymer surface, such as changing the hydrophilic character of the surface or change the pore structure [65, 66], which in theory can lead to better adhesion between layers of ZIFs and polymer support. To the author's knowledge, plasma treatment has not been investigated as a treatment for better adhesion between polymers and ZIF layers.

The robust stability of ZIFs has motivated intensive research efforts through the years. An article from Zhang et al. [67] contradicts this with ZIF-8, in which the study confirms that the ZIF-8 crystals can degrade in water due to the dissolution of ZIF-8. A sharp enhancement of water pervaporation flux and the disappearance of ZIF-8 structure on the α -alumina supported ZIF-8 membrane indicated that the ZIF-8 particles went degradation during water pervaporation. On the other hand, Park et al. [68] reported no change in crystallinity or porosity of ZIF-8 crystals after immersion in boiling water, refluxing organic solvents, or in alkaline solutions. The contradictory reports suggest that more studies are needed on the subject of ZIFs water stability. However, the studies mentioned have reported the water effects on ZIF crystals and not ZIFs immersed in membranes, hence the water stability could be different. There are no reports on water stability on ZIF membranes. Zhang et al. [69] converted the surface of MOFs from hydrophilic to hydrophobic to solve the problem of MOFs moisture sensitivity. The MOFs; MOF-5, HKUST-1 and ZnBT were successfully coated with hydrophobic PDMS without affecting their original crystalline nature and pore characteristics.

Chapter 3

Experimental

This section will go through the experimental procedures of the laboratory work completed in this thesis. This includes membrane characterization techniques, such as compatibility experiments, contact angle measurements and morphological characterization. The membrane preparation techniques will be explained for composite membranes and multi-layered membranes. Furthermore, analytical method development and validation with GC/MS will be justified. At last, the experimental aspects of the pervaporation study will be explained.

3.1 Materials

The membrane support was microporous polypropylene Celgard 2400 (25 μm thick, average pore diameter 0.0043 μm and 41% porosity), polysulfone (MWCO 20k) was purchased from Alfa Laval, Denmark, polymer Teflon AF2400 ($T_g=240^\circ\text{C}$) was supplied from DuPont, the solvent electronic liquid FC-72 was ordered from 3M.

Membranes used for compatibility tests: PTMSP was ordered from Gelest, EU. PIM-1 was made in the lab by step polymerization between 5,5,6,6-tetrahydroxy-3, 3,3,3-tetramethyl-1,10-spirobisindane and an aromatic chlorinated monomer, PDMS was made out of a two component kit, Sylgard 184, all products have been purchased from Sigma Aldrich.

ZIF-8 and ZIF-L, zeolite imidazolate frameworks containing respectively Zn^{2+} (Basolite Z1200) and $\text{Zn}(\text{NO}_3)_2 \cdot 6\text{H}_2\text{O}$ (98%), 2-methylimidazole (Hmim) (99%) were supplied from Sigma-Aldrich. The PVDF membrane used for ZIF-L filtration is from Millipore with an average pore size of 0.68 μm .

Triethylene glycol (99%, boiling point 166°C) and the internal standard triethylene glycol monoethyl ether were purchased from Sigma-Aldrich, and aqueous triethylene glycol solutions of different solution for use as feed in pervaporation experiments were prepared by mixing triethylene glycol with de-ionized water at specific concentrations. Methanol, ethanol, hexane and acetone were all purchased from Sigma-Aldrich.

3.2 Characterization techniques

3.2.1 Compatibility experiments

In pervaporation, the upstream side of the membrane is in direct contact with the liquid feed solution. Of that reason, it is important to know the effect TEG and water have to the membrane material. Swelling measurements were performed by submerging different self standing membranes in TEG. The weight of the membrane pieces were reported before submerging and at chosen time intervals after submerging. Time intervals of weights reported were 1h, 2h, 4h, 6h, 24h, 2 days, and 7 days after submerging. To ensure no residues of TEG was left on the membrane surface, the membranes were swiped with paper prior to weighing. The measurements reported in this work were the average of two pieces of each membrane sample. The solvent uptake (SU) was calculated by Equation 3.2.1

$$SU(\%) = \frac{W_s - W_d}{W_d} \times 100 \quad (3.2.1)$$

Where W_s is the weight of the TEG-swollen membrane and W_d is the dry weight of the self standing membrane.

3.2.2 Contact angle measurement

The contact angles of TEG and water on the samples were measured using a drop shape analysis system based on the Sessile droplet method with an Optical tensiometer. A picture of the contact angle apparatus is illustrated in Figure 3.2.1. The volume of the droplet placed on the polymer surfaces were between $4\mu\text{L}$ and $7\mu\text{L}$. The apparatus was calibrated with a calibration ball prior to every sample collection. The contact angles reported in this work were the average of the at least 3 different points on the sample surface and more than 100 angle measurements by the software.

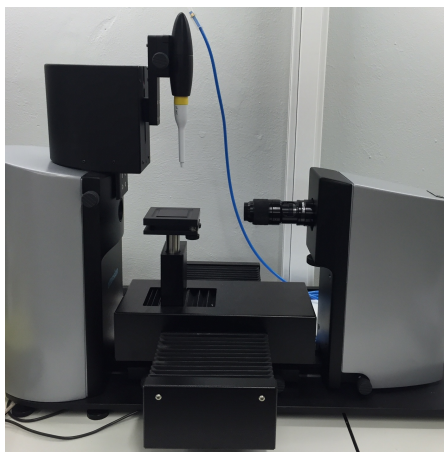


Figure 3.2.1: Contact angle apparatus.

Contact angle measurements give information about the wettability of the material, or the hydrophilicity of the material. If a membrane is hydrophilic, the contact angle between the droplet and the membrane surface will have an angle of less than 90 degrees. With less affinity to the material, the contact angle will be greater than 90 degrees [17]. The possible configurations of a droplet deposited on a solid surface in case of different affinities are shown schematically in Figure 3.2.2.

If a membrane is porous, the liquid droplet will penetrate into the pores of the membrane if wetting occurs ($\theta < 90^\circ$). The interaction between the liquid droplet and the porous membrane can be described by the Young Laplace equation:

$$\Delta p = -\frac{2\gamma_l}{r} \cos\theta \quad (3.2.2)$$

If the pressure difference $\Delta p > 0$, the droplet will go through the pores of the membrane and liquid wetting will occur. The wettability of the membrane material depends on pore size r , surface tension of the liquid γ_l and the surface energy of the membrane material θ . Wetting of the pores in the porous membrane can cause pore condensation in pervaporation, which reduces transport over the membrane. Less wetting can be obtained by choosing materials with smaller pores or using liquid with higher surface tension γ_l . Examples of commercially available hydrophobic porous materials that can be used as membrane layer are PP and PTFE [17].

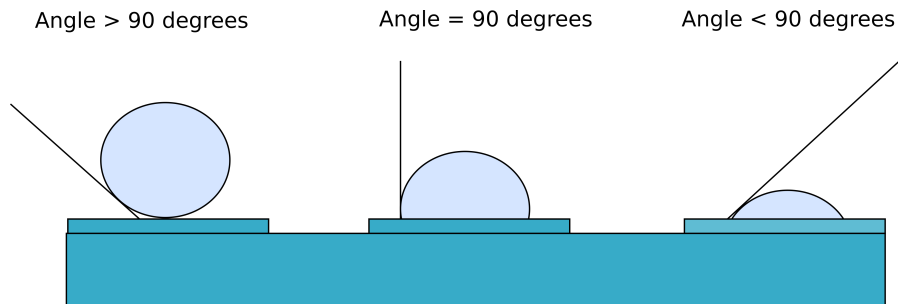


Figure 3.2.2: Contact angles of liquid droplets on a solid material.

3.3 Membrane preparation

3.3.1 Composite membranes

Several composite membranes with and without nanoparticles were prepared. First, one pure polymer composite membrane was made with porous support of polypropylene and thin skin layer of Teflon AF2400. The composite membranes containing nanoparticles were prepared by two techniques; dip coating porous support in nanoparticle solution (Technique A) or attaching a nanoparticle sublayer on the porous the support by filtration of nanoparticle solution (Technique B). The nanoparticles used were ZIF-L and ZIF-8 and the porous support tested was polypropylene. However, due to detachment of nanoparticle layer and porous support, polysulfone (PSf) was also tested with Technique B. An overview of the different membranes made is given in Table 3.3.1. Membranes with number 1-4 were made with technique A and membrane number 5-9 were made with Technique B.

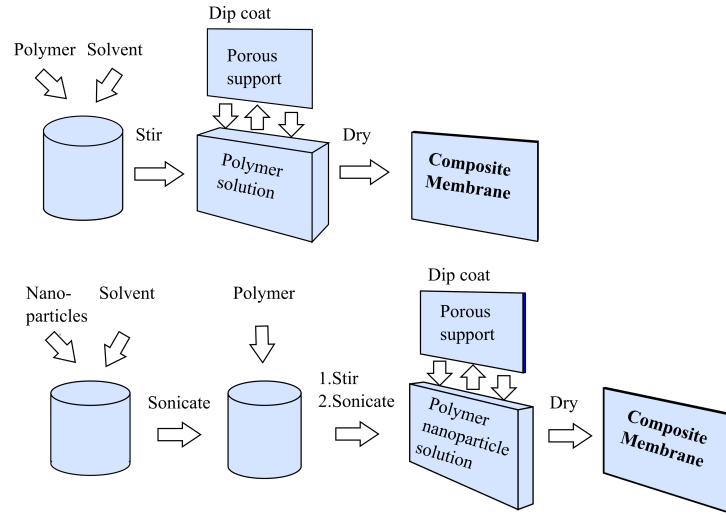


Figure 3.3.1: Technique A: dip coating procedure for composite membranes. Dip coating with pure polymer (top), Dip coating with nanoparticles in polymer solution (bottom).

Table 3.3.1: Overview of the composite membranes that were experimentally made.

Nr.	Technique	Porous support	Sublayer	Thin skin layer
1	A	PP	-	AF2400
2	A	PP	-	ZIF-L and AF2400 MMM
3	A	PP	-	ZIF-8 and AF2400 MMM
4	A	PP	ZIF-8 and AF2400 MMM	AF2400
5	B	PP	ZIF-8 particle layer	-
6	B	PP	ZIF-L particle layer	-
7	B	PP	ZIF-L particle layer	AF2400
8	B	PSf	ZIF-L particle layer	-
9	B	PSf	ZIF-L particle layer	AF2400

ZIF-L nanoparticles were synthesized following a procedure previously reported [36, 43, 44]. At room temperature, 0.59 g of $Zn(NO_3)_2 \cdot 6H_2O$ and 1.30 g of Hmim were dissolved separately in 40 mL deionized water before the two parts were mixed together and stirred for 4 h. The molar ratio between Hmim and zinc used was 1:8. The suspension was subsequently filtered through a hydrophilic microporous PVDF membrane. The produced filter cake was dispersed and rinsed with deionized water. The rinse and filtration processes were repeated three times and repeated another three times with acetone instead of water. The resulting filter cake was vacuum dried at 30°C, producing a white powder of ZIF-L particles.

The composite membranes obtained by Technique A were dip coated on one side of the porous polypropylene support with Teflon AF2400 polymer solution. The dip coating procedure with and without nanoparticles is illustrated in Figure 3.3.1. The composite membranes with a skin layer containing nanoparticles had to undergo sonication in a sonication bath in order to agitate the nanoparticles. A solution of ZIF-L particles and solvent was sonicated for 4-5 hours with a temperature less than 40°C by frequently changing the water and adding ice to the bath. Polymer was added to the solution and stirred overnight. Solvent was frequently added to replace the solvent evaporated during the sonication process. The sonicating procedure was repeated with the polymer in the ZIF-L solution. Within 10 minutes after the sonication procedure was finished, the solution was coated on the porous support of polypropylene. The porous polypropylene was dip coated with the same technique as explained over. The porous support was fixed on a glass plate using aluminum tape to avoid the solution to go to the back side of the porous support. The coating was performed by submerging the porous support 10 seconds in the polymer solution, dry it in 10-20 degrees angle at room temperature, turn the plate 180 degrees and dip coat for another 10 seconds. The membrane was left to dry 4 hours, before put in a vacuum oven to dry overnight in 60°C. After drying, a thin polymer coating was obtained at one side of the flat sheet membrane.

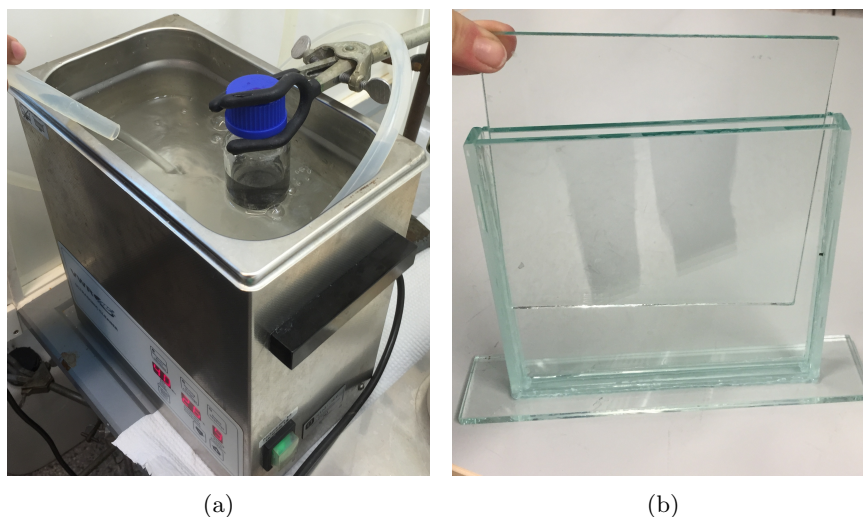
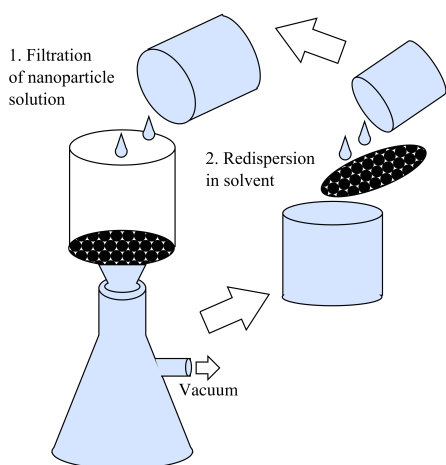


Figure 3.3.2: Membrane preparation apparatus. a) Sonication bath. b) Dip coating glass equipment.

3.3.2 Multi-layered membrane development

The composite membranes obtained by Technique B were made by by filtrating a nanoparticle solution through the porous support resulting in a particle sublayer on top of the porous support. The nanoparticle solution consisted of 1wt% ZIF-L in ethanol solution. The filtration was performed with a sintered plate used to sustain the thin polymeric samples and the setup had a transmembrane pressure of 2 bar obtained by a vacuum pump. The procedure of Technique B is illustrated in Figure 3.3.3a. After the procedure, the membranes were dried overnight in a vacuum oven at 40°C.

The surface of the PP porous support was modified with oxygen gas plasma using a Plasma cleaner Femto apparatus. A piece of polypropylene was placed inside of the plasma cleaner, parameters were adjusted and the surface was automatically plasma treated. A picture of the Plasma apparatus is shown in Figure 3.3.3b. Parameters tested were: effects of plasma treatment time, percentage of oxygen in plasma chamber and different power settings on the instrument. The enhanced hydrophilic character was measured with contact angle measurements and the adhesion improvement was studied with scanning electronic transmission microscopy.



(a)



(b)

Figure 3.3.3: a) Filtration procedure of preparing composite membranes with a crystalline layer of nanoparticles (Technique B). b) Plasma cleaner Femto apparatus.

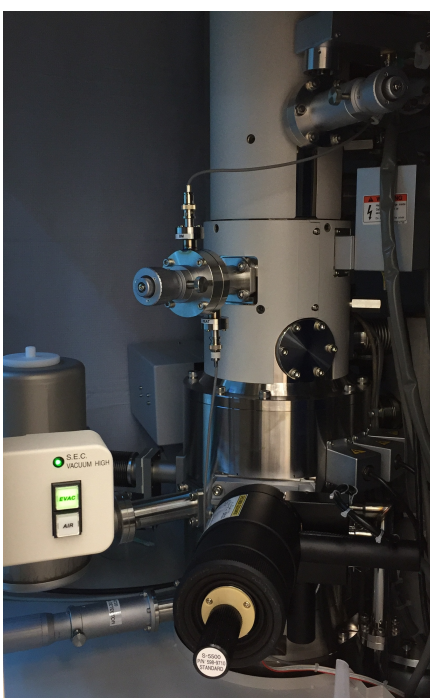
3.4 Morphological characterization

The morphology of the membranes was studied using scanning electron microscopy TM3030 PLUS and scanning transmission electron microscopy 5500 from HITACHI. Pictures of the microscopes are shown in Figure 3.4.1 To avoid charging of samples produced by the electron beam, all samples were coated with a conducting metal layer using a sputter coater Q150R from Quorum.

The samples were attached on a sample holder with a conductive tape, and coated with a 5nm thick gold layer for SEM TM3030 and a 5nm platinum/palladium for the S(T)EM 5500. For the cross-sectional stub in S(T)EM, silicon plates were used to fit the membrane to the cross section stub. The cross sections of the membranes were prepared by freeze-fracturing the membranes after immersion in liquid N_2 . Depending on the sample, different detector types were chosen, different magnifications were picked and the voltage was adjusted between 1kV and 30kV. The SEM TM3030 is able to have a voltage between 5kV and 10kV, while the S(T)EM 5500 can have a voltage between 1kV and 30kV. Low voltage was used to prevent melting of the polymer in the membranes.



(a) SEM TM3030 PLUS



(b) S(T)EM 5500 from HITACHI

Figure 3.4.1: Pictures of the electron microscopes used to study the membrane morphology.

Scanning Electron Microscopy

Both SEM TM3030 and S(T)EM 5500 are in-lens microscopes, which use an electron probe that detects signals from the interactions between the specimen and the electrons. Figure 3.4.2 shows an illustration of the SEM microscope. The signals can be from backscattered electrons (BSE), secondary electrons (SE) or X-rays (EDX) and the picture quality will depend on type of signal used [70, 71]. The S(T)EM has several advantages over SEM where S(T)EM 5500 can achieve resolution up to 0.4 nm with higher spatial resolution caused by addition of an extra detector (HAADF) and an EDX-system that gives 10 times better collection of X-rays compared to SEM [72].

The SEs are low-energy electrons, which leaves the sample as a result of several collisions, and the BSEs have higher energy than the SEs and have gone through one or several scatterings before leaving the surface. When a sample is bombarded with electrons, X-rays are emitted when the electrons go back to ground state after excitation, which detects backscattered electrons that have a relative large angle. In SEM, these electrons are added to the BSE detection.

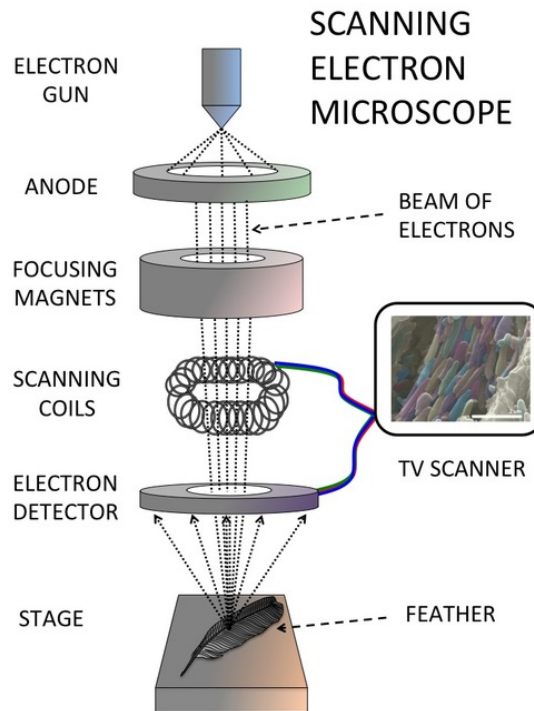


Figure 3.4.2: Illustration of a scanning electron microscope. (Reprinted from [73])

3.4.1 Effect of water exposure

In the pervaporation test, the membranes will be in direct contact with an aqueous solutions of TEG and water. The composite membranes containing nanoparticles were therefore flushed with water in order to check if the particles would wash off or if liquid water would have an effect on the nanoparticles. The membranes were placed in a membrane module and washed continuously with water for 2.5 hours and a picture of the experimental membrane washing module is shown in Figure 3.4.3a. SEM pictures were taken before and after the washing to spot any visible changes in the structure of the nanoparticles. Moreover, to protect the nanoparticles, half of the membranes were covered with a thin skin layer of AF2400 on top of the particle sub layer by dip coating (Technique A). With the assumption that the AF2400 layer completely protects the nanoparticles, only water vapor will be in contact with the nanoparticles. To investigate the effect of water vapor on the nanoparticles, both ZIF-L and ZIF-8 particles were placed in a humid cabinet for two weeks, which will create an environment with 100% humidity.

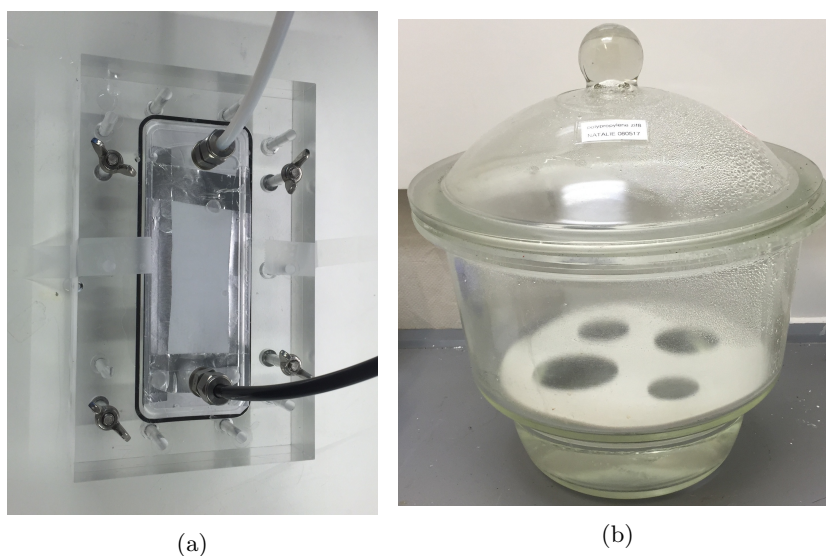


Figure 3.4.3: a) Picture of the membrane module used in water washing of the composite membranes. b) Picture of the humid cabinet.

3.5 Gas Chromatography Mass Spectrometer

Gas chromatography-mass spectrometry (GC/MS) is a powerful analytical technique for detection and identification of organic compounds in complex matrices. The GC/MS technology combines the the fine technique of separation in gas chromatography (GC) with the powerful analyzing tool of mass spectrometry (MS). The method has been widely used in fields of forensics, health care, research, food safety, and many others [74].

First, the gas chromatograph separates the compounds of a mixture by volatilization of the sample with respect to time in a specialized column. The sample is transferred from the injector, through the column and towards the mass spectrometer via a carrier gas (mobile phase), usually hydrogen or helium. A general requirement for the gas chromatograph is that the compounds should be able to vaporize without decomposition. How the components are separated is determined by the distribution of each compound in the mobile phase compared to the stationary phase with respect to time [75]. Figure 3.5.1 gives a schematic representation of the GC/MS.

Second, the mass spectrometer gives quantitative information of the components in the mixture, which can be obtained by analyzing the mass spectra of the compounds in the mixture. The separated components in the gas-phase are ionized as they enter the mass spectrometer. The mass spectra is all the data resulting from a GC/MS analysis based on the mass-to-charge ratio (m/z) of the components. The differences in the mass-to-charge ratio and different peaks in the mass spectra represent the fragmented ions and can reveal the structure of the molecule. Furthermore, the GC/MS is connected to a computer, which controls operational parameters of the system, such as temperature, amount of sample injected and gas flows. The computer handles all the information generated by the GC/MS, which can help identifying unknown compounds, quantitation of peaks and determine the concentration of a particular compound [75, 76].

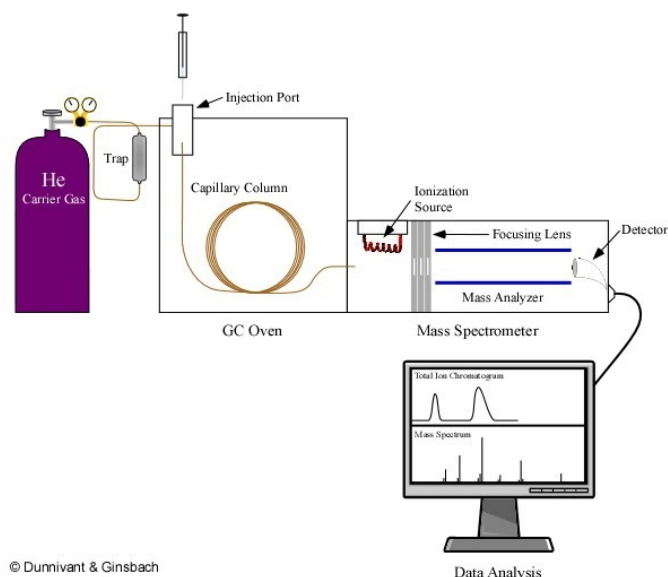


Figure 3.5.1: Illustration of GC/MS analytical tool. (Reprinted from [77])

3.5.1 Technical conditions

Analytical determinations of the permeate compositions were performed using an Agilent 7890A gas chromatograph coupled with an Agilent 5975C inert mass spectrometer operating in the selected ion monitoring (SIM) mode. The separation was performed using capillary column Agilent CP7596 with the film dimensions 30m x 320 μm x 1.07 μm . The inert gas used was Helium and the sample injector was split/splitless using a liner. A picture of the GC/MS is given in Figure 3.5.2.

3.5.2 Sample preparation

To analyze samples collected from the pervaporation setup, a calibration curve with standard solutions had to be created. The standard solutions were prepared by weighing accurate weight of TEG and water and diluting until the right concentration was reached. These known concentrations of the standard solutions were in the range of 20ppm to 1000ppm in 1mL vials. In addition, 100-200ppm of Internal standard was added to each vial. The intention with the internal standard is to measure the concentration ratio between the TEG and the internal standard to better quantify the concentration of TEG. The best internal standard is one that is chemically similar to the compound to be measured [74], and triethylene glycol monoethyl ether (TEG MEE) was chosen as it is a common internal standard for TEG GC analyses. The permeate samples collected had an unknown concentration of TEG and were diluted between 0-10 times with water on a weight basis. Internal standards were added to the diluted sample vials with approximately the same concentration as in the standard solutions.



Figure 3.5.2: Picture of the GC/MS setup.

3.5.3 Method development

The starting point of the GC/MS method development was a deficient method without clear component peaks or reproducibility. During preliminary GC/MS analysis, several GC parameters had to be customized for the detection of TEG. Parameters were; column oven temperature program, detector temperature, injection temperature, flow rate, split ratio, injection volume and gas flow rate. Each of the parameters were changed to observe the effect they had on the component peaks that were produced by the GC/MS. Furthermore, the liner in the GC/MS setup was changed from splitless liner to split liner because of problems related to the large expansion volume of water. Methanol with less expansion volume was also tested as the solvent. For the quantitative analysis, the mass analyzer was operated in the selected ion monitoring (SIM) mode. The ions selected to identify TEG were m/z : target 59, other 119, 43, 89 and the ions selected to identify TEG MEE were m/z : target 89, other 72 and 103. The mass spectra are shown in Figure 3.5.3.

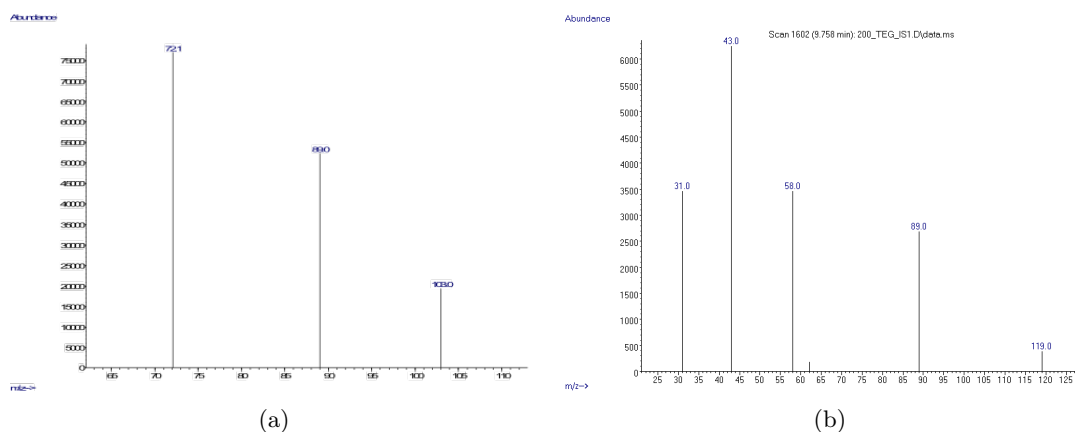


Figure 3.5.3: Graphs of the mass spectra obtained with GC/MS. a) Mass spectra of TEG MEE. b) Mass spectra of TEG.

3.5.4 Method validation

The method was validated according to the ISO/IEC 17025 requirements and the guidelines given by the International Council for Harmonisation (ICH)[78, 79]. The method was validated in terms of specificity, model correlation, limit of detection (LOD), limit of quantification (LOQ), repeatability, accuracy and possible carryover[80, 81].

The specificity is the ability to identify the components and to separate the target compound from impurities. This is a general test performed in start of the method validation on the responses from the chromatograms produced. To measure specificity, Signal to Noise (S/N) ratio tests were performed on the TEG and TEG MEE peaks. The specificity's tolerance for error in the chromatogram is set to 20% relative standard deviation (RSD), which indicates that the S/N ratio should be less than 2.5. The calculations are given in Appendix[82, 83]. Ten samples of the control standard solutions were used to confirm the method's specificity. The specificity test was successful if the S/N ratio was less than 2.5 of the retention time at the target compound.

The quadratic calibration model was checked by analyzing control standards with 100ppm, 200ppm, 400ppm and 600ppm of TEG in water. The concentration of the internal standard was 150ppm. The quadratic calibration parameters were calculated by least-square regression, and the squared correlation coefficient (R^2) was used to estimate the model's fit to the data. All quantitative results of TEG areas were corrected using the internal standard signal.

The limit of detection (LOD) of an analytical procedure is the lowest amount of target compound in a sample that can be detected. The detection limit was estimated as the TEG concentration that responds to a S/N ratio of 2 (25% RSD). The limit of quantitation (LOQ) of an analytical procedure is the lowest amount of target compound in a sample which can be quantitatively determined with suitable accuracy and was set to 10% RSD. The S/N ratio is a tool that can be used to separate the peaks from the noise. However, when the peaks are large, the S/N ratio is not a tool that should be used when explaining the methods reliability.

Repeatability is a measure of precision under the same operating conditions over a short time span. The repeatability was tested by running ten samples of standard control solutions with three different concentrations of TEG and calculating the % RSD. At high TEG concentrations (more than 500ppm TEG), the repeatability was considered acceptable when the % RSD was lower than 10%, and with low concentrations the acceptable value was 20%.

The accuracy of the method is was tested with the purpose to show that the concentration found from the calibration curve is accurate compared to the real concentration of the standard solutions. The accuracy was performed based on five concentrations (100ppm, 200ppm, 300ppm, 400ppm and 500ppm) and three replicates of each sample was injected. The percentage of recovery and % RSD was reported.

Carryover is when sample residue in the syringe is transferred from one injection to another injection. This effect can cause less accuracy and reproducibility of the samples. The carryover effect was evaluated by injecting a sequence of five standard samples with 500ppm TEG and five blank samples. To ensure the absence of the carryover effect, the S/N ratio from the blank samples should be less than 3.

3.6 Pervaporation

3.6.1 Experimental setup

The flow chart of the experimental setup in Figure 3.6.1 illustrates the working principle of the pervaporation experiment [84]. The membrane was mounted inside a membrane module shown in Figure 3.6.2b with a sintered plate used to sustain the thin polymeric samples, which had an effective surface area of 37.8cm^2 . The liquid feed is continuously pumped to the membrane module with a flow rate of $0.2\text{-}1.2\text{L/h}$, which is placed inside of a temperature controlled cabinet shown in Figure 3.6.2a. During the pervaporation process, the downstream side pressure is maintained with a vacuum of $3\text{-}4\text{mbar}$ pressure by means of a vacuum pump causing the liquid to evaporate on the permeate side of the membrane. A cold liquid N_2 (LN2) trap is placed before the pump to prevent the vapors to enter the pump and also to prevent emission of vapors from the pump outlet.

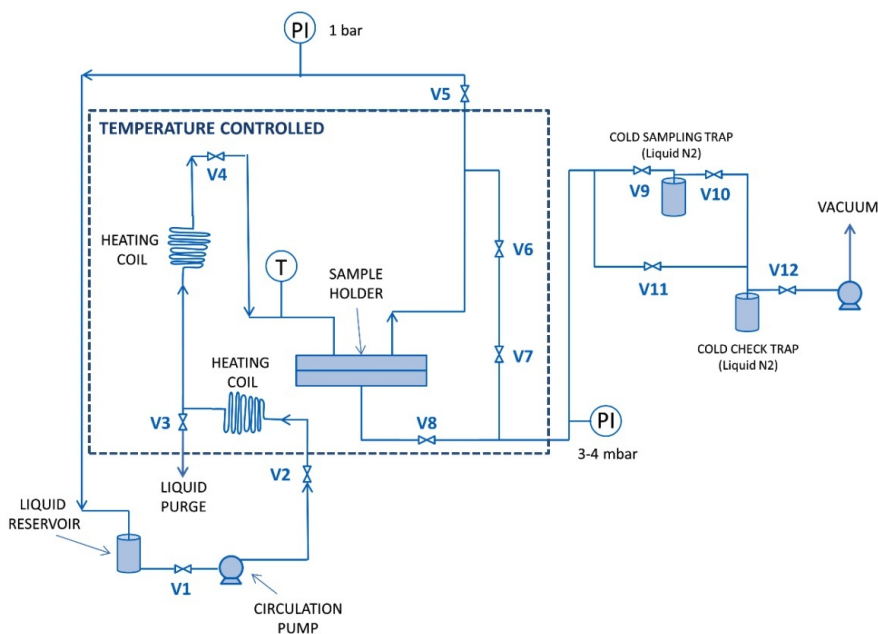


Figure 3.6.1: Experimental pervaporation setup. T = temperature; V1-V12 = valve number 1-12. (Reprinted from [84])

After washing the membrane upstream side, the liquid is recirculated back to the feed tank. The vaporized permeate is collected in a cold sampling trap, weighed and collected for further analyzing. The sampling trap was washed with warm water for at least 10 minutes to avoid contamination of permeate. The permeate composition was analyzed with gas chromatography mass spectrometer (GC/MS) Hewlett-Packard 5890 (SeriesII) and with Fourier transform infrared spectroscopy. Solutions with different $TEG - H_2O$ concentration in the range from 10-100% water were used as liquid feed, and temperatures in the range of $40\text{-}65^\circ\text{C}$ were considered. All the experiments were repeated three times to guarantee the validity of the experimental data.

In order to avoid contamination of one water concentration in another concentration of water, the setup was cleaned between the different concentration tests. Water was circulated 4 times, each time reticulating minimum 10 minutes. Furthermore, water was tapped out, and the setup was dried with compressed air from the topside to the downside of the membrane module. The speed of the liquid flow was calculated by recording time and amount of liquid pumped into the liquid reservoir.

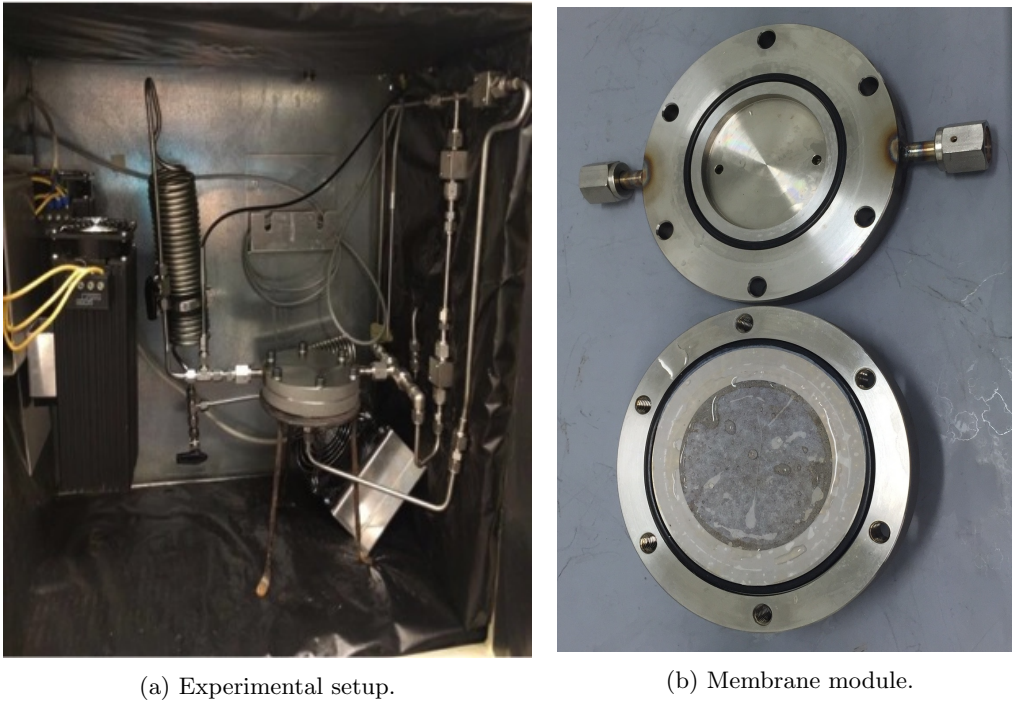


Figure 3.6.2: Pictures of the experimental pervaporation setup.

The performance of a membrane separation is often determined by the total flux through the membrane and the selectivity. In a pervaporation experiment, the flux is measured as:

$$J_i = \frac{Q}{At} \quad (3.6.1)$$

in which Q is the total mass permeated over time t and A is the membrane area. In a laboratory setup, the total amount of permeate of a single measurement is weighed, divided by the time of the experiment and the membrane area.

Chapter 4

Results and Discussion

This section will go through the results obtained from the experimental work. First, compatibility measurements with submerging tests and contact angle tests are discussed. Second, morphological characterization of the composite membranes PP-AF2400, PP-AF2400-ZIF-8 and PP-AF2400-ZIF-L are presented and discussed. Third, the results from the analytical method development and validation of GC/MS are obtained. All the results leading to the pervaporation experiments, in which pervaporation performance of PP-AF2400 and PP-AF2400-ZIF-L were discussed with the focus on effects of temperature and feed content, plus effects of aging on the pervaporation performance. At last, further improvements of experimental membrane preparation techniques and the investigation of the innovative multi-layered membrane are presented.

4.1 Compatibility measurements

In order to screen possible candidates as materials for membrane pervaporation, the compatibility of different polymers with TEG was examined. To avoid wetting of the membrane material and pore condensation, dense membranes were chosen over porous membrane materials [84]. This is confirmed by contact angle measurements of the porous support polypropylene (PP) in Section 4.1.2. Dense membrane materials were selected according to the following factors: high chemical stability, low cost and high H_2O flux ensured by the material. When the most suitable membrane material was identified, contact angle measurements were performed to find whether the membrane surface is wetted by water or TEG.

4.1.1 Submerging test

Different membrane materials were investigated by submerging membrane samples in TEG and studying the liquid uptake over time. For long-term operational stability, chemical stability is required, hence membranes that absorb negligible amount of TEG are preferred for the pervaporation process so that no long term swelling phenomena can jeopardize the membrane operational stability. In particular, three cases can be observed during compatibility tests: weight loss and

dissolution of the membrane due to poor chemical stability; weight increase due to swelling of the membrane; constant weight, indicating a stable membrane with chemical stability and no swelling. If pure TEG swells the membrane, it is expected that TEG can go through the membrane during pervaporation, resulting in a poor TEG-water separation.

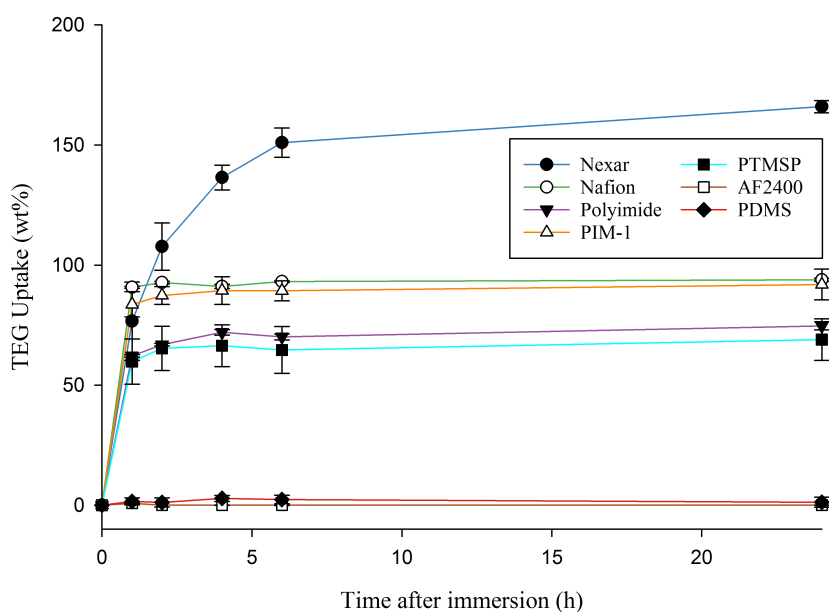


Figure 4.1.1: TEG uptake over time for different membranes.

In this experiment, two hydrophilic membranes, and five hydrophobic membranes were considered: Nexar, a sulfonated block copolymer [85], Nafion, a perfluorosulfonic ionomer [86], polyimide (6FDA-Durene) a glassy polymer with rigid imide groups, PIM-1, a polymer with intrinsic microporosity, PTMSP, a glassy polyacetylene-based polymer [87], PDMS a rubbery polymer with an organosilicate-based structure and AF2400, a glassy PTFE copolymer [88]. The TEG uptake of the different membranes as a function of time is given in Figure 4.1.1. The graph illustrates the first 24 hours of immersion as the change after 24 hours was insignificant. All the membranes were submerged for minimum two weeks at room temperature.

Two hydrophilic membranes Nexar and Nafion were considered. These two membranes have both a hydrophobic backbone and a hydrophilic tail that ensures high H_2O transport. The hydrophobic backbone gives the membranes the mechanical stability. None of the membranes showed any weight decrease, indicating that TEG did not dissolve any of the polymeric samples and the chemical stabilities in TEG were good. However, both membranes experienced excessive TEG uptake. The Nexar membrane had the largest TEG uptake with a weight increase of 150% compared to its initial dry weight. The middle block of the pentablock copolymer is a sulfonated group attributing the hydrophilicity to the polymer and the TEG uptake (Figure 4.1.2b). Geise et al. studied the water uptake of pentablock copolymers and found that the sulfonated group is the cause of the high water uptake. As the degree of sulfonation increased, the water uptake also

increased [89]. Nafion is a perfluorosulfonic acid (PFSA) membrane, which has shown excellent chemical and thermal stability (Figure 4.1.2a)[86]. Nevertheless, Nafion underwent significant TEG uptake (90% of the initial weight). PSFA membranes have shown to have high fuel permeability (especially methanol), resulting in loss of fuel when using the membrane in a methanol fuel cell [90]. Even though TEG is a much larger molecule than methanol, both TEG and methanol are in the alcohol family and the uptake test shows that TEG can easily be absorbed by Nafion, suggesting that the membrane should not be considered for further characterization.

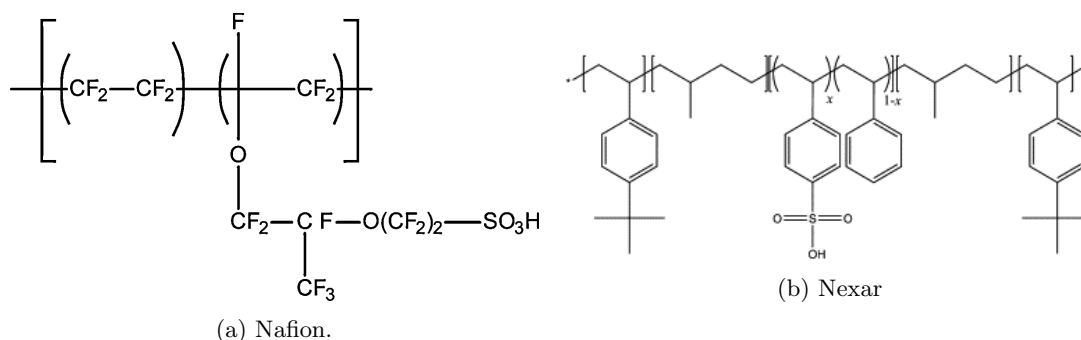


Figure 4.1.2: Molecular structure of a) Nafion [91] and b) Nexar [89].

Five hydrophobic membranes were considered. They are all high free volume polymers, which should ensure high H_2O transport in despite of their hydrophobicity. Among the polymers tested, there were four glassy polymers and one rubber polymer (PDMS). PTMSP (poly[1-(trimethylsilyl)-1-propylene]) is the most permeable polymer commercially available and its high FFV is associated with the rigid backbone chain with bulky trimethylsilyl side groups (Figure 4.1.3). The TEG uptake with PTMSP was found to be high (70% of the initial weight). PIM-1 (Figure 4.1.3) is a glassy polymer that has been used in pervaporation with the desirable property of intrinsic microporosity, which in solid state behaves like molecular sieves [92]. However, PIM-1 underwent excessive TEG uptake (90% of the initial weight), making it undesirable for TEG dehydration with pervaporation. Scholes et al. [93] examined the water uptake tendencies for PIM-1 and PTMSP. It was found that both membranes followed a behavior of adsorption within the micro voids of the membrane, in which PIM-1 underwent significant water uptake.

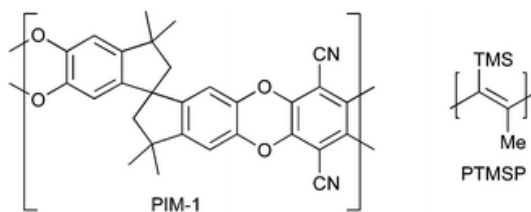


Figure 4.1.3: Molecular structure of PIM-1 and PTMSP [94].

Polyimide has been reported to be an excellent candidate as pervaporation membrane material, as it has superior chemical and physical stability and is water selective. The rigid backbone in the imide ring in 6FDA-Durene causes the membrane to have low swelling properties (Figure 4.1.4a) [95]. However, despite the low swelling properties of polyimide, the membrane experienced TEG uptake (70% of the initial weight), hence it can lead to relevant swelling, affecting the membrane stability [96].

Membranes that did not undergo any significant uptake were PDMS and AF2400. The molecular chains in polydimethylsiloxane (PDMS) have high mobility and is the only rubbery polymer tested. PDMS is well known for removing organics from aqueous solutions or the dehydration of ethanol with pervaporation [97]. PDMS has shown stable PV performance, has a low cost and has the ability to form excellent thin films. However, PDMS membranes have generally shown low fluxes and separation factors in the separation of alcohols and water [98]. The low selectivity is due to the highly flexible molecular chains.

Teflon AF2400[®] is on the other side, a glassy polymer. The molecular chains in this polymer have less mobility and with rigidity. Teflon AF2400[®] is well known for its high fractional free Volume (FFV) and therefore high permeability values for light gases and vapors. The Teflon AF family is composed by PTFE copolymers with different amount dioxole monomers in the polymeric chains (Figure 4.1.4c) [10]. In view of their rigid, glassy nature, the separation factor should be higher. Nonetheless, the AF polymer membranes are permeable to water. Huang et al. compared three per-fluoro membranes for dehydration of ethanol-water mixtures with pervaporation [9]. It was reported that perfluoro-polymers absorb less than 1% liquid in water/ethanol mixtures, and of that reason the water permeance through the membrane is independent of water/ethanol concentration [9]. On the other side, water permeance has been reported to be low in AF2400, requiring an ultra-thin layer to achieve competitive permeances. Due to low TEG uptake, high chemical stability and high fractional free volume, AF2400 membranes were further characterized.

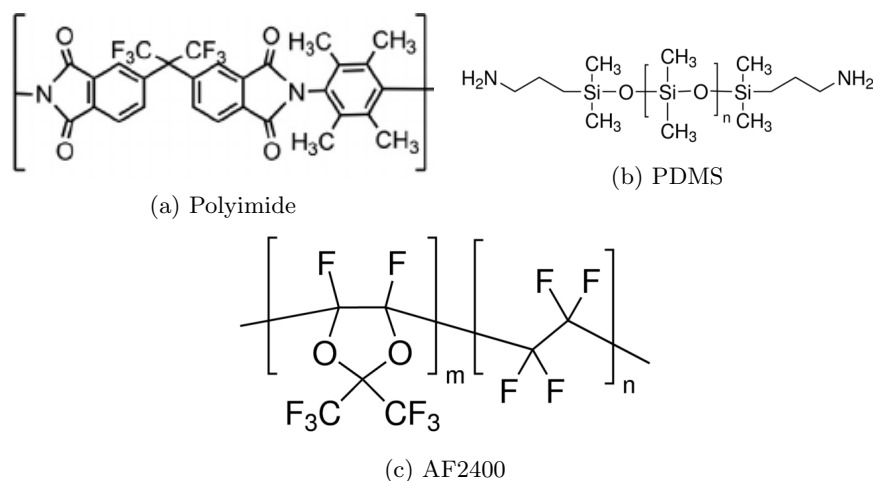


Figure 4.1.4: Molecular structure of a) Polyimide [99] b) PDMS [100] c) AF2400 [101].

4.1.2 Contact angle

In the specialization project, contact angles of AF2400 and PP was tested with water and TEG. Because of the importance of these results, they are presented in the present study. Water and TEG contact angle measurements are summarized in Figure 4.1.5. The Figure show that the hydrophobicity of PP and Teflon is similar expecting little change in hydrophobicity after coating of the polypropylene membrane. Both PP and teflon AF2400 have especially low surface energies, and therefore a low wetting tendency and high hydrophobicity. As expected, these characteristics are found on the composite membranes with thin skin layer of Teflon AF2400. For both membranes, the contact angle for H_2O is higher than for TEG, due to less surface tension compared to H_2O , indicating that the membranes have better affinity to TEG compared to water. However, in the case of TEG, the difference between the contact angles in PP and Teflon increases. The contact angle in PP decreases from 120° to 85° , while the contact angle in Teflon AF2400 decreases from 123° to 100° .

The only angle less than 90° was the pure porous polypropylene polymer support with pure TEG. Wetting of the pores in the porous membrane can cause pore condensation, which reduces transport over the membrane. Capillary condensation can happen because of high interaction between gas molecules and pore walls of the membrane, which can cause blockage of pores and flux reduction [102]. It is shown that capillary condensation is more dependent of solute chemistry rather than solute size where high affinity between the solute and the membrane material result in more capillary condensation [103].

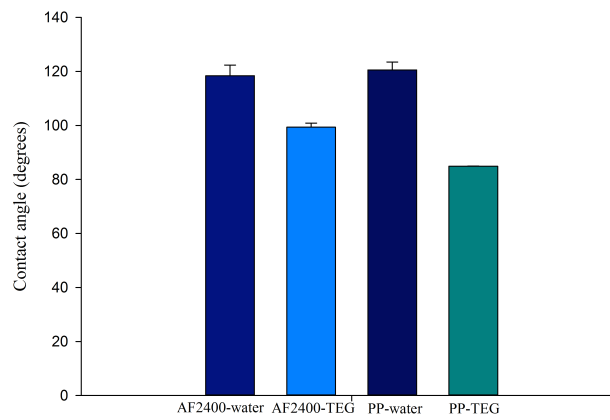


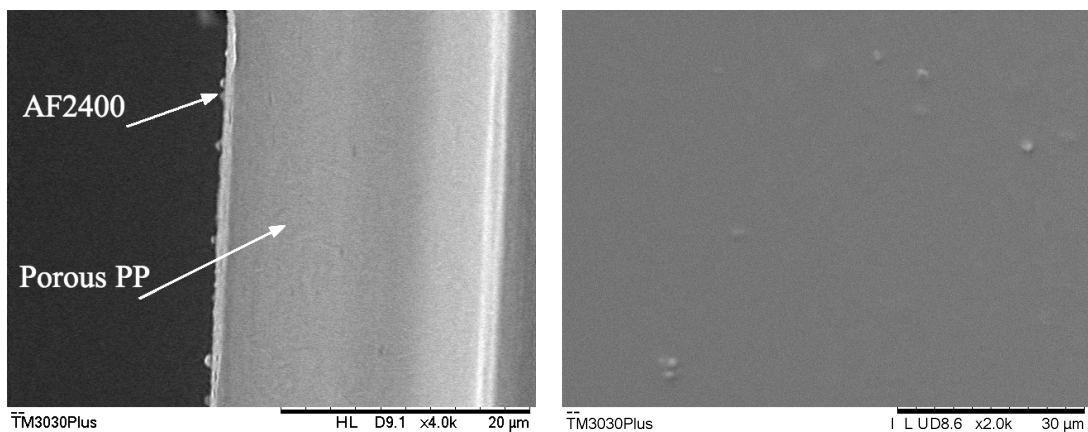
Figure 4.1.5: Contact angle measurements of AF2400 and PP with water and TEG.

4.2 Morphological characterization

4.2.1 Composite membrane PP-AF2400

Several composite membranes with and without nanoparticles were made by dip coating porous support in a solution of AF2400. The microstructure of the composite membranes was observed by SEM and S(T)EM. In composite membranes, it is particularly important to examine the cross section of the membranes, as the thickness and interface properties will directly affect the separation.

Figure 4.2.1 give the membrane morphology of the PP-AF2400 composite membrane made of 1 wt% AF2400 solution. The thickness of the top layer of the membrane was measured to be $1.7 \pm 0.3 \mu\text{m}$. The SEM image of the cross section showed clearly the presence of a two-layer structure with the rough texture of the porous support and uniform, dense top layer. In addition, the surface of the composite membrane was found to be uniform and fully covered the porous support. Furthermore, no interfacial voids or detachment were observed in the cross-sectional morphology, which proved that the AF2400 layer had been coated successfully.



(a) Cross section image.

(b) Surface image.

Figure 4.2.1: SEM images of PP-AF2400 composite membrane

4.2.2 ZIF particles

The morphology of ZIF-8 and ZIF-L was characterized with S(T)EM and can be seen in Figure 4.2.2. The ZIF-8 particles had a circular, almost hexagon shape with an average measured diameter of 400 ± 80 nm. Most literature data report a ZIF-8 diameter between 100-200 nm[36, 104], hence it is possible that the ZIF-8 particles in this image are agglomerated.

When adding the ZIF-8 particles in a polymer matrix, the particles will be sonicated before and after adding the polymer to ensure a well dispersion of ZIF-8 particles in the polymer matrix. The morphology of ZIF-L particles had the distinct leaf shape, sized with an average length of 0.9 ± 0.2 μm and an average thickness of 0.9 ± 0.2 μm . The size and shape of the ZIF-L particles are comparable to literature data [36]. When using nanoparticles as a filler in polymer matrixes, the dispersion is vital for a successful separation. The filler size can affect the polymer-filler interactions. With a smaller filler size, the surface area is larger and can provide greater polymer-filler interactions and enhance the polymer-filler compatibility[53].

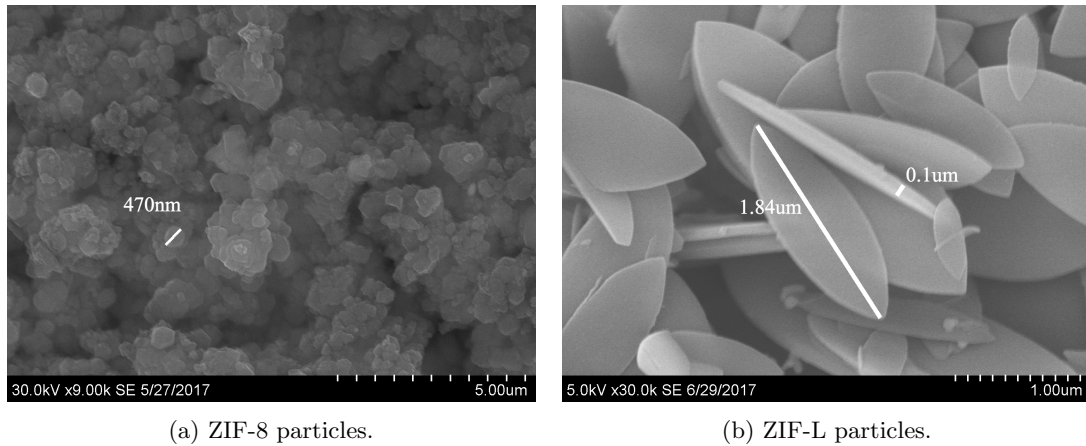


Figure 4.2.2: S(T)EM images of the ZIF particles characterized. a) ZIF-8 particles. b) ZIF-L particles.

4.2.3 Nanocomposite membrane

Porous nanoparticles (ZIF-8 and ZIF-L) were embedded in the dense top layer of the composite membrane, with the purpose of enhancing the separation properties of the membrane. The porous structure of the ZIFs can in theory enhance the water permeation through the membrane due to lower diffusion resistance in the porous structure [35]. However, to achieve this, the membrane has to be defect free and there should not be any discontinuity between the polymer and the nanoparticles. To study this effect, a morphology study of the immersed nanoparticles is carried out.

In order to get a proper dispersion of the nanoparticles in the polymeric matrix, sonication was used and its effect on the nanoparticles was examined. The ZIF-L particles were sonicated 4x40 minutes and for 8x40 minutes, and S(T)EM pictures from the morphology study are shown in Figure 4.2.3. In Figure 4.2.3a, the MMM was sonicated four times and the images show apparent particle agglomeration due to stacking and agglomeration of nanosheets. It appears that the discontinuity of the ZIF-L particles were near the surface of the membrane, which may affect the separation performance of the membrane. In comparison to Figure 4.2.3b that was sonicated eight times, the nanoparticles were better dispersed in the polymer matrix. However, it appears that the ZIF-L nanoparticles were partly chopped in pieces due to the intense sonication procedure.

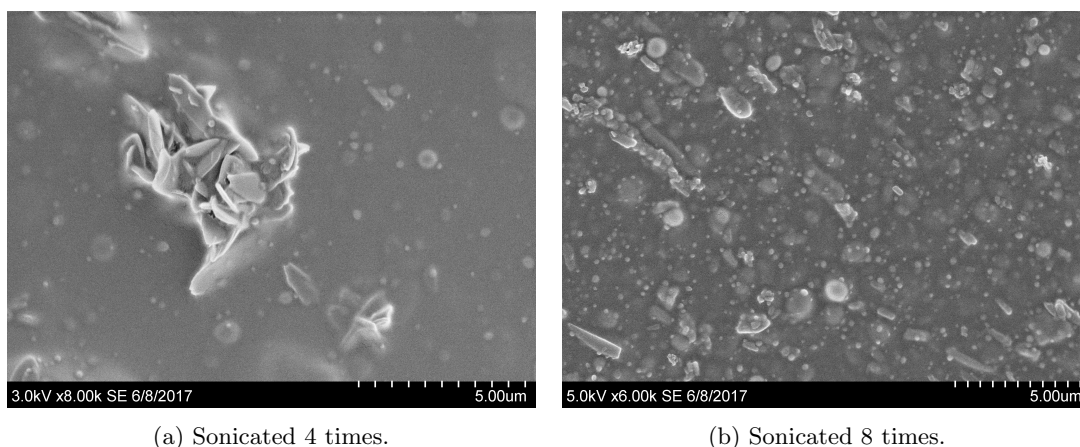


Figure 4.2.3: S(T)EM images: comparison of 4 and 8 sonications of ZIF-L in the coating layer of composite membranes with PP coated with MMM of AF2400 and ZIF-L. a) sonicated 4 times. b) sonicated 8 times.

From Figure 4.2.3, it can be seen that size and shape of the nanoparticles were not uniform, and the distinct leaf shape of ZIF-L can not be observed from the surface images after eight sonication processes. If the agglomeration creates sieves larger than the kinetic diameter of TEG, the selectivity in the pervaporation will drastically decrease. On the other side, the purposed water channels of ZIF-L [36] illustrated in 2.2.5 can be affected by the decomposition of the ZIF-L leaf shape, possibly leading to less molecular sieving effect for water molecules.

The composite membranes containing ZIF-L nanoparticles were further investigated in the pervaporation of water and TEG. Figure 4.2.4 shows cross sectional S(T)EM images of the composite membrane with AF2400 and ZIF-L. S(T)EM images were taken before and after pervaporation and no clear differences was observed, indicating that pervaporation did not have a great impact on the membrane morphology. The average thickness of the dense polymer layer with ZIF-L particles was measured to be $3.3 \pm 0.8 \mu\text{m}$, out of 25 measurements. It is also possible that the ZIF-L particles slowed down the deposition of MMM on top of the porous support resulting in a thickness difference. A solution to reduce the coating thickness could be to decrease the concentration of the dip coating solution. An interfacial gap between the porous support and the dense layer can be observed in the cross-sectional images. However, the gap could be due to detachment when ice-fracturing the membranes for cross sectional study.

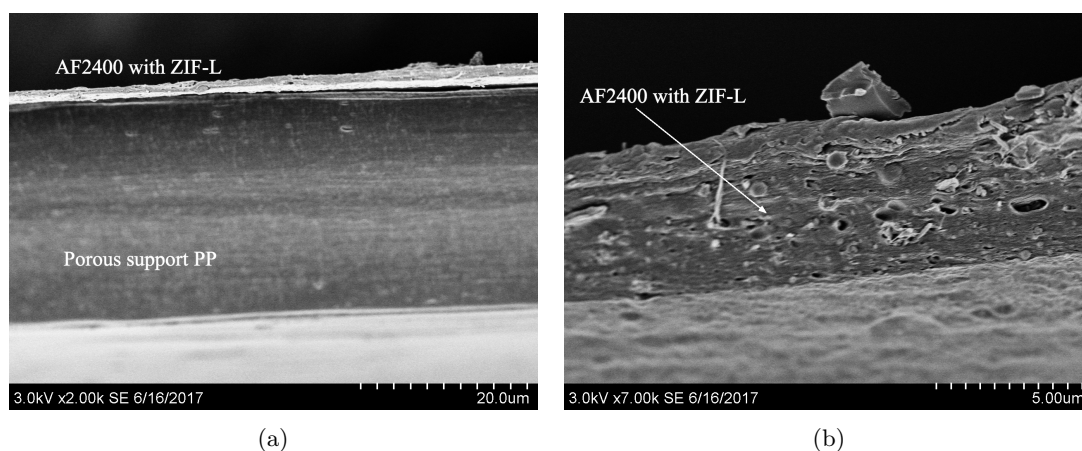


Figure 4.2.4: S(T)EM images of composite membranes with PP coated with MMM of AF2400 and ZIF-L. a) Cross-sectional image of PP-AF2400-ZIF-L. b) Cross-sectional image of PP-AF2400-ZIF-L, zoomed in on the dense layer of AF2400-ZIF-L.

The top layer with ZIF-L in the polymer matrix in Figure 4.2.4b shows that the nanoparticles are surrounded by empty spaces in the polymer matrix. This could be that there exist interfacial voids between the inorganic nanoparticle and the polymer with a "sieve in cage" structure, suggesting that there is detachment of the polymeric chains from the particle surface. Avoiding voids present in the membrane structure is difficult with polymers that are rigid and glassy, such as AF2400. Avoiding voids refers to maintaining flexibility of the polymer chains during membrane preparation and a solution could be to cast at an elevated temperature to maximize stress relaxation [37]. Interfacial voids were also discovered when casting pure self standing membranes with ZIF-8 particles in the polymer matrix of AF2400, and can be seen in Appendix C, Figure .0.2b. The interfacial voids were observed to be even larger in the ZIF-8 compared to ZIF-l, contradicting the statement that a smaller filler size can provide greater polymer-filler interactions and can enhance the polymer-filler compatibility [53].

Composite membranes with PP and ZIF-8 nanoparticles embedded in the AF2400 polymer matrix were also made. From the SEM pictures of the thin coating layer in the composite membrane with nanoparticles, it can be observed that there is clear aggregation of nanoparticles in the polymer matrix, suggesting that the sonication procedure was not completely successful in spite of

being sonicated eight times. Furthermore, the S(T)EM images in Figure 4.2.5a show that the ZIF-8 particles protruded the membrane surface instead of being immersed in the polymer matrix.

Water washing of the membranes removed nanoparticles from the membrane surface (seen from Figure 4.2.5), producing defects that are unacceptable for further testing. For this reason, either the dispersion of the particles must be improved, or another Teflon AF2400 layer must be added on top of the coated composite membrane to protect the nanoparticles; however, adding a layer will result in higher membrane thickness, and therefore higher transport resistance (i.e. lower flux). In Figure 4.2.5c-4.2.5d, the nanoparticle composite membranes are coated with respectively one and two layers of AF2400. The picture contrast is lower in the S(T)EM images of the composite membranes with layers of AF2400, indicating that the surface is more smooth, and with less particles protruding the surface. Water washing tests were performed on the PP-AF2400-ZIF-8-AF2400 membranes. Surface images before and after water wash indicate that no nanoparticles were removed.

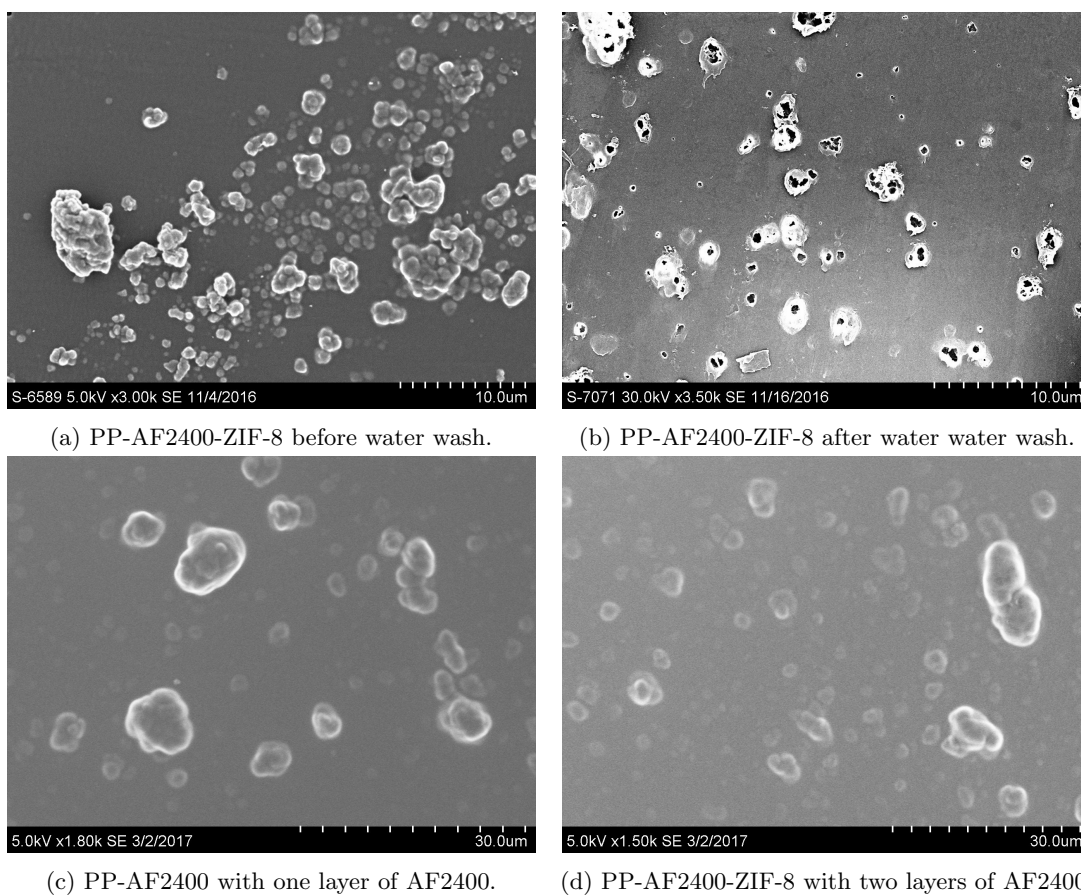


Figure 4.2.5: S(T)EM surface images composite membrane PP-AF2400-ZIF-8 before and after water wash. a) PP-AF2400-ZIF-8 before water wash. b) PP-AF2400-ZIF-8 water water wash. c) PP-AF2400-ZIF-8-AF2400 after water wash.

4.3 Gas Chromatography Mass Spectrometer

One part of this research project was to develop a method of analyzing TEG in aqueous solutions with gas chromatography mass spectrometry (GC/MS). The development of the GC/MS method was vital to the pervaporation study, in which the TEG-water composition gives information of membrane performance (separation factor and permeability). No similar GC/MS measurements have been carried out in the research group prior to this project. The customized method with the selected GC parameters are summarized in Table 4.3.3. GC/MS is a powerful analytical tool that combines two analytical techniques where the gas chromatograph separates components in a mixture with respect to time, and the mass spectrometer provides the structural information of the components [105].

4.3.1 Method development

Method development for GC/MS is a time demanding process where different parameters have to be adjusted to attain clear component peaks and reproducibility of results. Parameters of interest are: oven temperature program, detector temperature, injection temperature, flow rate, split ratio, injection volume and gas flow rate. To see the effects of the different parameters, every single parameter was tested at a time, and every test took between 2-24 hours, depending on the program chosen. The results of the GC-parameters found with method development are summarized in Table 4.3.3. All the steps towards finding this method is introduced by illustrating the chromatograms resulted from the different parameters tested with the GC-MS and can be found in Figure 4.3.1-4.3.4

Table 4.3.1: GC parameters.

	Rate [$^{\circ}\text{C}/\text{min}$]	Temp. [$^{\circ}\text{C}$]	Hold time [min]	Total time [min]
Oven temperature	Initial 8	80 200	1 5	21
Detector temperature	250 $^{\circ}\text{C}$			
Injection temperature	200 $^{\circ}\text{C}$			
Flow rate	9 mL/min			
Split ratio	2			
Injection volume	0.4 μL			
Gas flow rate	He: 25 mL/min			

Most challenges correlated to GC/MS are related to the injection of samples, especially when high concentration of H_2O are present in the sample to be analyzed. The large expansion of water after vaporization can cause effects like backflash and carryover, which result in inconsistent results. Backflash is when the vapor cloud expands beyond the inlet liner, resulting in poor sample transfer to the column and irreproducible peak shapes. To avoid all problems related to backflash a suitable injection volume should be found. From a solvent expansion calculator by the supplier of liners (Restek corporation), in our case the suitable amount of sample injected

should be less than $0.5\mu\text{L}$ [106]. All samples were therefore injected with $0.5\mu\text{L}$. Reducing the amount of sample even lower will result in a smaller electronic signal of the component (abundance) and can affect the detection limit. In addition, the syringe size in our case was $10\mu\text{L}$ and the minimal amount of sample injected by the syringe was $0.2\mu\text{L}$. The small amount of injected sample compared to the syringe size could affect the repeatability. Further optimization of the amount of sample injected will therefore be done on a later stage of the method development. Carryover is when sample residue in the syringe or from the injection port is transferred from one injection to another injection. To avoid this, the syringe was washed 2 times before and 6 times after each injection with a water-methanol (1:1) mixture. To completely sure that no sample residue from one injection would affect the next sample, a vial with pure water was placed between each sample vial.

The first parameter tested was the change of liner from splitless to split. Split injection is a method to split the injected sample into parts, so not all sample is directed to the head of the GC column [74]. The reason for the change was that there had not been observed repeatability and reliable results on an earlier stage of the testing. First, the amount of split must be optimized. Splits were tested in the range of 2 to 30 with TEG concentrations between 10ppm and 1000 ppm. Figure 4.3.1 illustrates the effect of changing the split from 10 to 2 with a TEG concentration of 500 ppm, the abundance is higher and the splits are better separated. The x-axis gives the retention time of the different components (TEG and TEG MEE) and the y-axis shows the abundance of the analyte. A high abundance is a large electronic signal from the compound detected is connected to high concentration of the component. The ratio of TEG and TEG MEE is used in GC calibration to better quantify the concentration of TEG. The component at retention time 7.7 min is the TEG peak and the component at retention time represents the internal standard TEG MEE. The ideal split was found to be 2 in the case of TEG-water solutions in the range of 100 ppm to 1000 ppm. It can be seen that the split of 10 was too large as the abundance was low and the peaks of TEG and TEG MEE could not be separated from each other, whereas with the split of 2, the abundance was higher and the peaks were a distance apart. However, there can be observed a tail of analyte after the TEG peak, between the retention time of TEG and TEG MEE (respectively at retention time 7.6 min and 8.4 min), which can affect the precision of the results. The next step of the method development was therefore to examine the effect of temperature program.

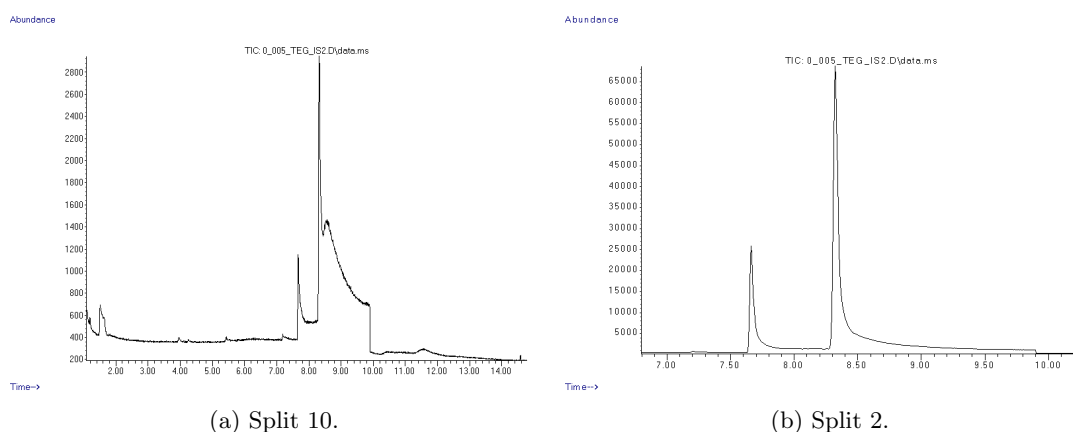


Figure 4.3.1: Effect of changing split from 10 to 2.

The temperature was adjusted to achieve separate and reproducible peaks in the chromatograms. The sample is transferred from the injector, through the column and towards the mass spectrometer via a carrier gas of helium. How the components are separated is determined by the distribution of each compound in the mobile phase compared to the stationary phase with respect to time [75]. With different temperature programs, the components will vaporize differently and the results will differ.

The goal is to achieve clear component peaks, not too close to each other and without a connecting tail. TEG is a polar compound that is highly soluble in water and TEG MEE has similar chemical structure. As the rest of the glycols, TEG is not focused in a narrow band in the GC-analysis. It is rather overlapping with the condensed water and can stick to the column walls, which can cause split peaks and irreproducible results. The temperature can be either adjusted in the oven or at the injection port. The injection temperature was adjusted between 200°C and 250°C, the initial oven temperature was in the range 40°C to 100°C, the maximum oven temperature was 200-300 °C and the temperature increase was adjusted between 8°C/min and 25°C/min. Table 4.3.2 show an overview of all the different temperatures programs in the oven that were tested, in which the blue color shows what parameter that was changed. Figure 4.3.2 illustrates how the temperature program can affect the results.

Table 4.3.2: Summation of the different temperature oven programs that were tested.

Test	Initial T[°C]	Max T[°C]	$T_{Increase}$ [°C/min]
1	80	200	25
2	40	200	25
3	60	200	25
4	75	200	25
5	90	200	25
9	100	200	10
6	80	-	8
7	70	300	20
8	40	250	10

The effect of changing the initial oven temperature from 40°C to 75°C with a temperature increase of 25°C/min is shown in Figure 4.3.2. The chromatograph with initial 75°C gave a much sharper peak compared to the test with 40°C as the initial oven temperature. Other temperature tested are shown in Table 4.3.2, in which 60°C gave similar results as 40°C and 80°C-90°C gave similar results to 75°C, suggesting that the ideal initial oven temperature should be in the range of 75-90°C. However, the repeatability of the results with 75°C as inlet temperature was not satisfactory. The ratio between the peaks of TEG and TEG MEE changed from different runs, suggesting that another parameter should be tested. Several methods of changing the temperature program is suggested by different sources. However, with different technical conditions and various analytes, the best way of finding the effect of temperature program is by trial and error analysis.

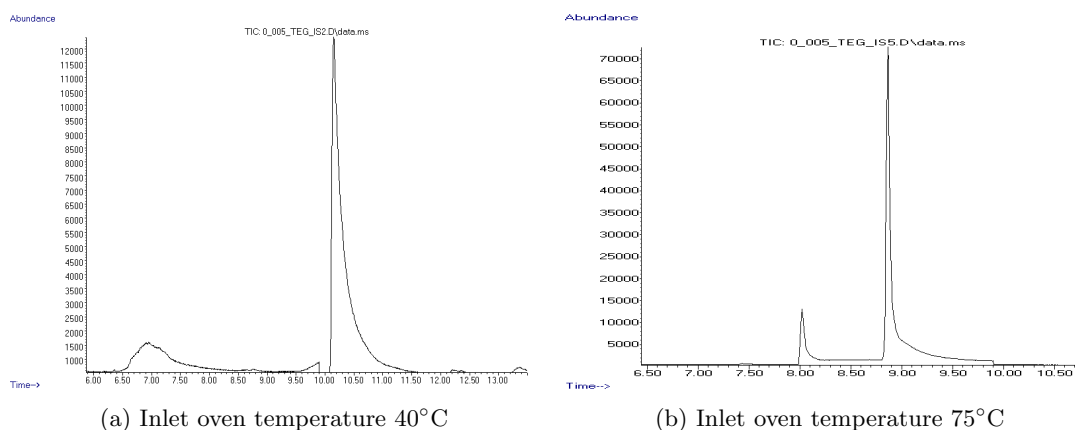


Figure 4.3.2: Effect of changing the inlet oven temperature from 40°C to 75°C.

The oven temperature program from the supplier of GC-MS equipment (Restek corporation) suggested a temperature increase of 8°C/min instead of 25°C/min with a high initial oven temperature of 80°C [107]. Data from the Restek corporation suggests that it is possible to detect glycol amounts down to a range 1-10 ppm in aqueous solutions. However, this method was for a GC apparatus with a flame ionization detector (FID) that measures the concentration of organic species in a gas stream instead of a mass spectrometer [105]. From Figure 4.3.3, it can be seen that the tail between the two peaks disappeared. Due to slower temperature increase, the retention was also higher. Repeated testing of this temperature program was rather successful, in which the ratio of the peaks was reproducible. Further testing and optimization was done with the basis of this particular temperature program.

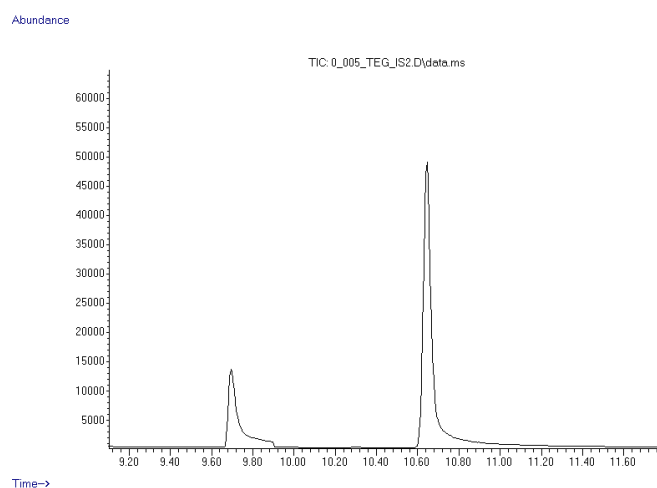


Figure 4.3.3: Restek GC temperature program.

Now that the temperature program in the oven was found, further optimization can be done with the sample injection. By lowering the injection temperature from 250°C to 200°C, the vapor cloud into the liner will also decrease, resulting in less chance of backflash. This was tested and no noticeable change was observed, therefore the injection temperature was kept at 200°C. To be on the safe side, the amount of sample injected was adjusted to 0.4 μ L. The challenge here is the detection limit. Figure 4.3.4 show the difference between 0.5 μ L and 0.4 μ L of sample injected at 100 ppm of TEG. The abundance of the 0.5 μ L sample was higher than the abundance for the 0.4 μ L, indicating a lower detection limit for 0.5 μ L compared for 0.4 μ L. However, the unwanted effect of backflash is more important to avoid, therefore 0.4 μ L was chosen for the next stage of the method testing: method validation.

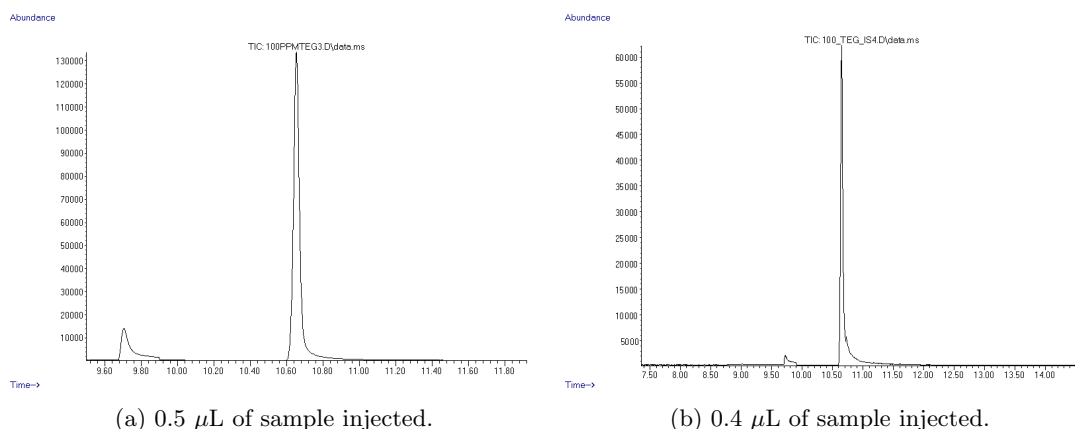


Figure 4.3.4: The effect of different amount of sample injected. a) 0.5 μ L b) 0.4 μ L.

When testing the developed GC-MS method on unknown TEG samples, it is vital to know the approximate concentration range of the sample. The final concentration of the internal standard should be approximately in the mid-range of the expected concentration of the compound being measured. In this study permeate samples with extremely low concentrations of TEG were tested. If feed samples with higher concentration of TEG were to be tested (for example 70% TEG), the sample must be diluted due to difficulties of vaporizing pure TEG. In addition, higher concentration samples result in more maintenance and shorter lifetime of GC-MS equipment such as liner or column. With this method, it is recommended to dilute the sample to a concentration range within 100ppm and 2000ppm.

4.3.2 Method validation

To be certain that the method found is valid and can give trustable data for analyzing TEG in aqueous solution, a validation process was performed. The essence of method validation is to test the electronics, the equipment, the specimen and the method parameters found in the method development. It is also a tool to find how low concentrations of analyte that can be analyzed with precision (LOQ) or what the lowest concentration that can be detected is (LOD). The method found was validated according to ISO/IEC 17025 requirements and the guidelines given by the International Council for Harmonisation (ICH)[78, 79].

The following parameters were obtained: quadratic regression coefficient of $R^2 > 0.99$, limit of detection (LOD) of 50ppm, limit of quantitation (LOQ) 150ppm, repeatability at low and high concentration in (RSD%). In addition repeatability and accuracy were satisfactory and no carry over effects were observed. A summary of the validation parameters can be found in Table 4.3.3.

Table 4.3.3: Parameters for the validation of the GC-MS method.

Parameter	Value
LOD	50ppm
LOQ	150ppm
RSD% low concentration	18.61%
RSD% high concentration	2.81%

Ten samples of the control standard solutions were tested to confirm the method's specificity. Five of the samples contained TEG in aqueous solutions, while the rest were blank samples. The specificity was successful as the S/N ratio was higher than 2.5 at the retention time of the target compound for the five samples with TEG and water.

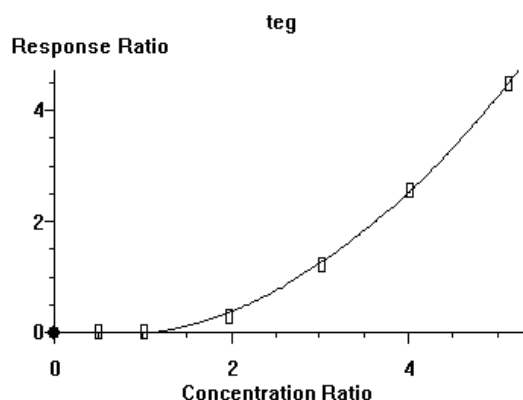


Figure 4.3.5: A picture of a typical calibration curve with quadratic regression force (0,0).

The quadratic regression curve fit to the data for samples with 50ppm, 100ppm, 200ppm, 300ppm, 400ppm and 500ppm can be found in Figure 4.3.5. The response ratio between TEG and TEG MEE is plotted against the concentration ratio of the known standard samples and TEG MEE.

From the graph, it is clear that the limit of quantitation is 150ppm, as the response ratio from the calibration curve for all concentrations below 100ppm is around zero. However, it is possible to detect concentrations lower than 100ppm, but it is not possible to quantify the data correctly. Therefore, the detection limit was found to be 50ppm with a S/N ratio of 2.5.

Repeatability was calculated as the the relative standard deviation (% RSD), after running ten samples of control standards with four different concentrations. The repeatability can be found in Table 4.3.4 for approximately 100ppm, 150ppm, 500ppm and 984 ppm TEG in aqueous solutions. The repeatability of low concentrations (100 ppm) was found to be 18.6% RSD and high concentration (1000 ppm) at 2.8% RSD, which were all acceptable numbers to the requirement set. In addition, it can be observed that % RSD for 100ppm is over the requirement for the quantitation limit (15% RSD), while 150ppm is under, setting the limit of quantitation to 150ppm.

Table 4.3.4: Method repeatability.

Injection	1.Conc. (ppm)	2.Conc. (ppm)	3.Conc. (ppm)	4.Conc. (ppm)
1	124.9	151.5	493.9	975.7
2	78.5	160.0	476.5	974.3
3	113.8	118.4	489.9	973.4
4	106.7	140.9	483.1	977.3
5	81.4	149.9	476.1	972.0
6	93.3	145.8	479.8	972.5
7	92.0	135.3	499.9	979.8
8	60.0	131.9	482.8	976.1
9	99.9	132.7	483.3	971.3
10	96.0	144.9	484.3	973.9
AVR	96.2	141.1	480.8	984.5
RSD%	18.61	8.028	1.560	2.808

The accuracy of the test was reported to prove that the concentrations calculated by the computer (based on the quadratic regression model) was correct compared to the real concentration of the standard solutions. The method accuracy can be found in Table 4.3.5. The relative concentrations of all tested samples were in the range of 98-125% and the % RSD was less than 5. The 100 ppm is under the concentration of quantitation and showed a much higher relative concentration and % RSD compared to the other samples tested, indicating that the quantitation limit is correctly set.

Table 4.3.5: Method accuracy.

Relative conc. %	Real Conc. (ppm)	Test nr.	Conc. found
125%	96.3	1	115.9
		2	129.2
		3	116.9
		Average	120.7
		% RSD	4.992
99%	191.7	1	193.2
		2	187.7
		3	191.2
		Average	190.7
		% RSD	1.182
98%	297.1	1	293.8
		2	289.4
		3	291.0
		Average	291.1
		% RSD	0.617
100%	395.5	1	392.7
		2	398.0
		3	396.9
		Average	395.87
		% RSD	0.584
103%	485.8	1	488.6
		2	486.8
		3	487.0
		Average	487.4
		% RSD	0.344

4.4 Pervaporation

Due to minimal literature on dehydration of TEG with pervaporation, experimental data is needed to validate computational models for process analysis. Pervaporation experiments for the separation of water from TEG were performed on two composite membranes: one polypropylene coated with AF2400 (PP-AF2400) and one with polypropylene coated with MMM of AF2400 and ZIF-L (PP-AF2400-ZIF-L).

In order to examine the effect of feed composition on the performance of the composite membranes, experiments were carried out in feed water concentration ranging from 1wt% to 30wt%. This H_2O concentration in TEG range is relevant to industrial applications for natural gas dehydration by TEG. In addition, experiments with pure water was carried out to study the water flux through the membranes. The effect of temperature was examined ranging from 30°C to 60°C. At last, the pure polymer composite membrane PP-AF2400 was compared with the composite membrane with nanoparticles PP-AF2400-ZIF-L to see the effect of the addition of ZIF-L particles to the dense AF2400 top layer. The thickness of the dense layer in the PP-AF2400 membrane was measured to be $1.7 \pm 0.3 \mu\text{m}$ and for the PP-AF2400-ZIF-L, the thickness was measured to be $3.3 \pm 0.8 \mu\text{m}$. When comparing the membranes, it is important to take the thickness into account since a thinner dense layer is proportional to the membrane flux.

It is worth mentioning that the pervaporation data from 20wt% water in the feed has been removed from data sets due to unexpectedly high TEG concentration (10 times higher compared to 90wt% and 80wt%), possibly from an experimental error, such as contamination of the permeate. A similar graph to Figure 4.4.1b with the data set from 20wt% water in the feed can be found in Figure E.0.3 in Appendix E. In addition, the amount of permeate in 1wt% TEG was so small that it was only possible to extract permeate from 50°C and one sample from 60°C.

4.4.1 Pervaporation performance of PP-AF2400

Effect of feed composition

The total flux and the TEG concentration in the permeate are plotted as a function of feed water concentration as presented in Figure 4.4.1. The total flux through the membrane at 50°C was 80.31g/m²h with a feed water concentration of 10wt%. The total flux increased with higher water content in the feed. At a feed water concentration of 10wt%, the amount of TEG found in the permeate at 50°C was 531ppm, an already extremely low concentration of TEG. When increasing the amount of water in the feed, the permeate was further enriched with water resulting in a TEG concentration of less than 100ppm in the permeate. The TEG flux through the membrane appeared to be quite independent of the water concentration. Except when having the lowest water concentration of water (1wt%), the TEG flux was slightly lower. TEG is a polar compound, which can form hydrogen bonding between the hydroxyl groups and water. However, the TEG flux and the TEG concentration in the permeate is extremely low, and the variations are small over a broad range of water concentrations. From the morphological study, no significant faults in the membrane were found. However, there will always be a number of TEG molecules that will permeate through the membrane due to chemical potential difference across the membrane. Other possibilities for the TEG presence could be experimental errors or the fact that the limit of detection (LOD) for TEG in water by GC-MS is reached when having less than 100ppm TEG in aqueous solutions.

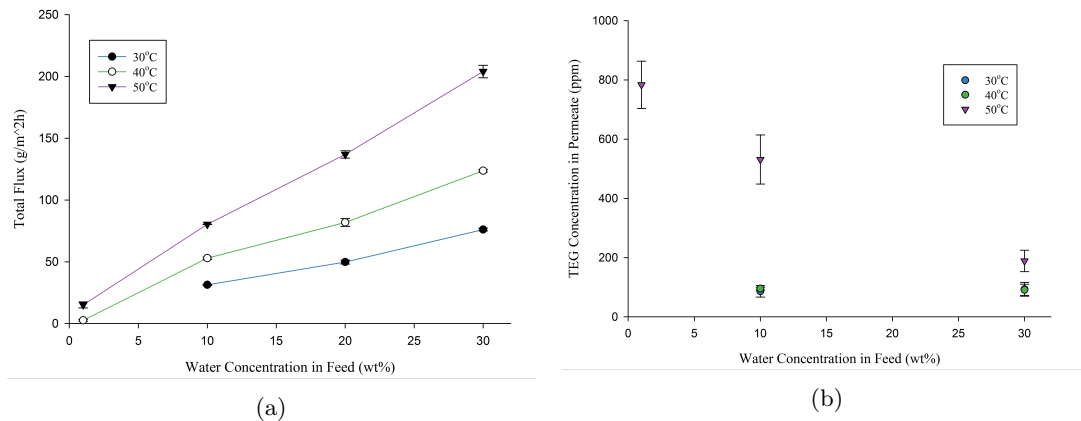


Figure 4.4.1: Effect of water concentration in feed. a) Total flux. b) TEG concentration in permeate.

In Figure 4.4.2, the water flux and the TEG flux through the membrane are plotted as a function of water concentration in the feed. The water flux at a temperature of 50°C and a feed water content of 10wt% is 80.26g/m²h. With a higher water concentration in the feed, the water flux increased almost linearly and at a feed water content of 30%, the water flux was 201.61g/m²h. The TEG flux at a feed water content of 10% water was found to be 0.04g/m²h. From the equation of permeance 2.1.10, there should be a linear relationship between the driving force ($x_i\gamma_i p_i^0$) and the water flux. When increasing the water fraction in the feed, the flux will increase proportionally. Similar trends have been observed for dehydration of ethylene glycol [52].

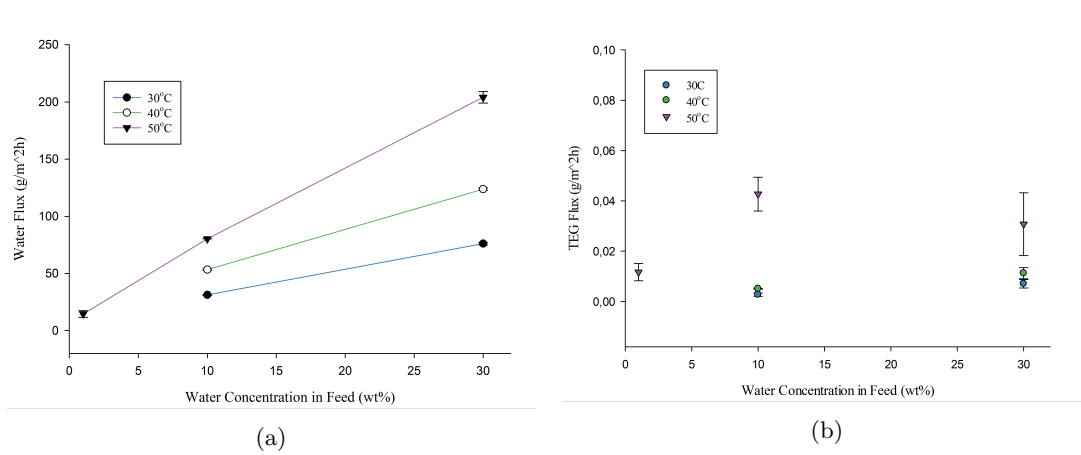


Figure 4.4.2: Effect of water concentration in feed. a) Water Flux. b) TEG flux.

The separation factor as a function of water concentration in the feed is given in Figure 4.4.3. At a feed water concentration of 10wt% and a temperature of 50°C, the separation factor was 16581. All values are over 10000, which is an extremely good separation factor, suggesting that high TEG recovery can be expected for the separation process. Increasing the feed water concentration from 10wt% to 30wt% resulted in decreasing selectivity from 100000 to 25000 with a temperature of 30°C. As explained earlier, this trade-off between permeation flux and selectivity is common in pervaporation, which makes it challenging to develop membranes that can exhibit both high permeation flux and exceptional selectivity [108].

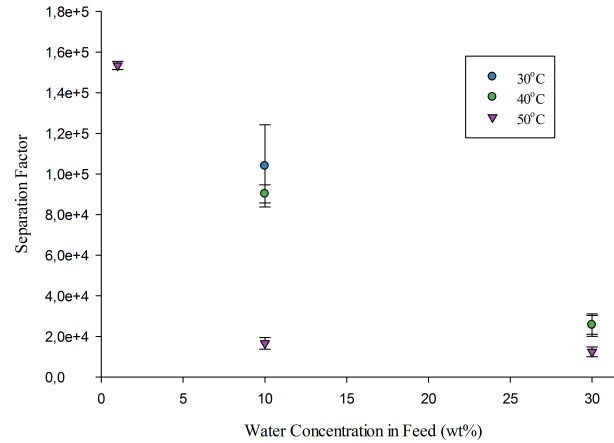


Figure 4.4.3: Separation factor as a function of water concentration in feed in PP-AF2400 membrane.

From Section 4.1, compatibility tests showed that TeflonAF2400 absorbs less than 1wt% TEG, and the contact angle of both TEG and water is $>90^\circ$, indicating that the water flux through the membrane is mainly based on size exclusion and not chemical affinity as in hydrophilic pervaporation dehydration. The question is, can the membrane compete with hydrophilic membranes on the market? Due to water swelling, the flux of hydrophilic membranes are generally larger, compared to those of hydrophobic membranes. Dogan et al. [25] separated water from EG with pervaporation with $30\mu\text{m}$ thick membrane, in which the total flux was $311\text{g}/\text{m}^2\text{h}$ at 30°C and 90wt% EG in the feed. The hydrophobic composite membrane of PP-AF2400 in this study gave a total flux of $31\text{g}/\text{m}^2\text{h}$ at 30°C with 90wt% EG as feed solution, a tenfold lower compared to the hydrophilic membrane of chitosan and zeolite. To increase the flux to compete with the chitosan membrane, the dense layer of AF2400 could be decreased to 100nm, or other variations could be done, such as the addition of porous nanoparticles. On the other side, the separation factor with the AF2400 membrane was much higher compared to the hydrophilic membrane, giving the AF2400 potential and incentive for further research efforts.

Starting from the fluxes obtained from the experiments, the permeance of H_2O and TEG were also calculated. The partial pressure on the downstream side was kept below 5mbar and can be considered negligible, hence the permeance equation from section 2.1.1 becomes:

$$\frac{P_i}{l} = \frac{J_i}{(x_i \gamma_i p_i^0)} \quad (4.4.1)$$

where P_i/l is the permeance of component i and is dependent on both composition and temperature. x_i is the mole fractions of component i in the liquid feed, p_i^0 is the saturation pressure of pure component i at the given T and γ_i is the activity coefficient of species i . In order to determine the activity coefficient of TEG and water for the calculation of permeance, an activity model from Parrish [109] was used and the calculations were performed in a Matlab model provided by Kristin Dalane. The values found for the activity coefficients of TEG and water at different temperatures and water contents can be found in Appendix I, Table .0.1 and Table .0.1.

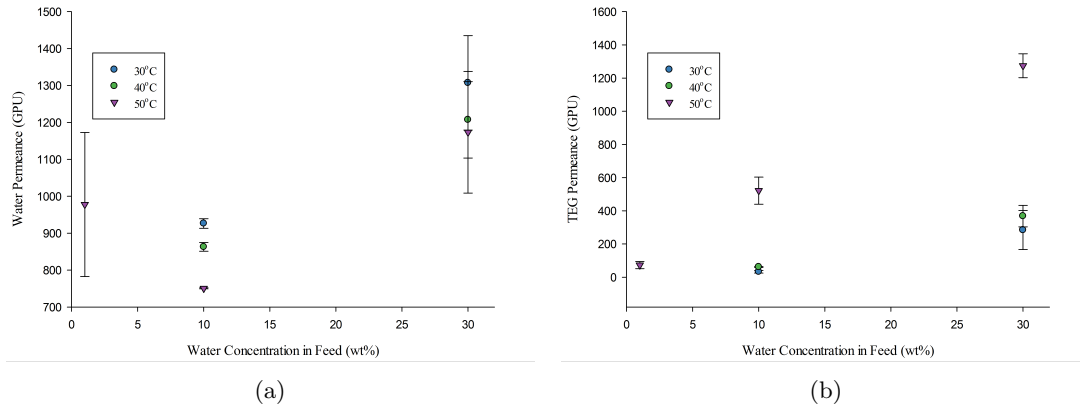


Figure 4.4.4: Effect of water concentration in feed on a) water permeance and b) TEG permeance.

The permeance as a function of feed water concentration is given in Figure 4.4.4. At feed water concentration of 10% and temperature of 50°C, the water permeance was 751GPU. With 1wt% water in the feed, the water concentration throughout the experiment decreased, hence the standard deviation in the data of the permeance was large. Excluding the permeance for 1wt% water, the water permeance increases with higher water concentration in the feed. The TEG permeance shows a similar trend. At feed water content of 10% and temperature of 50°C, the TEG permeance was found to be 522GPU. A higher water permeance compared to TEG permeance indicates a water selective membrane.

Huang et al. [9] showed that the water permeance of AF membranes was independent of feed concentration and the average permeance at 75°C and 0.5 μ m thick membranes was measured to be 2900GPU. The average permeance of this dataset with 50°C was 1000GPU. However, when taking the difference of thickness into account, the permeability of the AF membrane from Huang et al. would be 1450Barrer, which is comparable with this pervaporation study of AF2400 membrane. On the other side, the TEG permeance at 50°C showed almost an linear trend, in which the TEG permeance increased proportionally to higher water content in the feed.

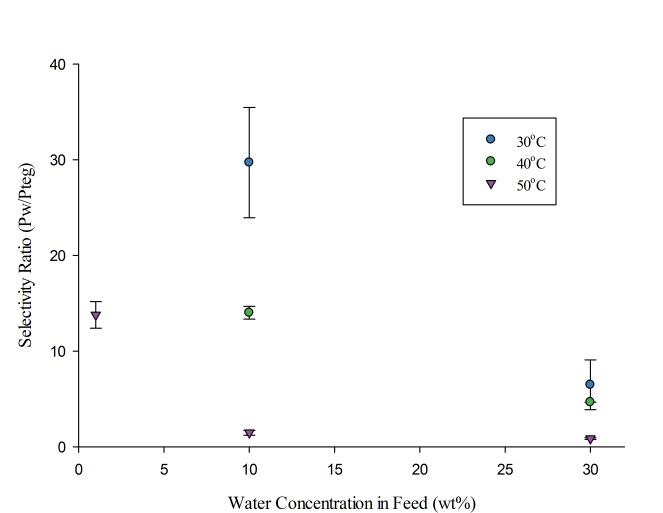


Figure 4.4.5: Effect of water concentration in feed on ideal selectivity in PP-AF2400 membrane.

Assuming a valid solution-diffusion model, the membrane separation performance can be determined as the ratio of permeance in terms of selectivity, defines as the ratio of the water and TEG permeance. This selectivity is in terms of intrinsic membrane properties and can be seen in Figure 4.4.5. Since the vapor pressure of TEG is extremely low (an order of 10^6 lower than for water), the TEG content in the permeate must be extremely low (lower than approximately 100ppm) to give a high selectivity. At a temperature of 30°C and a feed water concentration of 10wt%, the water selectivity is 30, which is decreased to 2.8 at 30wt% water in the feed. At a temperature of 40°C, the selectivity is 14 and at a feed water content of 10wt%, the selectivity is 3.4. At last, at a temperature of 50°C, the selectivity is found to be 1.5 with 10wt% water in the feed, which is decreased to 0.95 at a feed water concentration of 30wt%. With a selectivity less than 1, the membrane is not water selective. Summed up, the ideal conditions for the intrinsic membrane properties appears to be low water concentration in the feed with a low temperature, which can relate to industrial conditions in dehydration of TEG subsea.

Effect of temperature

The effect of the operating temperature on the water flux and TEG flux of the composite membrane with PP coated with AF2400 is shown in Figure 4.4.6. With pure water in the feed, the water flux through the membrane is $120\text{g}/\text{m}^2\text{h}$ at 30°C , and increases to $354\text{g}/\text{m}^2\text{h}$ at 50°C . When decreasing the feed water concentration to 10wt%, the water flux becomes $31\text{g}/\text{m}^2\text{h}$ with a temperature of 30°C . Increasing the temperature to 50°C , the water flux is enhanced to $80\text{g}/\text{m}^2\text{h}$. The TEG flux through the membrane at a feed water concentration of 10wt% is $0.0027\text{g}/\text{m}^2\text{h}$ and increases 20 times to $0.04\text{g}/\text{m}^2\text{h}$ with a temperature of 50°C . In general, the results indicate that all of the permeation fluxes increase with increasing feed operating temperature.

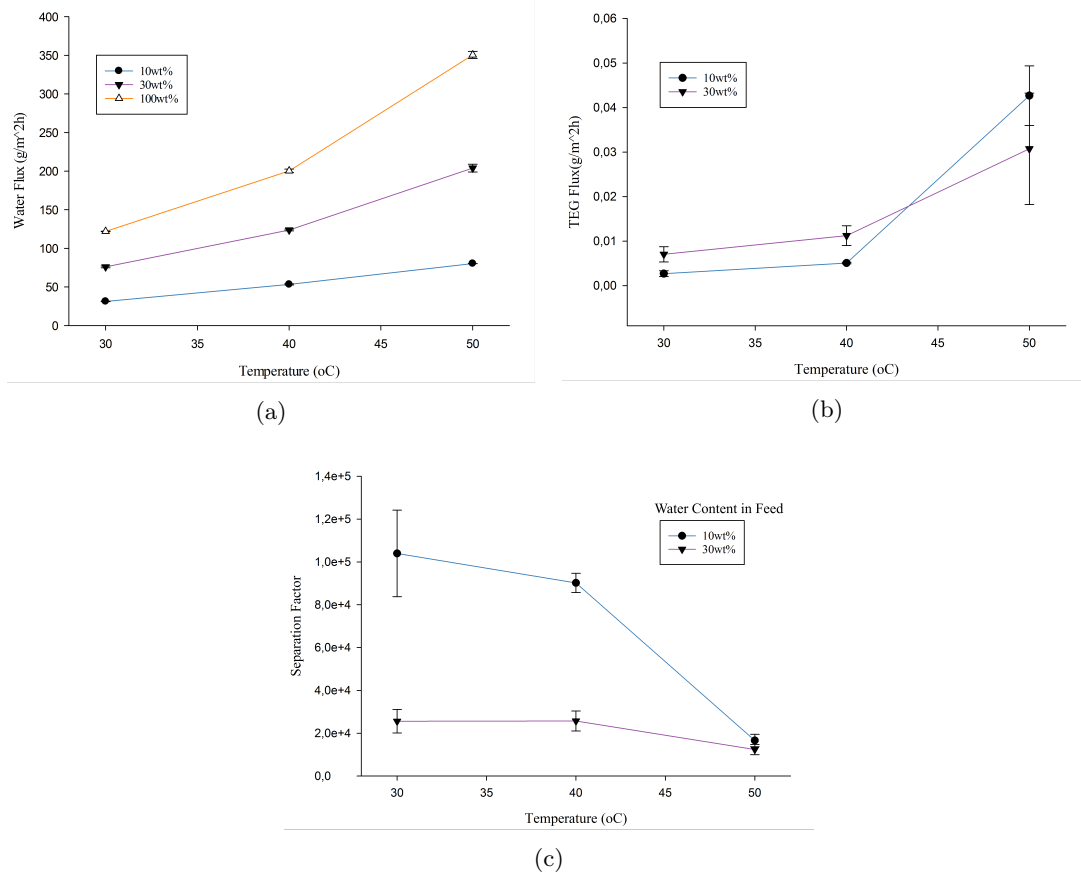


Figure 4.4.6: Effect of temperature on a) Separation factor b) TEG flux c) Selectivity as a ratio of the permeances.

The operating temperature can affect the permeation flux through the membrane in several ways. When increasing the temperature, the saturated vapor pressure of the penetrant will increase, which results in higher driving force and therefore larger mass transport through the membrane. In addition, when increasing the temperature, the diffusion through the membrane enhances. This effect is particularly effective for larger components, such as TEG compared to water, resulting

in more TEG permeation through the membrane at a higher temperature. With an increased temperature, the solubility will decrease. Since water is less condensable than TEG (critical temperature $H_2O \approx 647K$, $TEG > 700K$), water should be affected more by a decrease of solubility. In all, resulting in more TEG permeating through the membrane.

The temperature effect of the separation factor can be seen in Figure 4.4.6c. The graph shows that the separation factor decreases as the temperature is increased. The temperature dependence is more significant when having less water in the feed. This is directly connected to that the TEG flux is enhanced when increasing the temperature.

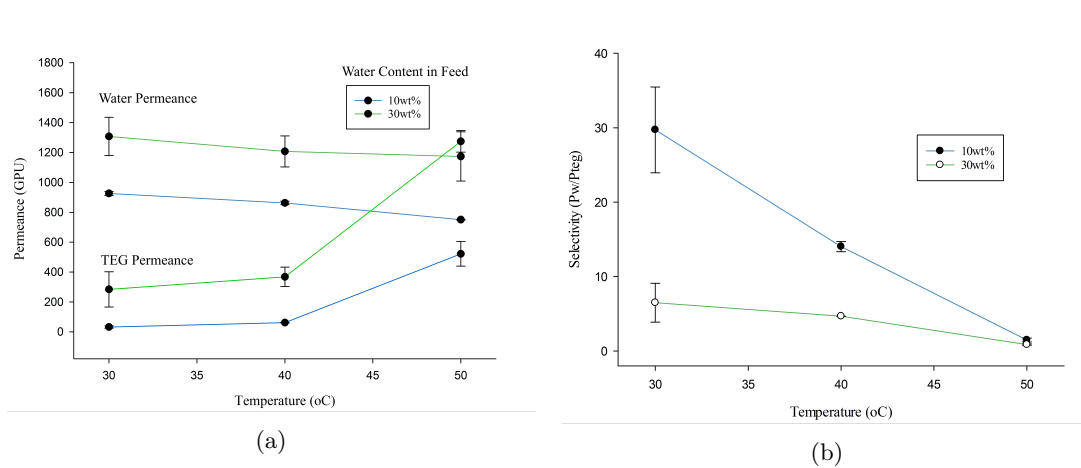


Figure 4.4.7: The effect of temperature on a) permeance and b) ideal selectivity.

The effect of temperature on permeance is shown in Figure 4.4.7a. Both water permeance and TEG permeance are plotted in the same graph. At a feed water concentration of 30wt% and a temperature of 30°C, the water permeance is 1307GPU and the TEG permeance is 284GPU. When increasing the temperature to 50°C, the water permeance becomes 1173GPU and the TEG permeance 1274GPU. At a feed water content of 10wt% and a temperature of 30°C, the water permeance is 926GPU and the TEG permeance is 33GPU. When increasing the temperature to 50°C, the water permeance becomes 751GPU and the TEG permeance 521GPU. The ratio of the permeances or the ideal selectivity is plotted against the temperature in Figure 4.4.7b. As the TEG concentration in the permeate increase with higher temperature, the intrinsic selectivities will consequently decrease. According to the solution-diffusion model, the permeance can be described in terms of solubility and diffusivity. With higher temperature, the diffusion through the membrane will increase. Solubility has rather an opposite effect with temperature. Solubility is normally an exothermic process where higher temperature leads to a lower absorption of the permeant. In view of high free volume of AF2400, the diffusion of penetrant with a large kinetic size (such as TEG) is generally hindered by the glassy nature of the polymer. With a higher temperature, the fraction of free volume will increase and an increase in FFV resulted in high TEG permeance. Based on the results it is expected that the diffusivity has a larger effect on the TEG flux compared to the sorption effect[17].

The temperature dependence of the permeance can be analyzed through an Arrhenius relationship where the logarithmic permeance is plotted against reciprocal temperature, shown in Figure 4.4.8. The slope of the trend line can describe the apparent activation energy, which can quantitatively describe the temperature dependence on the permeance. It is of interest to consider the details in the activation energies due to variations in the mixture composition of water and TEG. The activation energies are dependent on physicochemical properties of the penetrants and the interactions between the permeating components and the polymer.

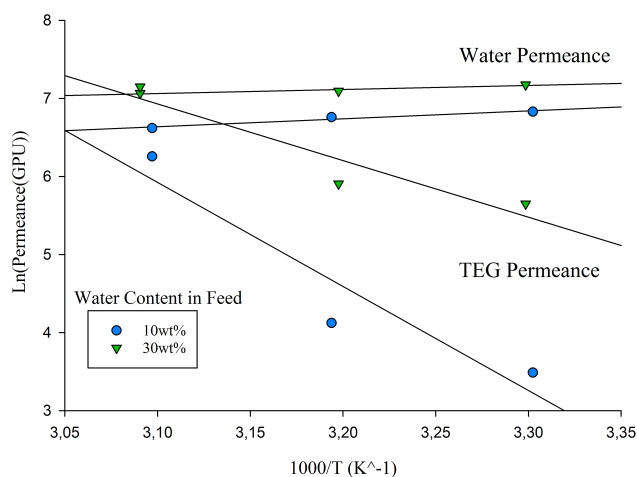


Figure 4.4.8: Arrhenius type of relation with permeance of water and TEG.

The graphs of water permeance show relative good linearity for the experimental data as the values of the regression coefficients R^2 are close to unity (0.95 and 0.92) indicating the experimental data fits the Arrhenius equation well. However, this is not the case with the TEG permeance, in which the regression coefficients R^2 are less than 0.9 (both 0.89) indicating the experimental data to fit the Arrhenius equation to less extent. The reason could be that the limit of detection of TEG in water was reached in GC-MS analysis and the standard deviations are high. At a feed water concentration of 10wt%, the apparent activation energy is -8.45kJ/mol for water and 110.90kJ/mol for TEG. When increasing the feed water concentration to 30wt%, the apparent activation energy for water is -4.29kJ/mol and for TEG 60.26kJ/mol. TEG requires more energy to permeate through the membrane compared to water, which can be explained by the difference in kinetic size of the two components.

4.4.2 Pervaporation performance of PP-AF2400-ZIF-L

Effect of feed composition

To study the effect of the addition of ZIF-L in the membrane on the separation performance, ZIF-L was added to the dense layer of AF2400 and pervaporation experiments were performed. Only the effect of feed composition was tested with the PP-AF2400-ZIF-L membrane with feed water concentration ranging from 10wt% to 30wt% at a temperature of 40°C. All the results were compared with the data obtained from pervaporation experiments with PP-AF2400. When comparing PP-AF2400 and PP-AF2400-ZIF-L it is important to have in mind the differences in membrane thickness of the two membranes since smaller thickness will result in higher flux. The thickness of PP-AF2400-ZIF-L was approximately twice as thick as PP-AF2400, hence expecting twice as high flux through the membrane.

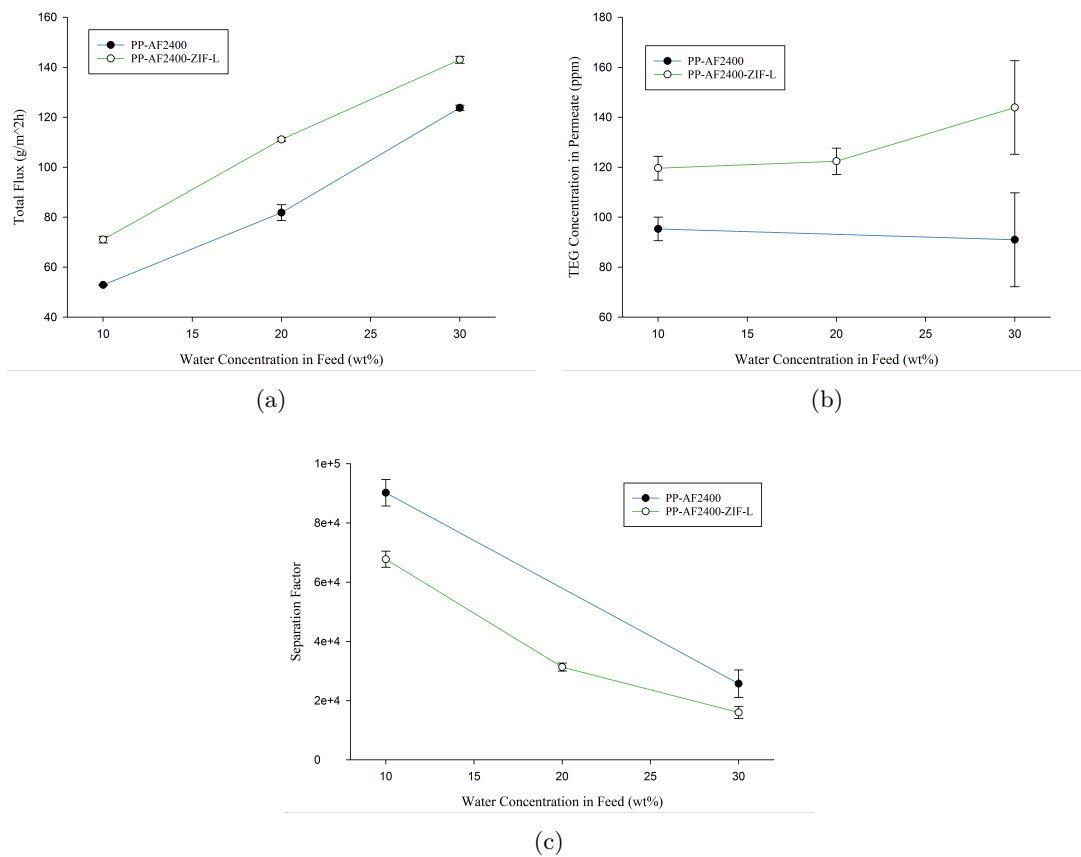


Figure 4.4.9: A comparison of PP-AF2400 with and without ZIF-L. The effect of feed water concentration on a) Total flux b) TEG concentration in permeate d) Separation factor.

The total flux, TEG concentration in the permeate and separation factor are plotted against water concentration in feed in Figure 4.4.9. At a feed water concentration of 30wt% and 10wt%, the total fluxes through the membrane are respectively $143\text{g}/\text{m}^2\text{h}$ and $71\text{g}/\text{m}^2\text{h}$. The TEG concentration in the permeate at a feed water content of 30wt% is 144ppm, whereas with a feed water content of 10wt%, the TEG concentration in the permeate is 120ppm. All the trends with water concentration of the PP-AF2400-ZIF-L membrane are similar to the membrane without ZIF-L particles: total flux increases with water concentration, TEG flux is extremely small, but is slightly enhanced with higher water concentration in feed. In general, the addition of ZIF-L to the dense AF2400 layer enhanced both total flux and TEG concentration in the permeate. Compared to PP-AF2400, the membrane with ZIF-L particles had an increased water flux of $20\text{g}/\text{m}^2\text{h}$ extra, indicating that the addition of the porous ZIF-L particles made the membrane more porous and easier for water to pass. However, the addition of ZIF-L particles also increased the TEG concentration in the permeate resulting in lower separation factor compared to the pure PP-AF2400 membrane. At a feed water concentration of 10wt%, the separation factor was found to be 67800 and at a feed water concentration of 30wt%, the separation factor was 16000.

To examine if the addition of ZIF-L to AF2400 affected the total hydrophilicity of the MMM, compatibility test and contact angle test were performed on AF2400-ZIF-L. The results are presented in Table 4.4.1 and show that the addition of 7wt% ZIF-L in the membrane did not change the uptake of TEG, nor changed the hydrophilicity of the surface. Thus the enhanced flux can not be explained by enhanced hydrophilicity of the surface, but primarily of a more porous structure, letting the water and TEG diffuse easier through the membrane.

Table 4.4.1: Compatibility tests of AF2400-ZIF-L.

	TEG uptake	Contact angle with water
AF2400-ZIF-L (7wt%)	0	$118\pm 6^\circ$

The morphological studies of the PP-AF2400-ZIF-L membrane show that the ZIF-L particles are not homogeneously dispersed into the AF2400 matrix, which could be the explanation of higher TEG flux. If the agglomeration of ZIF-L particles create pores larger than the kinetic diameter of TEG, more TEG could pass and the separation factor will decrease. Liu et al. [36] incorporated both ZIF-L and ZIF-8 particles into sodium alginate (SA) matrix for dehydration of ethanol using pervaporation technology. In their experiment, both separation factor and flux was enhanced, suggesting that the dispersion of ZIF-L particles in the SA matrix was more successful compared to the dispersion of ZIF-L in AF2400. The dispersion of ZIF-L in AF2400 has been shown to be challenging due to the different nature of the polymer (hydrophobic) and the nanoparticles (hydrophilic). As a consequence, more research is required to better the dispersion and to achieve the desirable alignment of ZIF-L particles that creates the so called "water channels". However, the separation factor with AF2400-ZIF-L was a factor of 10^4 larger than the separation factor of the SA-ZIF-L, which can be due to the water swelling of the hydrophilic SA matrix.

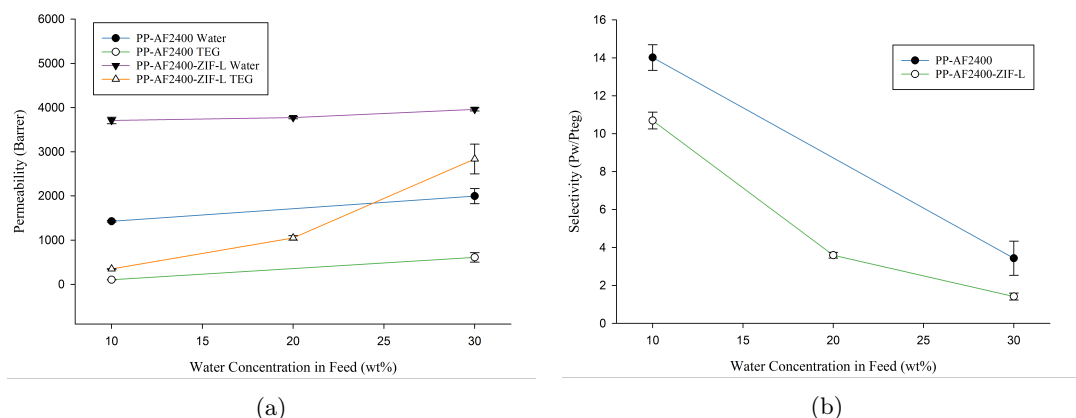


Figure 4.4.10: Effect of water concentration in feed on a) permeability b) ideal selectivity.

The permeabilities of water and TEG are given as a function of the feed water concentration in Figure 4.4.10a. At a water concentration of 10wt%, the water permeability is 3708Barrer and the TEG permeability is 347 Barrer. When increasing the water content in the feed to 30wt%, the water permeability is enhanced to 3959Barrer and the TEG permeability increases to 1890 Barrer. When comparing the PP-AF2400-ZIF-L membrane to the PP-AF2400 membrane, both water permeability and TEG permeability increased with the addition of ZIF-L in the top layer of the composite membrane. In general, the water permeability was enhanced by a factor of 2000 Barrer, which is an impressive improvement of the membranes intrinsic properties. However, the TEG permeability increased when having a higher water content in the feed.

At last, the ratio of the permeabilities as a function of the water concentration are given in Figure 4.4.10b. At a water concentration of 10wt%, the water selectivity is 10.70 and increasing the feed water content to 30%, the water selectivity decreases to 1.4. Similar to the separation factor, the intrinsic selectivities are in general lower with the addition of ZIF-L into the top layer of AF2400, suggesting not perfect dispersion of ZIF-L into the AF2400 matrix and the classical trade-off between selectivity and permeation flux still exists.

4.4.3 Effects of aging

The long-term operational stability of the membrane is a vital factor for industrial applications, and it is especially important as the membrane is intended to be moved for subsea separation. The water flux was studied at three different stages of the continuous pervaporation separation: at the start of the run, at approximately 1000h and at 1500h of aging. The 30°C was studied at 1200h of aging instead of 1500h of aging. The aging data is reported with three temperatures (30, 40 and 50°C) as relative variations of the flux plotted against the aging time measured in hours. At 1000 hours of aging, the total permeation flux of the membranes had decreased by less than 5% for all temperatures and at 1500h of aging, the flux had decreased by 12% for the highest temperature, 3% and 6% for respectively 40°C and 30°C. From literature, it is expected that the highest temperature should show the highest aging rate for AF2400 [110]. This is comparable with the 50°C, however, not with the aging data from 40°C and 30°C. Since the difference is so little between 40°C and 30°C, experimental errors could be the reason for the deviation to the literature data. On the other side, aging of less than 12% is minimal aging, demonstrating the favorable operation stability and suggesting the desirable structural stability of the composite membranes with PP-AF2400.

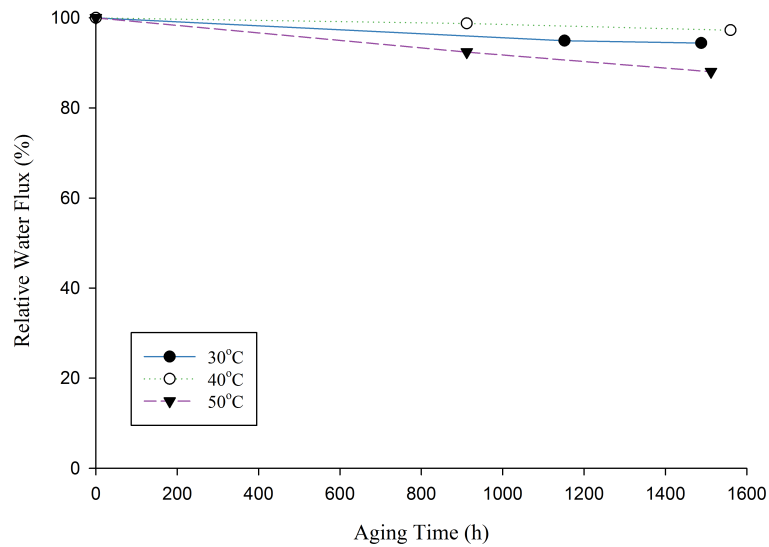


Figure 4.4.11: The relative aging expressed as percentage of the flux relative to the first flux measured plotted against time in hours.

4.4.4 Comparison to literature data

A comparison of the pervaporation data obtained in this study and literature data can be seen from Figure 4.4.12. The research has mainly been focused on the dehydration of MEG, therefore the comparison has been done with literature data of polymeric membranes in the dehydration of EG with pervaporation. As the total flux and separation factor is dependent of temperature and amount of TEG/EG in the feed, all data has been given with it's specific temperature and EG amount in the feed. All data reported has a flat sheet configuration.

The comparison shows that the separation factor obtained in this study is a factor of 100 larger than the separation factors obtained from comparable literature data. As the kinetic size of TEG is larger than MEG, it is expected that the separation factor for dehydration of TEG is larger than for MEG [12]. However, the total flux trough the membrane is amongst the lowest with a total flux less than $150\text{g}/\text{m}^2\text{h}$ for all experiments. The addition of ZIF-L to the polymer matrix enhanced the flux slightly, but more effort should be done to increase the flux. Decreasing the thickness of the dense layer would decrease the resistance and increase the total flux.

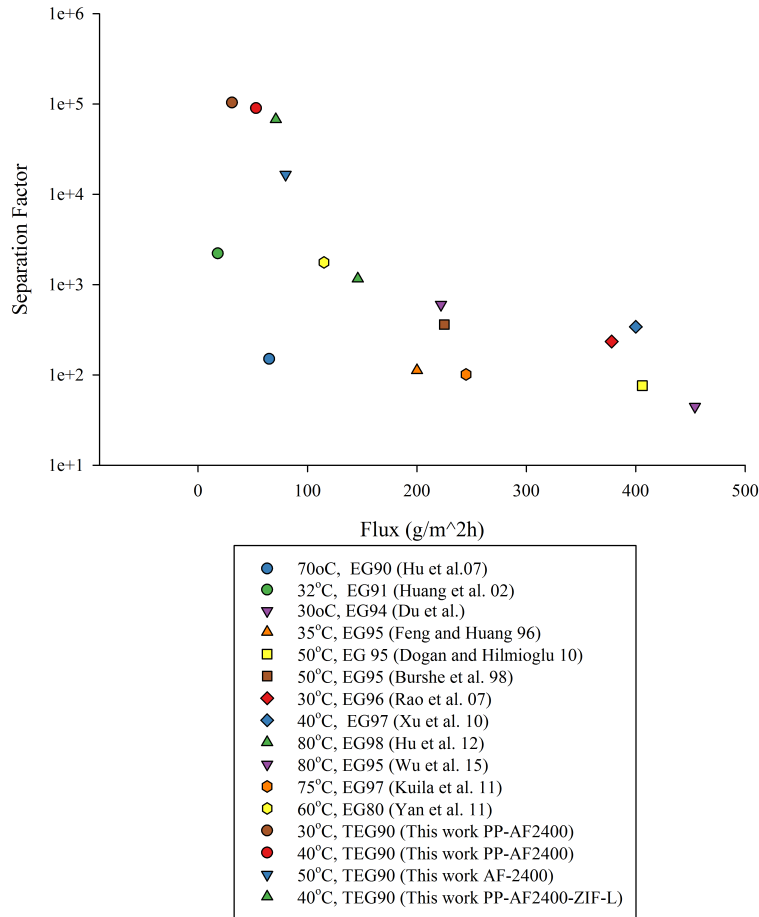


Figure 4.4.12: A comparison of literature data and the obtained data for pervaporation.

4.5 Further membrane development

In this section, possible directions for membrane development have been investigated. Several stages of improvement of the composite membranes were considered. First, the dip coating process of pure AF2400 was examined. Second, a new innovative multi-layered membrane with porous support coated with an inorganic particle layer was examined. Plasma treatment was performed to enhance the adhesion between the porous support and ZIF-L layer. Furthermore, the effect of water exposure to the inorganic ZIF-L layer was studied and the multi-layered membrane was coated with AF2400 to avoid effects of water exposure. Due to the limited amount of time, these membranes have not been tested in terms of pervaporation performance, but they can be considered for further testing in the future.

4.5.1 Optimizing the dip coating process

The dip coating technique was examined. The ideal skin layer should be as thin as possible to enhance high permeation flux, be selective and homogenous without any faults. Three different concentrations of AF2400 were tested with respectively 0.1wt%, 0.5wt% and 1wt% AF2400 in a solution of electronic liquid. The AF2400 layer dipped in 0.1wt%, 0.5wt% and 1wt% AF2400 were respectively measured to be $690\pm 150\text{nm}$, $830\pm 184\text{nm}$ and $1480\pm 230\text{nm}$. Doubling the submerging time with 1wt% AF2400 solution to 20 seconds gave a measured thickness of $1840\pm 240\text{nm}$ and dipping the porous support four times gave a thickness of $2060\pm 380\text{nm}$. The results from the dip coating examination is given in Figure 4.5.1. All the thin skin layers of AF2400 were observed to have a uniform character and covering the porous support, which indicates that it is possible to coat thinner AF2400 layers with the dip coating process.

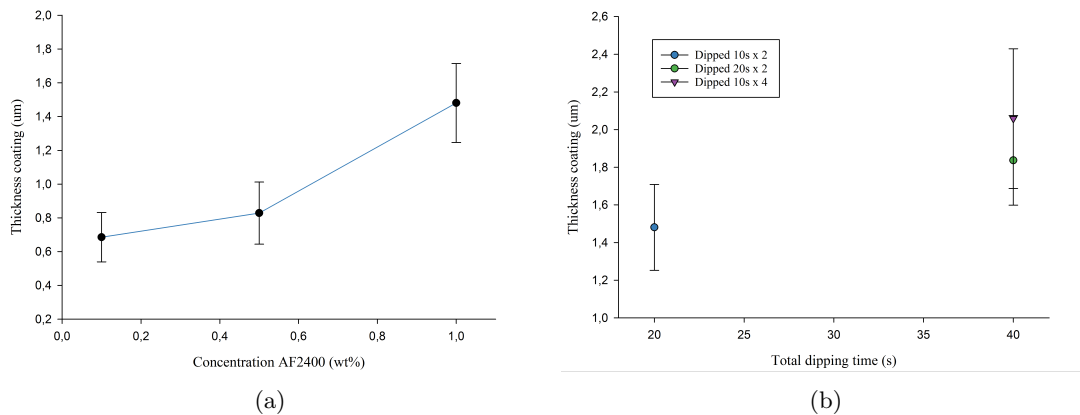


Figure 4.5.1: Examination of the dip coating technique. a) Thickness of coating as a function of AF2400 concentration. b) Thickness of coating as a function of total dipping time.

4.5.2 Multi-layered membrane development

Porous support with an inorganic particle layer

One part of this project was to develop new, innovative membranes for future pervaporation study. This was a first attempt of making multi-layered composite membranes with inorganic ZIF layer on polymer support. A morphological study was performed on the membranes made, in which cross-sectional images are vital to understand the compatibility between the layers. The ideal multi-layered membrane should consist of a low-cost, mechanically stable porous support, and a thin selective particle layer with an alignment that creates water channels, which render the molecular sieving effect for water molecules [36, 59]. If the nanoparticles are sensitive to the liquid environment, a thin protective polymer layer can be coated on top of the crystalline ZIF layer.

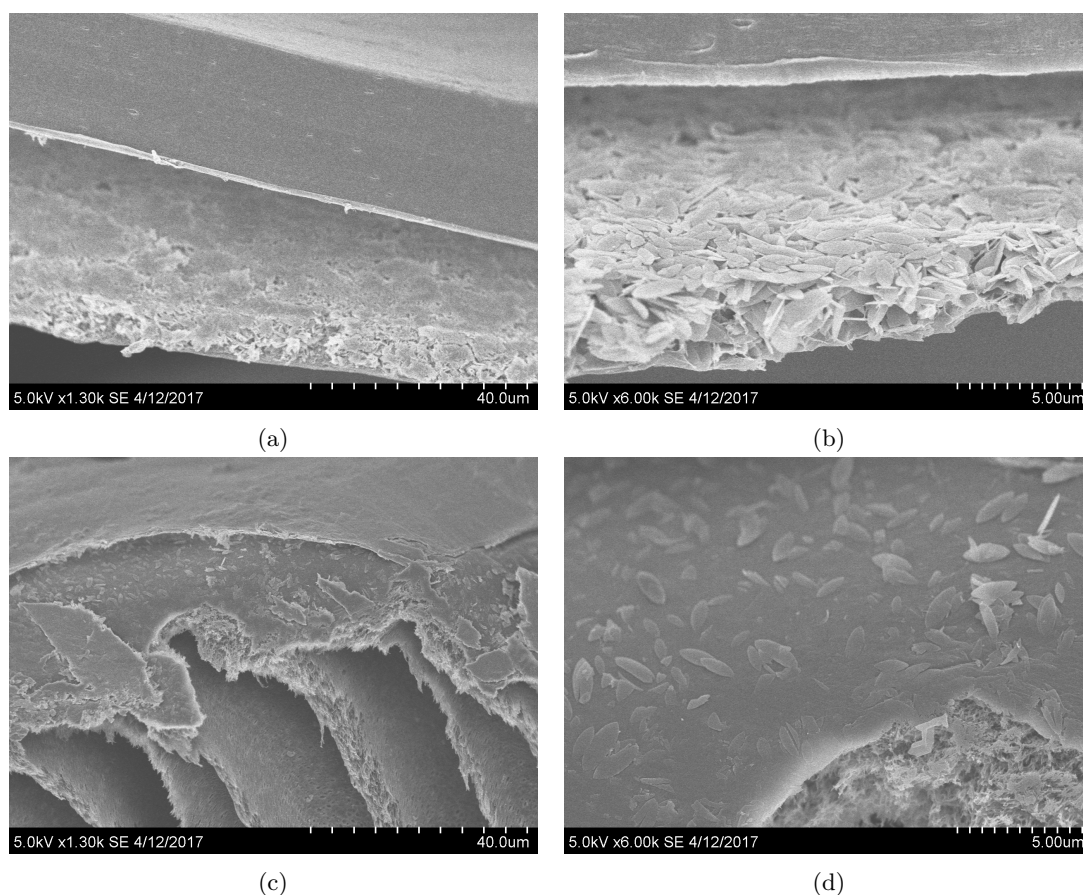


Figure 4.5.2: S(T)EM images of multi-layered membranes with PP and a crystalline layer of ZIF-L. a) and b) Cross-sectional PP with a crystalline layer of ZIF-L. c) and d) Cross-sectional images of PSf with a crystalline layer of ZIF-L.

Polypropylene (PP) and Polysulfone (PSf) were coated with ZIF-L particles and the cross-sectional S(T)EM images are given in Figure 4.5.2. The thickness of the crystalline particle layers were measured to be $2.1 \pm 0.4 \mu\text{m}$ for the PP membrane and $0.2 \pm 0.1 \mu\text{m}$ for the PSf membrane. From Figure 4.5.2a-4.5.2b, the cross section of PP with ZIF-L particle layer is given. The particle layer on the PP is indicated uniform stacking of ZIF-L nanosheets, suggesting that using ZIF-L as a particle layer is promising in the development of future multi-layered membranes. However, a large interfacial gap can be observed between the PP support and the ZIF-L layer, indicating poor adhesion between PP and crystalline ZIF-L layer. Modification of the polymer support is needed to enhance the adhesion between the porous support and the ZIF-L layer, or choose another porous support with better compatibility to ZIF-L layer. A similar poor adhesion was also observed when coating PP with ZIF-8.

Figure 4.5.2c-4.5.2d give the membrane morphology of the PSf membrane with a crystalline ZIF-L layer. Since the pore size of the PSf membrane is much larger than for PP, it is logical that the ZIF-L particles will intrude the pore structure of PSf. The effect of ZIF-L inside of the pore structure of PSf could enhance water flux with higher porosity or decrease the water flux with a blockage of the open pore structure [37, 111]. However, the purpose of this study was to develop new multi-layered membranes for the TEG-water separation and to achieve a layer of ZIF-L on top of polysulfone, hence a solution is to add an ultra-thin polymer layer on PSf before growing ZIF-L particles.

Plasma treatment to improve of adhesion between PP and particle layer

With the intention to enhance the adhesion between PP and the crystalline ZIF-L layer, plasma treatment was performed on the PP surface. The PP membrane surface was treated with oxygen plasma, which should enhance the hydrophilic character of the membrane surface and possibly change the pore structure of the porous support. Figure 4.5.3 illustrates the effect of plasma treatment to the surface of the PP support, which is measured by contact angle measurements. The untreated porous support had a contact angle with water of $113 \pm 3^\circ$ and with 8 minutes of oxygen plasma the angle was measured to be $43 \pm 1^\circ$. The surface was transformed from hydrophobic to hydrophilic.

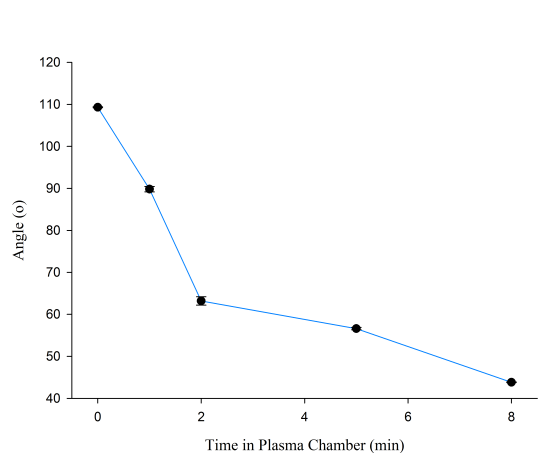


Figure 4.5.3: The effect of plasma treatment on the contact angles of water on PP.

In addition, the plasma treated PP was coated with a crystalline layer of ZIF-l and cross-sectional images of the multi-layered membrane before and after plasma treatment can be found in Figure 4.5.4. Before plasma treatment, the interface between PP and ZIF-L was observed to be smooth with a large interfacial gap between the layers, while with oxygen plasma treatment, the surface was more rough and the ZIF-L flakes were attached to the PP surface. The improvement of adherence between the layers is most likely due to the change in surface pore structure of the PP. On the other side, visual inspections of the membrane adhesion did not show any difference before and after plasma treatment, where the crystalline layer detached easily under stress. Pictures of the detachment of the crystalline layer are shown in Figure B-.0.1 in Appendix B.

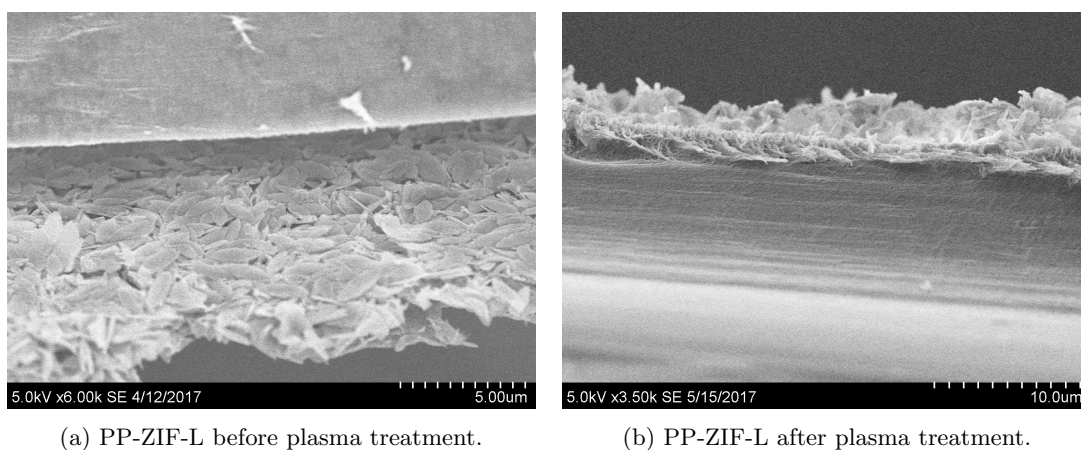


Figure 4.5.4: Effect of plasma treatment on adhesion between PP and ZIF-L. a) Before plasma treatment. b) After plasma treatment.

Effect of water exposure

In the development of composite membranes, it was observed that the ZIF particles were affected by the exposure of liquid water. This was further investigated by washing the crystalline layer of ZIF-L with water for 2.5 hours. In addition, the crystalline layers of ZIF-L and ZIF-8 were exposed to 100% humidity over 10 days. S(T)EM pictures were taken before and after the water wash, and the morphological differences were observed.

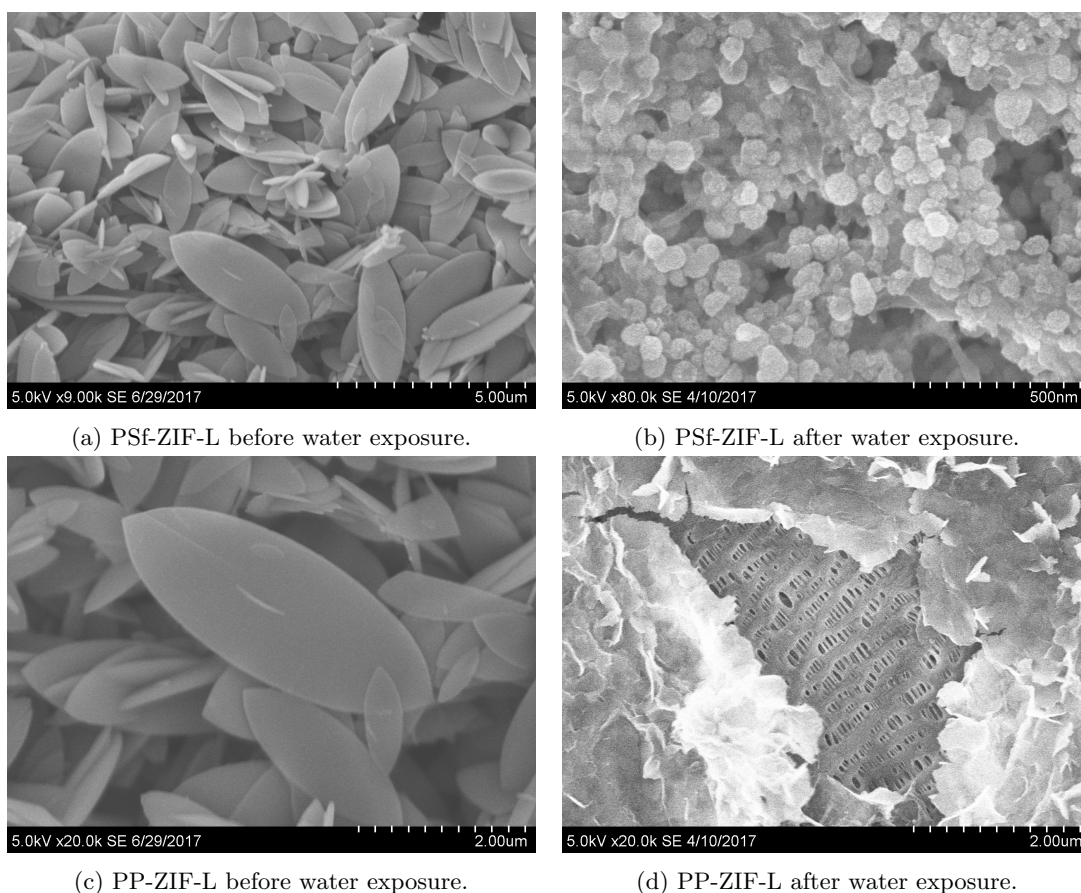


Figure 4.5.5: S(T)EM surface images of ZIF-L particles before and after liquid water exposure. a) Porous support of PP and ZIF-L layer before water exposure. b) Porous support of PP and ZIF-L layer after water exposure. c) Porous support of PSf and ZIF-L layer before water exposure. d) Porous support of PSf and ZIF-L layer before water exposure.

Figure 4.5.5a - 4.5.5b show surface images of polypropylene coated with crystalline ZIF-L layer before and after water exposure and Figure 4.5.5c - 4.5.5d give surface images of polysulfone coated with ZIF-L before and after water exposure. Before water wash, the ZIF-L particles had the distinct leaf shape with a particle size of $1.9 \pm 0.9 \mu\text{m}$, while after water wash the particles consisted either of a dense layer or a particle layer with circular particles in the size $73 \pm 12 \text{nm}$. The dense layer was created when the thickness of the ZIF-L layer was less than $1 \mu\text{m}$, suggesting further degradation of the ZIF-L particles. The circular particles of the washed ZIF-L resemble the shape and size of the ZIF-8 particles [112].

S(T)EM images of the ZIF-L crystalline layer that was exposed to 100% humidity for 10 days can be found in Figure 4.5.6. The ZIF-L particles were partly chopped, but the ZIF-L shape was still intact. ZIF-8 was also exposed to 100% humidity for 10 days, but no change was observed through S(T)EM characterization.

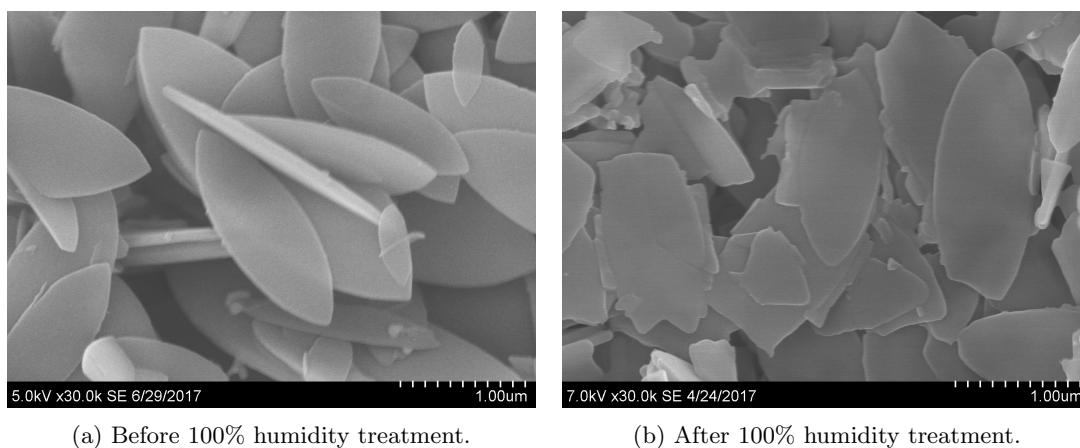


Figure 4.5.6: Effect of 100% humidity on ZIF-L particle layer. a) ZIF-L layer before humidity exposure. b) ZIF-L layer after humidity exposure.

To determine the particle degradation, more research is required with other analytical tools, such as X-ray diffraction (XRD) for identifying crystal structure or Fourier transform infrared spectroscopy (FT-IR) to examine the chemical species present in the samples. Contradicting results of the degradation of ZIF-8 have been found. Zhang et al. [67] confirmed that the ZIF-8 crystals can degrade in water due to the dissolution of ZIF-8, while Park et al. [68] reported no change in crystallinity or porosity of the ZIF-8 particles after water exposure. No research has been found on the degradation of ZIF-L, however, it is reasonable to predict same effect since the ZIFs consist of the same building blocks. On the other side, degradation of a crystalline layer could be different compared to MMM with the same ZIF particles. No research has been found on the degradation of ZIFs in MMM. For this study, the degradation of ZIF-L particles with water exposure indicates the importance of complete polymer cover of the ZIF particles in the MMM. Of that reason, a protective layer of AF2400 was coated on top of the ZIF-L particle layer and S(T)EM images of multi-layered membranes with AF2400 can be found in Figure 4.5.7.

Porous support coated with an inorganic particle layer and a AF2400 layer

Due to water degradation, multi-layered membranes with a protective layer of AF2400 on top of the ZIF-L layer were made. The membranes were washed with water for 2.5 hours, dried and morphology was studied. Cross-sectional S(T)EM images of the membranes after water wash can be seen in Figure 4.5.7a-4.5.7b with respectively PP and PSf as porous support. The top layer of AF2400 show exceptional good adhesion to the crystalline ZIF-L layer, which is a promising founding for further membrane development of multi-layered membranes. Furthermore, the morphology of the ZIF-L layer was not affected by water washing, indicating well covered AF2400 layer and potential for the use in future pervaporation studies.

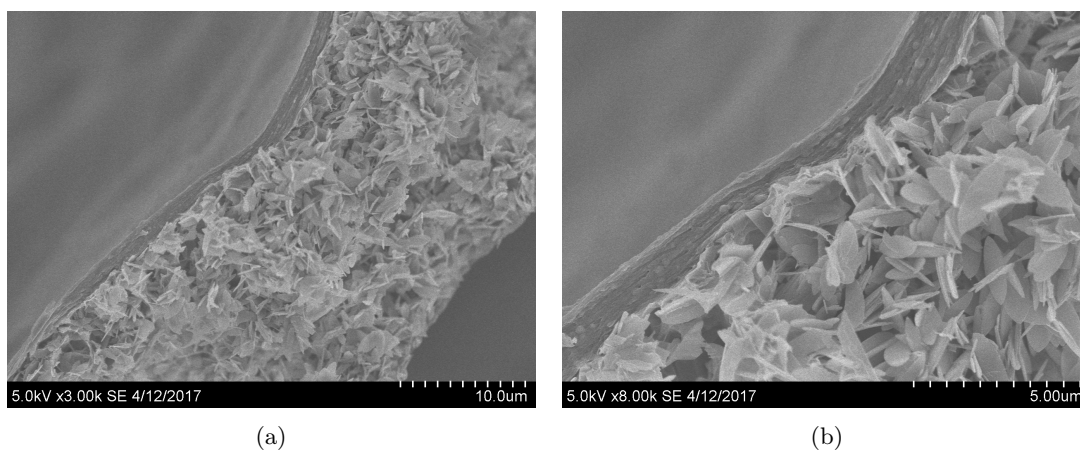


Figure 4.5.7: S(T)EM images of multi layered membrane with PP-ZIF-L coated with a layer of AF2400.

Chapter 5

Conclusion

The aim of this thesis was to examine the use of pervaporation technology with membranes for the regeneration of Triethylene glycol (TEG) in natural gas dehydration. Experimental data for pervaporation is needed as there exist minimal literature for the dehydration of TEG with pervaporation technology.

The first part was to identify membrane materials suitable for pervaporation of TEG-water solutions. Compatibility tests confirmed AF2400 as a suitable membrane material for pervaporation with 0% TEG uptake and contact angles higher than 90° for TEG and water. Morphological characterization with SEM/S(T)EM proved successful coating of PP with AF2400 with a thickness of $1.7 \pm 0.3 \mu\text{m}$. ZIF-L nanoparticles in AF2400 were well dispersed after sonicating 8x40minutes. The membrane with ZIF-L particles was therefore further tested in pervaporation studies.

Pervaporation experiments with PP-AF2400 were performed and effect of temperature and feed water concentration were studied. Results obtained from the pervaporation study show excellent separation factor of water from TEG (>10000), but rather low water flux through the membrane. With 10% water content in the feed the water flux was measured to be $31.28 \text{g}/\text{m}^2\text{h}$ with 30°C and increased proportionally with increasing temperature to $80.26 \text{g}/\text{m}^2\text{h}$ with 50°C. The water flux also increased with higher water content in the feed from $14.58 \text{g}/\text{m}^2\text{h}$ with 1% feed water content to $201.61 \text{g}/\text{m}^2\text{h}$ with 30% water in the feed at 50°C. The amount of TEG in the permeate was extremely low (between 72ppm and 864ppm) and increased slightly with increasing temperature and decreased with higher water content in the feed. The water permeance enhanced with with higher temperature and was found to be 54.01GPU at 30°C at 10% feed water content, increasing to 862.11GPU at 50°C. As the TEG amount in the permeate increased with increased temperature, the TEG permeance also increased from 32.69GPU at 10% feed water content at 30°C, increasing to 521.74GPU at 50°C, resulting in a selectivity of less than 1 when studying the intrinsic selectivity. The membrane showed long-term stability as the pervaporation experiments were performed over a time span of 1500 hours.

The effect of adding ZIF-L nanoparticles to the dense layer of AF2400 in the composite membrane was studied with different feed water concentrations. All the pervaporation experiments with PP-AF2400-ZIF-L were performed with a temperature of 40°C. The addition of ZIF-L enhanced the water flux through the membrane from $53.33 \text{g}/\text{m}^2\text{h}$ with PP-AF2400 to $71.02 \text{g}/\text{m}^2\text{h}$ with PP-AF2400-ZIF-L with a feed water concentration of 90%. However, more TEG was found in the

permeate with the addition of ZIF-L, resulting in a lower separation factor. The TEG permeability was increasing from 101.87 Barrer with PP-AF2400 to 347.05 Barrer for PP-AF2400-ZIF-L, resulting in a lower intrinsic selectivity compared to the PP-AF2400 membrane. In addition, the water permeability also increased from 2160.19 Barrer for PP-AF2400 to 3708.60 Barrer for PP-AF2400-ZIF-L. On the other side, the separation factor was still extremely high (>10000), suggesting that the addition of ZIF-L to the composite membrane with PP and AF2400 enhanced the overall separation performance of the membrane.

In addition, improvement and investigation of membrane factors were performed. The dip coating technique was optimized, in which 1wt% AF2400 solution dipped 10seconds x 2 was found to give a thin and uniform AF2400 layer on PP. Innovative multi-layered membranes were examined, in which the best membrane found was a plasma treated PP with ZIF-L layer and a protective AF2400 layer. It was also found that ZIF-L particles are affected by water exposure, hence it is important to cover the ZIF-L particles with AF2400.

The present work clearly showed that AF2400 thin composite membranes are suitable to be used in pervaporation for TEG dehydration in subsea conditions, as they comply with subsea requirements. Further developments need to be done to optimize the membrane performance, but the results clearly identified a suitable membrane design for subsea operation.

Chapter 6

Suggestions for Future Research

Due to minimal information on dehydration of TEG by pervaporation, more experimental pervaporation data is required. In this study, composite membranes with Teflon AF2400 with and without nanoparticles were tested. The chemical compatibility tests showed that PDMS did not suffer any TEG uptake, hence PDMS can be tested as a membrane material in pervaporation membranes. To increase the permeation fluxes through the membrane, a thinner layer of AF2400 on PP can be tested in pervaporation. A suggestion is to coat the PP with 0.1wt% solution of AF2400, as this layer had a uniform character and covered the porous support. A thinner layer of AF2400 with ZIF-L particles is also worth testing. Further research is needed to improve the dispersion of nanoparticles in the AF2400 matrix. ZIF-L particles should not be partly chopped, which was observed in this study. Less ZIF-8 particle aggregation is necessary to test PP-AF2400-ZIF-8.

With the GC/MS, a column specialized for glycols can be tested to achieve a lower detection limit and quantitation limit for TEG in water. After suggestions from the supplier of GC/MS equipment, another split liner is suggested: "R23312 Topaz Liner Cyclosplitter 4mm x 6.3 x 78.5 for Agilent GCs".

With the multi-layered membranes, the plasma treated PP membrane with thin ZIF-L layer coated with AF2400 can be tested in pervaporation experiments. Another suggestion is to have a mixed matrix membrane of ZIF-L and AF2400 on top of the ZIF-L particle layer to enhance permeation flux and adhesion between the ZIF-L layer and the protective layer of AF2400. In addition, to determine how water affects the ZIF-L, more research is required. Analytical tools suggested are: X-ray diffraction (XRD) for identifying crystal structure or Fourier transform infrared spectroscopy (FT-IR) to examine the chemical species present in the samples.

Bibliography

- [1] Chapter 9 - natural gas dehydration. In Poe William A. Speight James G. Mokhatab, Saeid, editor, *Handbook of Natural Gas Transmission and Processing*, pages 323 – 364. Gulf Professional Publishing, Burlington, 2006.
- [2] Richard W. Baker and Kaaeid Lokhandwala. Natural gas processing with membranes: an overview. *Industrial & Engineering Chemistry Research*, 47(7):2109–2121, 2008.
- [3] Maurice Stewart and Ken Arnold. Part 2 - dehydration considerations. In Arnold Ken Stewart, Maurice, editor, *Gas Dehydration Field Manual*, pages 55 – 168. Gulf Professional Publishing, Boston, 2011.
- [4] Arthur L. Kohl and Richard B. Nielsen. Chapter 15 - membrane permeation processes. In Nielsen Richard B. Kohl, Arthur L., editor, *Gas Purification (Fifth Edition)*, pages 1238 – 1295. Gulf Professional Publishing, Houston, fifth edition edition, 1997.
- [5] Colin A. Scholes, Geoff W. Stevens, and Sandra E. Kentish. Membrane gas separation applications in natural gas processing. *Fuel*, 96:15 – 28, 2012.
- [6] Pervaporation versus evaporation. In Karl Wilhelm Bøddeker, editor, *Liquid Separations with Membranes: An introduction to barrier interference*, volume 11 of *Springer Berlin Heidelberg*, pages 81–104. Elsevier, 2008.
- [7] Bart Van der Bruggen and Patricia Luis. Chapter four - pervaporation. In Steve Tarleton, editor, *Progress in Filtration and Separation*, pages 101 – 154. Academic Press, Oxford, 2015.
- [8] P. Vandezande. 5 - next-generation pervaporation membranes: recent trends, challenges and perspectives. In Figoli Alberto Basile, Angelo and Mohamed Khayet, editors, *Pervaporation, Vapour Permeation and Membrane Distillation*, Woodhead Publishing Series in Energy, pages 107 – 141. Woodhead Publishing, Oxford, 2015.
- [9] Yu Huang, Jennifer Ly, Dung Nguyen, and Richard W. Baker. Ethanol dehydration using hydrophobic and hydrophilic polymer membranes. *Industrial & Engineering Chemistry Research*, 49(23):12067–12073, 2010.
- [10] Günter Dlubek, Jürgen Pionteck, Klaus Rätzke, Jan Kruse, and Franz Faupel. Temperature dependence of the free volume in amorphous teflon AF1600 and AF2400: A pressure-volume-temperature and positron lifetime study. *Macromolecules*, 41(16):6125–6133, 2008.
- [11] Roald R. Akberov, Azat R. Fazlyev, Alexander V. Klinov, Alexander V. Malygin, Mansur I. Farakhov, and Vera A. Maryakhina. Pervaporation technology for regeneration of diethy-

- lene glycol at russian complex gas treatment plants with the use of ceramic membranes hybsi. *Journal of Natural Gas Science and Engineering*, 26:670 – 682, 2015.
- [12] Kristin Dalane, Zhongde Dai, Gro Mogseth, Magne Hillestad, and Liyuan Deng. Potential applications of membrane separation for subsea natural gas processing: A review. *Journal of Natural Gas Science and Engineering*, 39:101 – 117, 2017.
- [13] Baker and Richard W. *Wiley*. Imperial College Press, 3 edition, 2014.
- [14] P. Shao and R.Y.M. Huang. Polymeric membrane pervaporation. *Journal of Membrane Science*, 287(2):162 – 179, 2007.
- [15] Xu and Tongwen. *Advances in Membrane Science and Technology*. Nova, New York, US, ninth dover printing, tenth gpo printing edition, 2009.
- [16] Haiqing Lin, Scott M. Thompson, Adrian Serbanescu-Martin, Johannes G. Wijmans, Karl D. Amo, Kaaeid A. Lokhandwala, Bee Ting Low, and Timothy C. Merkel. Dehydration of natural gas using membranes. part ii: Sweep/countercurrent design and field test. *Journal of Membrane Science*, 432:106 – 114, 2013.
- [17] J. Mulder. *Basic Principles of Membrane Technology*. Springer Netherlands, 2 edition, 1996.
- [18] J.G. Crespo and C. Brazinha. 1 - fundamentals of pervaporation. In Figoli Alberto Basile, Angelo and Mohamed Khayet, editors, *Pervaporation, Vapour Permeation and Membrane Distillation*, Woodhead Publishing Series in Energy, pages 3 – 17. Woodhead Publishing, Oxford, 2015.
- [19] Peter M. Budd. *High Free Volume Polymer*, pages 1–3. Springer Berlin Heidelberg, Berlin, Heidelberg, 2015.
- [20] Yan Wang, Tai Shung Chung, Bernard Weijie Neo, and Michael Gruender. Processing and engineering of pervaporation dehydration of ethylene glycol via dual-layer polybenzimidazole (pbi)/polyetherimide (pei) membranes. *Journal of Membrane Science*, 378(1–2):339 – 350, 2011. Membranes for a Sustainable Future Section.
- [21] A. Figoli, S. Santoro, F. Galiano, and A. Basile. 2 - pervaporation membranes: preparation, characterization, and application. In Angelo Basile, , Alberto Figoli, and Mohamed Khayet, editors, *Pervaporation, Vapour Permeation and Membrane Distillation*, Woodhead Publishing Series in Energy, pages 19 – 63. Woodhead Publishing, Oxford, 2015.
- [22] In Steve Tarleton, editor, *Progress in Filtration and Separation*, pages 671 – 684. Academic Press, Oxford, 2015.
- [23] Congli Yu, Chao Zhong, Yanmei Liu, Xuehong Gu, Gang Yang, Weihong Xing, and Nanping Xu. Pervaporation dehydration of ethylene glycol by naa zeolite membranes. *Chemical Engineering Research and Design*, 90(9):1372 – 1380, 2012.
- [24] Ruili Guo, Changlai Hu, Fusheng Pan, Hong Wu, and Zhongyi Jiang. Pva–gptms/teos hybrid pervaporation membrane for dehydration of ethylene glycol aqueous solution. *Journal of Membrane Science*, 281(1–2):454 – 462, 2006.
- [25] Hacer Dogan and Nilufer Durmaz Hilmioglu. Chitosan coated zeolite filled regenerated cellulose membrane for dehydration of ethylene glycol/water mixtures by pervaporation. *Desalination*, 258(1–3):120 – 127, 2010.

- [26] R. R. Akberov, A. R. Fazlyev, A. V. Klinov, A. V. Malygin, M. I. Farakhov, V. A. Maryakhina, and S. M. Kirichenko. Dehydration of diethylene glycol by pervaporation using hybsi ceramic membranes. *Theoretical Foundations of Chemical Engineering*, 48(5):650–655, 2014.
- [27] H.M. van Veen, Y.C. van Delft, C.W.R. Engelen, and P.P.A.C. Pex. Dewatering of organics by pervaporation with silica membranes. *Separation and Purification Technology*, 22–23:361 – 366, 2001.
- [28] Weixin Zhang, Yunpan Ying, Jing Ma, Xiangyu Guo, Hongliang Huang, Dahuan Liu, and Chongli Zhong. Mixed matrix membranes incorporated with polydopamine-coated metal-organic framework for dehydration of ethylene glycol by pervaporation. *Journal of Membrane Science*, 527:8 – 17, 2017.
- [29] Yoshio Morigami, Masakazu Kondo, Jun Abe, Hidetoshi Kita, and Kenichi Okamoto. The first large-scale pervaporation plant using tubular-type module with zeolite naa membrane. *Separation and Purification Technology*, 25(1–3):251 – 260, 2001.
- [30] Avelino Corma, Fernando Rey, Jordi Rius, Maria J. Sabater, and Susana Valencia. Supramolecular self-assembled molecules as organic directing agent for synthesis of zeolites. *Nature*, 431(7006):287–290, 09 2004.
- [31] Anne Julbe. Chapter 6 - zeolite membranes – synthesis, characterization and application. In Avelino Corma Jiří Čejka, Herman van Bekkum and Ferdi Schüth, editors, *Introduction to Zeolite Science and Practice*, volume 168 of *Studies in Surface Science and Catalysis*, pages 181 – 219. Elsevier, 2007.
- [32] Mengdong Jia, Klaus-Viktor Peinemann, and Rolf-Dieter Behling. Molecular sieving effect of the zeolite-filled silicone rubber membranes in gas permeation. *Journal of Membrane Science*, 57(2):289 – 292, 1991.
- [33] L. Donato, A. Garofalo, and C. Algieri. 3 - mixed-matrix membranes: Preparation and characterization for biorefining. In Alberto Figoli, , Alfredo Cassano, , and Angelo Basile, editors, *Membrane Technologies for Biorefining*, pages 61 – 84. Woodhead Publishing, 2016.
- [34] K.D. Byrne, W.S. Schmitt, and G.J.P. Fleming. Preparation of metal organic frameworks for reinforcement of glass-ionomer restoratives. *Dental Materials*, 30, Supplement 1:e71 – e72, 2014. Abstracts of the Academy of Dental Materials Annual Meeting, 8-11 October 2014 - Bologna, Italy.
- [35] Anh Phan, Christian J. Doonan, Fernando J. Uribe-Romo, Carolyn B. Knobler, Michael O’Keeffe, and Omar M. Yaghi. Synthesis, structure, and carbon dioxide capture properties of zeolitic imidazolate frameworks. *Accounts of Chemical Research*, 43(1):58–67, 2010. PMID: 19877580.
- [36] Keteng Cao Sankar Nair Xuanxuan Cheng Jing Zhao Hassan Gomaa Hong Wu Guan-hua Liu, Zhongyi Jiang and Fusheng Pan. Pervaporation performance comparison of hybrid membranes filled with two-dimensional ZIF-L nanosheets and zero-dimensional ZIF-8 nanoparticles. *Journal of Membrane Science*, 523:185 – 196, 2017.
- [37] Theodore T. Moore and William J. Koros. Non-ideal effects in organic–inorganic materials for gas separation membranes. *Journal of Molecular Structure*, 739(1):87 – 98, 2005. smart membranes and molecular cavity.

- [38] Isabelle Masselin, Xavier Chasseray, Laurence Durand-Bourlier, Jean-Michel Lainé, Pierre-Yves Syzaret, and Daniel Lemordant. Effect of sonication on polymeric membranes. *Journal of Membrane Science*, 181(2):213 – 220, 2001.
- [39] L. Ansaloni and L. Deng. 7 - advances in polymer-inorganic hybrids as membrane materials. In P.M. Visakh, Gordana Markovic, and Daniel Pasquini, editors, *Recent Developments in Polymer Macro, Micro and Nano Blends*, pages 163 – 206. Woodhead Publishing, 2017.
- [40] Z. Gao, Y. Yue, and W. Li. Application of zeolite-filled pervaporation membrane. *Zeolites*, 16(1):70 – 74, 1996.
- [41] Crystallography Open Database. Zif-8 metal organic framework. <http://www.chemtube3d.com/solidstate/MOF-ZIF8.htm>, 2017. [Online; accessed 11-July-2017].
- [42] Guorong Wu, Mingchen Jiang, Tingting Zhang, and Zhiqian Jia. Tunable pervaporation performance of modified mil-53(al)-nh₂/poly(vinyl alcohol) mixed matrix membranes. *Journal of Membrane Science*, 507:72 – 80, 2016.
- [43] Rizhi Chen, Jianfeng Yao, Qinfen Gu, Stef Smeets, Christian Baerlocher, Haoxue Gu, Dunru Zhu, William Morris, Omar M. Yaghi, and Huanting Wang. A two-dimensional zeolitic imidazolate framework with a cushion-shaped cavity for co₂ adsorption. *Chem. Commun.*, 49:9500–9502, 2013.
- [44] Rizhi Chen Zexian Low Ming He Jefferson Zhe Liu Zhaoxiang Zhong, Jianfeng Yao and Huanting Wang. Oriented two-dimensional zeolitic imidazolate framework-1 membranes and their gas permeation properties. *The Royal Society of Chemistry*, 3:15715–15722, 2015.
- [45] Changlai Hu, Ruili Guo, Ben Li, Xiaocong Ma, Hong Wu, and Zhongyi Jiang. Development of novel mordenite-filled chitosan–poly(acrylic acid) polyelectrolyte complex membranes for pervaporation dehydration of ethylene glycol aqueous solution. *Journal of Membrane Science*, 293(1–2):142 – 150, 2007.
- [46] Sara Sorribas, Alina Kudasheva, Eduardo Almendro, Beatriz Zornoza, Óscar de la Iglesia, Carlos Téllez, and Joaquín Coronas. Pervaporation and membrane reactor performance of polyimide based mixed matrix membranes containing mof hkust-1. *Chemical Engineering Science*, 124:37 – 44, 2015. Metal-Organic Frameworks for Emerging Chemical Technologies.
- [47] Chao-Hsiang Kang, Yi-Feng Lin, Yao-Sheng Huang, Kuo-Lun Tung, Kai-Shiun Chang, Jung-Tsai Chen, Wei-Song Hung, Kueir-Rarn Lee, and Juin-Yih Lai. Synthesis of ZIF-7/chitosan mixed-matrix membranes with improved separation performance of water/ethanol mixtures. *Journal of Membrane Science*, 438:105 – 111, 2013.
- [48] Dihua Wu, Jeff Martin, Jennifer Du, Yufeng Zhang, Darren Lawless, and Xianshe Feng. Thin film composite membranes comprising of polyamide and polydopamine for dehydration of ethylene glycol by pervaporation. *Journal of Membrane Science*, 493:622 – 635, 2015.
- [49] P.T. Nguyen, E. Lasseguette, Y. Medina-Gonzalez, J.C. Remigy, D. Roizard, and E. Favre. A dense membrane contactor for intensified {CO₂} gas/liquid absorption in post-combustion capture. *Journal of Membrane Science*, 377(1–2):261 – 272, 2011.

- [50] Tao Li, Yichang Pan, Klaus-Viktor Peinemann, and Zhiping Lai. Carbon dioxide selective mixed matrix composite membrane containing ZIF-7 nano-fillers. *Journal of Membrane Science*, 425:235 – 242, 2013.
- [51] Darren Bradshaw, Ashesh Garai, and Jia Huo. Metal-organic framework growth at functional interfaces: thin films and composites for diverse applications. *Chem. Soc. Rev.*, 41:2344–2381, 2012.
- [52] Steve Yijie Hu, Yufeng Zhang, Darren Lawless, and Xianshe Feng. Composite membranes comprising of polyvinylamine-poly(vinyl alcohol) incorporated with carbon nanotubes for dehydration of ethylene glycol by pervaporation. *Journal of Membrane Science*, 417–418:34 – 44, 2012.
- [53] Shaofei Wang Shengnan Yu Fusheng Pan Hong Wu Yifan Li, Guangwei He and Zhongyi Jiang. Recent advances in the fabrication of advanced composite membranes. *Royal Society of Chemistry*, 1:10058–10077, 2013.
- [54] Sanjay G. Chaudhri, Bhavika H. Rajai, and Puyam S. Singh. Preparation of ultra-thin poly(vinyl alcohol) membranes supported on polysulfone hollow fiber and their application for production of pure water from seawater. *Desalination*, 367:272 – 284, 2015.
- [55] Gui Min Shi and Tai-Shung Chung. Thin film composite membranes on ceramic for pervaporation dehydration of isopropanol. *Journal of Membrane Science*, 448:34 – 43, 2013.
- [56] Lingxiang Zhu Weiguang Jia Haiqing Lin Moon Kattula, Koushik Ponnuru and Edward P. Furlani. Designing ultrathin film composite membranes: the impact of a gutter layer. *Nature*, (15016 (2015)), 2015.
- [57] George Xomeritakis, Sankar Nair, and Michael Tsapatsis. Transport properties of alumina-supported mfi membranes made by secondary (seeded) growth. *Microporous and Mesoporous Materials*, 38(1):61 – 73, 2000.
- [58] Maria Pilar Bernal, George Xomeritakis, and Michael Tsapatsis. Tubular MFI zeolite membranes made by secondary (seeded) growth. *Catalysis Today*, 67(1):101 – 107, 2001. Catalysis in Membrane Reactors.
- [59] Eva Barankova, Xiaoyu Tan, Luis Francisco Villalobos, Eric Litwiller, and Klaus-Viktor Peinemann. A metal chelating porous polymeric support: The missing link for a defect-free metal-organic framework composite membrane. *Angewandte Chemie International Edition*, 56(11):2965–2968, 2017.
- [60] Eva Barankova, Neelakanda Pradeep, and Klaus-Viktor Peinemann. Zeolite-imidazolate framework ZIF-8 membrane synthesis on a mixed-matrix substrate. *Chem. Commun.*, 49:9419–9421, 2013.
- [61] Fernando Cacho-Bailo, Beatriz Seoane, Carlos Téllez, and Joaquín Coronas. Zif-8 continuous membrane on porous polysulfone for hydrogen separation. *Journal of Membrane Science*, 464:119 – 126, 2014.
- [62] Wanbin Li, Qin Meng, Congyang Zhang, and Guoliang Zhang. Metal-organic framework/pvdf composite membranes with high H₂ permselectivity synthesized by ammoniation. *Chemistry – A European Journal*, 21(19):7224–7230, 2015.

- [63] Hyuk Taek Kwon and Hae-Kwon Jeong. In situ synthesis of thin zeolitic-imidazolate framework zif-8 membranes exhibiting exceptionally high propylene/propane separation. *Journal of the American Chemical Society*, 135(29):10763–10768, 2013. PMID: 23758578.
- [64] Li S. Lai, Yin F. Yeong, Kok K. Lau, and Mohd S. Azmi. Preliminary study on the synthesis of zif-8 membranes via in situ and secondary seeded growth methods. *Advanced Materials Research*, 1133:649–653, 01 2016. Date revised - 2016-12-01; Last updated - 2016-12-05.
- [65] Irena Gancarz, Gryzelda Poźniak, Marek Bryjak, and Włodzimierz Tylus. Modification of polysulfone membranes 5. effect of n-butylamine and allylamine plasma. *European Polymer Journal*, 38(10):1937 – 1946, 2002.
- [66] Alexander Fridman. *Plasma chemistry*. Cambridge University Press, 1 edition, 2008.
- [67] Hui Feng Zhang, Defei Liu, Ying Yao, Baoquan Zhang, and Y.S. Lin. Stability of zif-8 membranes and crystalline powders in water at room temperature. *Journal of Membrane Science*, 485:103 – 111, 2015.
- [68] Kyo Sung Park, Zheng Ni, Adrien P. Côté, Jae Yong Choi, Rudan Huang, Fernando J. Uribe-Romo, Hee K. Chae, Michael O’Keeffe, and Omar M. Yaghi. Exceptional chemical and thermal stability of zeolitic imidazolate frameworks. *Proceedings of the National Academy of Sciences*, 103(27):10186–10191, 2006.
- [69] Wang Zhang, Yingli Hu, Jin Ge, Hai-Long Jiang, and Shu-Hong Yu. A facile and general coating approach to moisture/water-resistant metal-organic frameworks with intact porosity. *Journal of the American Chemical Society*, 136(49):16978–16981, 2014. PMID: 25412280.
- [70] Graciela Wild Padua and Qin Wang. *Nanotechnology Research Methods for Food and Bioproducts (1)*. Wiley-Blackwell, Hoboken, US, 2012.
- [71] Syed Z. Abdullah, Pierre R. Bérubé, and Derrick J. Horne. {SEM} imaging of membranes: Importance of sample preparation and imaging parameters. *Journal of Membrane Science*, 463:113 – 125, 2014.
- [72] Nobuo Tanaka. *Scanning Transmission Electron Microscopy Of Nanomaterials: Basics Of Imaging And Analysis*. Imperial College Press, 2014.
- [73] Industrial Liaison office. Electron microscopy for biological sciences. <http://www.diamond.ac.uk/industry/Industry-News/Latest-News/Synchrotron-Industry-News-eBIC.html#>, 2016. [Online; accessed 27-Oct-2016].
- [74] O. David Sparkman, Zelda E. Penton, and Fulton G. Kitson. Chapter 1 - introduction and history. In Penton Zelda E. Kitson Fulton G. Sparkman, O. David, editor, *Gas Chromatography and Mass Spectrometry (Second edition)*, pages 2 – 13. Academic Press, Amsterdam, second edition edition, 2011.
- [75] Fernández Vidal Irene Teixidor Casamitjana Pilar title = Handbook of instrumental techniques for materials edition = 1 publisher = Centres Científics i Tecnològics. Universitat de Barcelona year = 2012 chapter = 6 pages = 1-12 Berdié Rabanaque, Lourdes.
- [76] Larsen Kitson, FG and McEwen. *Gas Chromatography and Mass Spectrometry*. Elsevier Science, 1 edition, 1996.
- [77] Frank M. Dunnivant. The gas chromatograph. http://people.whitman.edu/~dunnivfm/C_MS_Ebook/CH2/2_3.html, 2008. [Online; accessed 27-Jun-2017].

- [78] *Validation of Analytical Procedures: Text and Methodology Q2(R1)*. International Conference on Harmonisation of Technical Requirements for Registration of Pharmaceuticals for Human Use, 2005.
- [79] *ISO/IEC 17025:2005, General Requirements for the Competence of Testing and Calibration Laboratories*. International Organization for Standardization, 2005.
- [80] Nidal Jaradat Murad N. Abualhasan, Abdel Naser Zaid and Ayman Mousa. "GC method validation for the analysis of menthol in suppository pharmaceutical dosage form. *International Journal of Analytical Chemistry*, 2017, 2017.
- [81] Paola A. Magni, Tommaso Pacini, Marco Pazzi, Marco Vincenti, and Ian R. Dadour. Development of a GC-MS method for methamphetamine detection in calliphora vomitoria l. (diptera: Calliphoridae). *Forensic Science International*, 241:96 – 101, 2014.
- [82] Harry Prest Greg Wells and Charles William Russ IV. Signal, noise, and detection limits in mass spectrometry. Technical report, 2011.
- [83] The role of the signal-to-noise ratio in precision and accuracy. *LCGC Europe*, 19(1):12 – 16, 2006.
- [84] Knuutila H. Ansaloni L., Rennemo R. and Deng L. 3rd generation membrane contactors: amine permeation through the membrane interface. *UT-CCS*, 2016.
- [85] Gui Min Shi, Jian Zuo, Shyuan Hong Tang, Shawn Wei, and Tai Shung Chung. Layer-by-layer (lbl) polyelectrolyte membrane with nexar™ polymer as a polyanion for pervaporation dehydration of ethanol. *Separation and Purification Technology*, 140:13 – 22, 2015.
- [86] Satoru Kato, Kunio Nagahama, and Hidetaka Asai. Permeation rates of aqueous alcohol solutions in pervaporation through nafion membranes. *Journal of Membrane Science*, 72(1):31 – 41, 1992.
- [87] A. Morisato, Sankar S. S. Shen, H. C., Pinnau I. Freeman, B. D., and C. G. Casillas. Polymer characterization and gas permeability of poly(1-trimethylsilyl-1-propyne) [ptmsp], poly(1-phenyl-1-propyne) [ppp], and ptmsp/ppp blends. *Journal of Polymer Science Part B: Polymer Physics*, 34(13):2209–2222, 1996.
- [88] Luca Ansaloni, Asad Arif, Arlinda F. Ciftja, Hanna K. Knuutila, and Liyuan Deng. Development of membrane contactors using phase change solvents for CO2 capture: Material compatibility study. *Industrial & Engineering Chemistry Research*, 55(51):13102–13113, 2016.
- [89] G.M. Geise, B.D. Freeman, and D.R. Paul. Characterization of a sulfonated pentablock copolymer for desalination applications. *Polymer*, 51(24):5815 – 5822, 2010.
- [90] Jifu Zheng, Qingyi He, Chunli Liu, Ting Yuan, Suobo Zhang, and Hui Yang. Nafion-microporous organic polymer networks composite membranes. *Journal of Membrane Science*, 476:571 – 579, 2015.
- [91] R. S. L. Yee, R. A. Rozendal, K. Zhang, and B. P. Ladewig. Cost effective cation exchange membranes: A review (article). *Chemical Engineering Research and Design*, 90(7):950–959, 2012.
- [92] Peter M. Budd, Neil B. McKeown, and Detlev Fritsch. Polymers of intrinsic microporosity (PIMs): High free volume polymers for membrane applications. *Macromolecular Symposia*, 245-246(1):403–405, 2006.

- [93] Colin A. Scholes, Jianyong Jin, Geoff W. Stevens, and Sandra E. Kentish. Competitive permeation of gas and water vapour in high free volume polymeric membranes. *Journal of Polymer Science Part B: Polymer Physics*, 53(10):719–728, 2015.
- [94] Yulia Rogan, Ludmila Starannikova, Victoria Ryzhikh, Yuri Yampolskii, Paola Bernardo, Fabio Bazzarelli, Johannes Carolus Jansen, and Neil B. McKeown. Synthesis and gas permeation properties of novel spirobisindane-based polyimides of intrinsic microporosity. *Polym. Chem.*, 4:3813–3820, 2013.
- [95] K. L. Mittal. *Polyimides and Other High Temperature Polymers : Synthesis, Characterization and Applications*. Brill, 2003.
- [96] Sheng Xu and Yan Wang. Novel thermally cross-linked polyimide membranes for ethanol dehydration via pervaporation. *Journal of Membrane Science*, 496:142 – 155, 2015.
- [97] Mashallah Rezakazemi, Kazem Shahidi, and Toraj Mohammadi. Synthetic pdms composite membranes for pervaporation dehydration of ethanol. *Desalination and Water Treatment*, 54(6):1542–1549, 2015.
- [98] Stan Claes, Pieter Vandezande, Steven Mullens, Kristien De Sitter, Roos Peeters, and Marlies K. Van Bael. Preparation and benchmarking of thin film supported ptmsp-silica pervaporation membranes. *Journal of Membrane Science*, 389:265 – 271, 2012.
- [99] M. A. Geday B. Cerrolaza C. Carrasco N. Bennis A. Spadlo, R. Dabrowski and J. M. Oton. Selective crosslinking of polyimide for photonic devices. *Molecular Crystals and Liquid Crystals*, 502(1):185–194, 2009.
- [100] Sigma Aldrich. PDMS. <http://www.sigmaaldrich.com/materials-science/material-science-products.html?TablePage=113790985>, 2017. [Online; accessed 18-Jul-2017].
- [101] Sigma Aldrich. Poly[4,5-difluoro-2,2-bis(trifluoromethyl)]. <http://www.sigmaaldrich.com/catalog/product/aldrich/469629>, 2017. [Online; accessed 18-Jul-2017].
- [102] Sun-Tak Hwang. Fundamentals of membrane transport. *Korean Journal of Chemical Engineering*, 28(1):1–15, 2011.
- [103] Kew-Ho Lee and Sun-Tak Hwang. The transport of condensable vapors through a microporous vycor glass membrane. *Journal of Colloid and Interface Science*, 110(2):544 – 555, 1986.
- [104] Mohammad Amirilargani and Behrouz Sadatnia. Poly(vinyl alcohol)/zeolitic imidazolate frameworks (zif-8) mixed matrix membranes for pervaporation dehydration of isopropanol. *Journal of Membrane Science*, 469:1 – 10, 2014.
- [105] Larsen Barbara S. Kitson Fulton G McEwen, Charles N. *Gas Chromatography and Mass Spectrometry*. Elsevier Science, 1 edition, 1996.
- [106] Restek Corporation. Solvent expansion calculator. <http://www.restek.com/Technical-Resources/Chromatography-Calculators>, 2017. [Online; accessed 19-Jun-2017].
- [107] Techniques for Optimizing GC Analysis of Ethylene Glycol in Water. Standard, Restek Corporation, U.S.A., 2013.

- [108] Yeon Ki Hong and Won Hi Hong. Influence of ceramic support on pervaporation characteristics of ipa/water mixtures using pdms/ceramic composite membrane. *Journal of Membrane Science*, 159(1–2):29 – 39, 1999.
- [109] WM. R. Parrish. Phase behaviour of the triethylene glycol-water system and dehydration/regeneration design for extremely low dew point requirements. *Annual GPA Convention*, pages 3813–3820, 1986.
- [110] Rajkiran R. Tiwari, Zachary P. Smith, Haiqing Lin, B.D. Freeman, and D.R. Paul. Gas permeation in thin films of “high free-volume” glassy perfluoropolymers: Part i. physical aging. *Polymer*, 55(22):5788 – 5800, 2014.
- [111] Ze-Xian Low, Amir Razmjou, Kun Wang, Stephen Gray, Mikel Duke, and Huanting Wang. Effect of addition of two-dimensional ZIF-L nanoflakes on the properties of polyethersulfone ultrafiltration membrane. *Journal of Membrane Science*, 460:9 – 17, 2014.
- [112] Javier Sánchez-Laínez, Beatriz Zornoza, Sebastian Friebe, Jürgen Caro, Shuai Cao, Anahid Sabetghadam, Beatriz Seoane, Jorge Gascon, Freek Kapteijn, Clément Le Guillouzer, Guillaume Clet, Marco Daturi, Carlos Téllez, and Joaquín Coronas. Influence of ZIF-8 particle size in the performance of polybenzimidazole mixed matrix membranes for pre-combustion co2 capture and its validation through interlaboratory test. *Journal of Membrane Science*, 515:45 – 53, 2016.
- [113] Microsoft. Stdevp function. <https://support.office.com/en-us/article/STDEVP-function-1f7c1c88-1bec-4422-8242-e9f7dc8bb195>, 2016. [Online; accessed 20-Jun-2017].

Appendix A - Risk assessments

Risk assessments for the experimental laboratory work were performed and is given in this appendix. All risk analysis were performed in collaboration with co-supervisor. Basis for the risk assessments were HSE guidelines (NTNU online website), laboratory handbook (NTNU online website, printed version) and material safety data sheets (MSDS).



ID	10164	Status	Dato
Risikoområde	Risikovurdering: Helse, miljø og sikkerhet (HMS)	Opprettet	14.07.2016
Opprettet av	Natalie Therese Josefsen	Vurdering startet	14.07.2016
Ansvarlig	Natalie Therese Josefsen	Tiltak besluttet	
		Avsluttet	

Membrane preparation procedure

Gyldig i perioden:

7/14/2016 - 7/14/2019

Sted:

3 - Gløshaugen / 314 - Kjemi 4 / 1020 - 2. etasje / 4.16 / 4.218 / 4.220

Mål / hensikt

The present procedure refers to the preparation of lab scale membranes (casting solution amount up to 500 mL).

Bakgrunn

The preparation procedures include the preparation of the casting solution as well as solvent evaporation, deep coating and knife coating technique to obtain the membrane. It includes also the possible use of nanoparticles to obtain mixed matrix membranes.

A large variety of solvents, polymeric materials and nanoparticles can be used. In case of new activities, the present document should be updated accordingly.

Chemicals:

- organic solvents
- polymeric materials
- water
- nanoparticles (e.g. nano cellulose, metal organic frameworks)

Beskrivelse og avgrensninger

In case of use of toxic or harmful chemicals, the casting solution preparation and the membrane casting must be carried out inside a fume hood, wearing nitrile gloves, lab goggles, and lab coat.

In case of use of nanoparticles, the addition of nanoparticles into the casting solution must be carried out into a safety cabinet and use of gas mask if required by the MSDS of the chemical. The casting solution preparation and the membrane casting must be carried out inside a fume hood, wearing a mask for powders, nitrile gloves, lab goggles, and lab coat.

Forutsetninger, antakelser og forenklinger

In case of use of toxic or harmful chemicals or nanoparticles, the casting solution preparation and the membrane casting must be carried out inside a fume hood.

Vedlegg

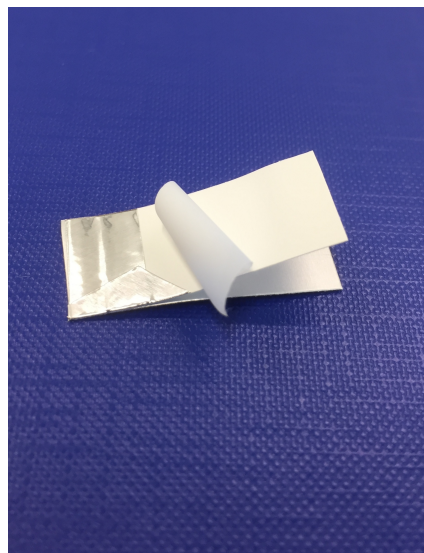
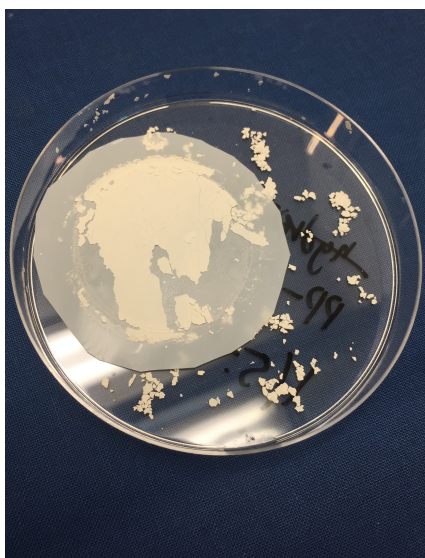
[Ingen registreringer]

Referanser

[Ingen registreringer]

Appendix B - Membrane images

Pictures the multi-layered membranes can be found in Figure .0.1. The pictures show the detachment of PP and the particle layers.

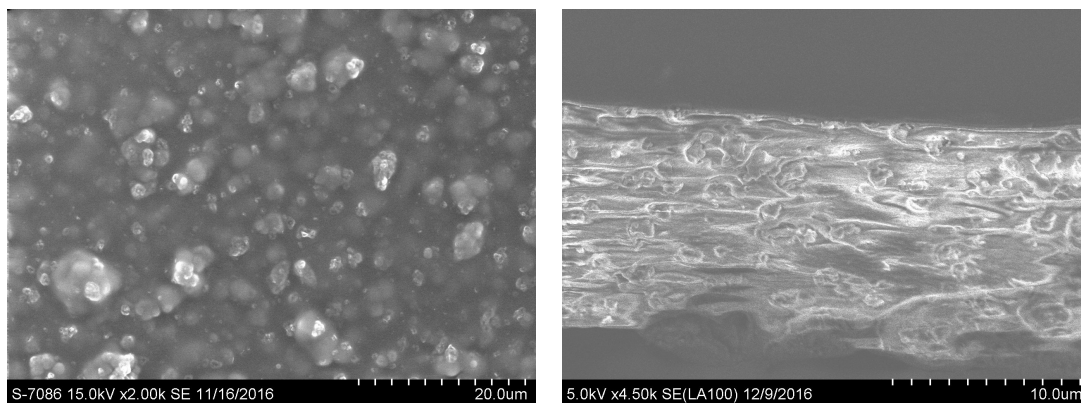


(a) Multi layered membrane of PP-ZIF-8 (b) Multi layered membrane of PP-ZIF-L-
AF2400

Figure .0.1: Pictures of the multi-layered membranes when detachment occurred.

Appendix C - S(T)EM images

STEM pictures of the mixed matrix membranes with ZIF-8 made in the specialization project can be found in Figure .0.2.



(a) Pure AF2400 self standing membrane.

(b) MMM with zifL immersed in AF2400.

Figure .0.2: Surface images of self standing membranes with AF2400, with and without zif-l nano particles. a) SEM surface image of pure AF2400 self standing membrane. b) S(T)EM surface image of MMM with zif-l immersed in AF2400.

Appendix D - standard deviation

The formula used to calculate the standard deviation (STD) in the experimental data is given in Equation .0.1 and the Microsoft excel command for the equation is STDEVP(number1,[number2],...) [113].

$$STD = \sqrt{\frac{\sum (x - \bar{x})^2}{n}} \quad (.0.1)$$

Where $(x - \bar{x})^2$ is the sample mean average and n is the sample size. The relative standard deviation (RSD) is widely used in analytical chemistry as a measure of precision and repeatability and is given by the Equation .0.2.

$$\%RSD = \frac{STD}{\bar{x}} \quad (.0.2)$$

Where \bar{x} is the sample average. If the method's precision should be less than 15% RSD, the S/N will be 3.33 given by Equation .0.3 [83] .

$$\%RSD = \frac{50}{(S/N)} \quad (.0.3)$$

Appendix E - Pervaporation graphs

A Figure of TEG concentration in the permeate as a function of water concentration in feed can be found in Figure .0.3.

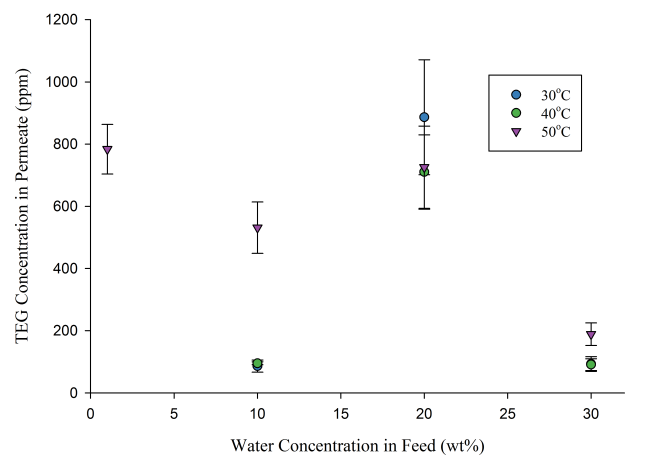


Figure .0.3: TEG concentration as a function of water concentration in feed.

Appendix F - Activity coefficients

Activity coefficients for water and TEG with different water concentrations and temperatures can be found in Table .0.1 and Table .0.2 [109].

Table .0.1: Activity coefficient of water

wt% water	30	20	10	1
mol% water	0.787444251	0.690456486	0.492874643	0.077662011
30	0.9086	0.8442	0.7518	0.5941
40	0.9516	0.8904	0.7853	0.6158
50	0.9776	0.9332	0.8236	0.6381
60	0.9872	0.9625	0.8654	0.6612

Table .0.2: Activity coefficient of TEG

wt% water	30	20	10	1
mol% water	0.787444251	0.690456486	0.492874643	0.077662011
0.6111	0.7563	0.9025	0.9979	
0.6133	0.742	0.8979	0.998	
0.6494	0.7401	0.8918	0.998	
0.7083	0.7599	0.8863	0.9979	

Appendix G - Apparent activation energy

Apparent activation energies found from an Arrhenius relationship of permeance can be found in Table .0.3.

Table .0.3: Activation energy found from permeance

	10wt%,water	10wt%,TEG	30wt%, water	30wt%,TEG
R^2	0,95	0,89	0,92	0,89
Slope	1,02	-13,34	0,52	-7,26
Ea	-8,45	110,90	-4,29	60,36